

# Controlling airborne cues to study small animal navigation

Marc Gershow<sup>1</sup>, Matthew Berck<sup>1</sup>, Dennis Mathew<sup>2</sup>, Linjiao Luo<sup>1</sup>, Elizabeth A Kane<sup>1</sup>, John R Carlson<sup>2</sup> & Aravinthan D T Samuel<sup>1</sup>

**Small animals such as nematodes and insects analyze airborne chemical cues to infer the direction of favorable and noxious locations. In these animals, the study of navigational behavior evoked by airborne cues has been limited by the difficulty of precisely controlling stimuli. We present a system that can be used to deliver gaseous stimuli in defined spatial and temporal patterns to freely moving small animals. We used this apparatus, in combination with machine-vision algorithms, to assess and quantify navigational decision making of *Drosophila melanogaster* larvae in response to ethyl acetate (a volatile attractant) and carbon dioxide (a gaseous repellent).**

Olfaction is a sophisticated sensory modality. Odor plumes from sources in an animal's environment are carried and mixed by chaotic air currents before reaching an animal's olfactory organ. From a complex olfactory signal, and the resulting time-varying activity of a panel of olfactory neuronal types, an animal strives to locate and discriminate odor sources<sup>1–3</sup>.

Olfactory computation may be studied using small invertebrates like *Caenorhabditis elegans* and *D. melanogaster*, which have small circuits and simple behaviors and are amenable to genetic manipulation<sup>4,5</sup>. Quantitative behavioral analysis, an important step in defining olfactory computations, is complicated by the difficulty of delivering precise airborne stimuli to freely moving animals. Classical behavioral assays for these animals quantify migration toward or away from droplets of odor<sup>6–9</sup>. In these assays, evaporation, convection and diffusion create spatially varying concentration gradients that change over time during each experiment. Droplet-based assays can be improved by calibrating the odor profile in closed plates using infrared spectroscopy<sup>8,9</sup>; however, gases such as carbon dioxide ( $\text{CO}_2$ ) that are not liquid at room temperature cannot be used, spatial or temporal gradients cannot be precisely defined, the odor profile cannot be held stable in time, and a relatively small experimental arena must be used, leading to lower throughput. An alternative is to deliver water-borne stimuli using microfluidic devices engineered to the shape and movements of each animal. Such devices constrain behavior to their specific geometries<sup>10–12</sup> and do not easily accommodate many animals including insect larvae.

We present a device (Fig. 1) that allows us to deliver airborne cues in defined spatial and temporal gradients to freely behaving animals. An array of miniature solenoid valves injects odorant cues into a laminar airflow directed across an experimental arena. The amount of airborne cue injected at each point can be dynamically regulated during each experiment. This device generated long-lasting, stable and highly reproducible spatiotemporal gradients of any gas, including  $\text{CO}_2$ , a salient cue for *D. melanogaster* and *Anopheles* sp. mosquito<sup>13,14</sup>, and features a large experimental arena that allows many small invertebrates to be studied simultaneously for extended periods of time.

Using our device, in combination with custom machine-vision software, the multianimal gait and track (MAGAT) analyzer (Fig. 2 and **Supplemental Fig. 1**), we quantified navigational decision making of *D. melanogaster* larvae in response to airborne cues with higher precision and throughput than has been possible with earlier methods. We examined *D. melanogaster* larva chemotaxis to an airborne attractant (ethyl acetate) and repellent ( $\text{CO}_2$ ) and discovered similarities between the larva's response to these gaseous cues and its navigation of thermal gradients.

## RESULTS

### Gradient generation

Our device creates airborne gradients in a square arena, 25 cm on a side, allowing extended observation of many animals per experiment and surpassing the throughput of single animal methods<sup>8,15</sup>. A slow laminar airflow ( $1.2 \text{ cm s}^{-1}$ ) is directed along the  $y$  axis of the arena. A row of miniature solenoid valves spaced 8 mm apart is used to generate gradients along the  $x$  axis. When each valve is open, a dose of gaseous cue is injected at a specific point along the  $x$  axis into the airflow. The opening of the valves and the odor-carrying airflow may be used to generate defined spatial and temporal gradients of any gaseous cue (Online Methods and **Supplementary Note 1**; detailed plans are available in **Supplementary Data**).

To characterize the gradients within the arena, we substituted its glass lid with an aluminum plate fitted with miniature gas detectors. We imposed a linear gradient by programming the fraction of time each valve was open to be in proportion to

<sup>1</sup>Department of Physics and Center for Brain Science, Harvard University, Cambridge, Massachusetts, USA. <sup>2</sup>Department of Molecular, Cellular and Developmental Biology, Yale University, New Haven, Connecticut, USA. Correspondence should be addressed to A.D.T.S. (samuel@physics.harvard.edu).

RECEIVED 24 AUGUST 2011; ACCEPTED 30 NOVEMBER 2011; PUBLISHED ONLINE 15 JANUARY 2012; DOI:10.1038/NMETH.1853

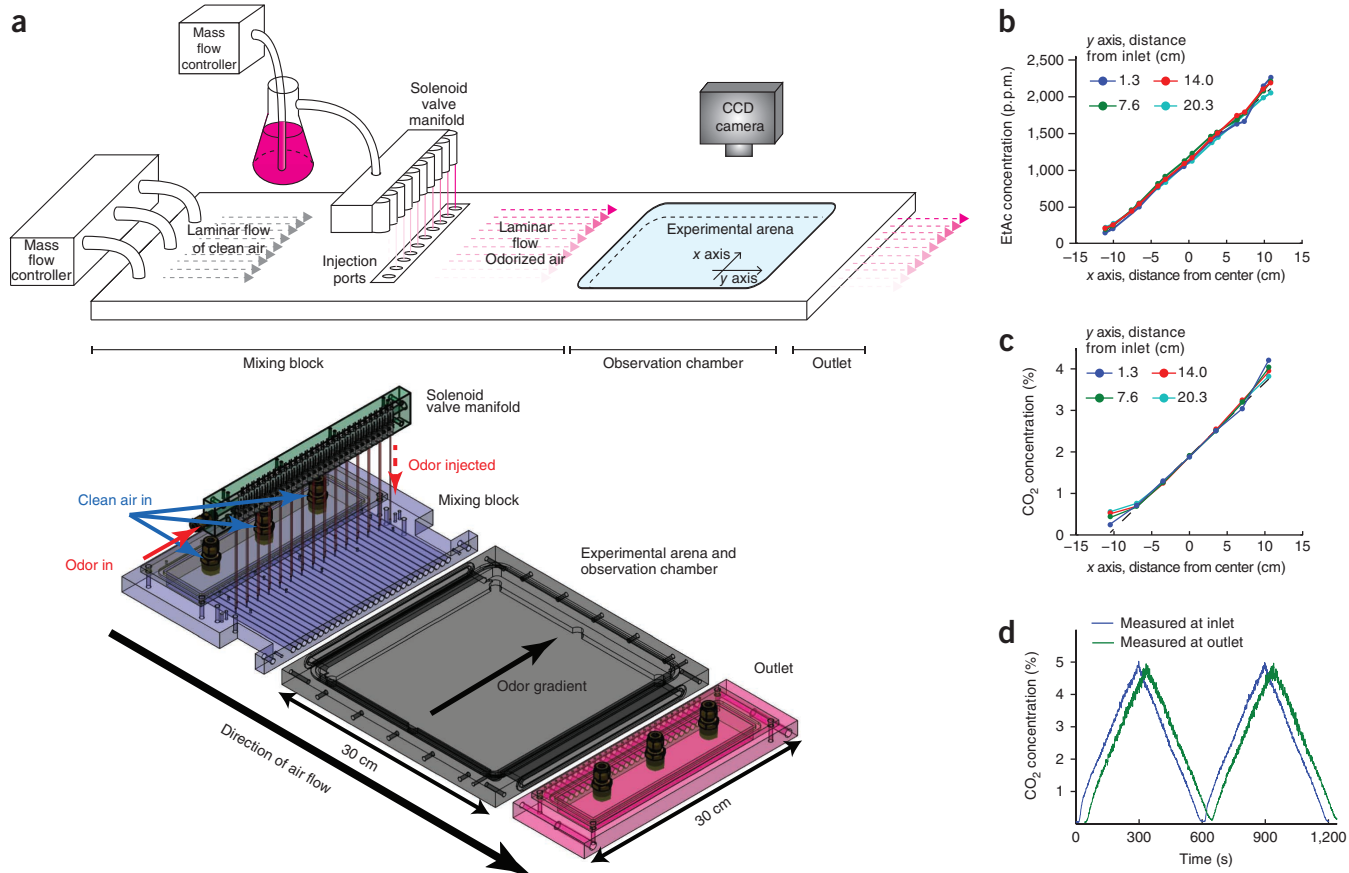


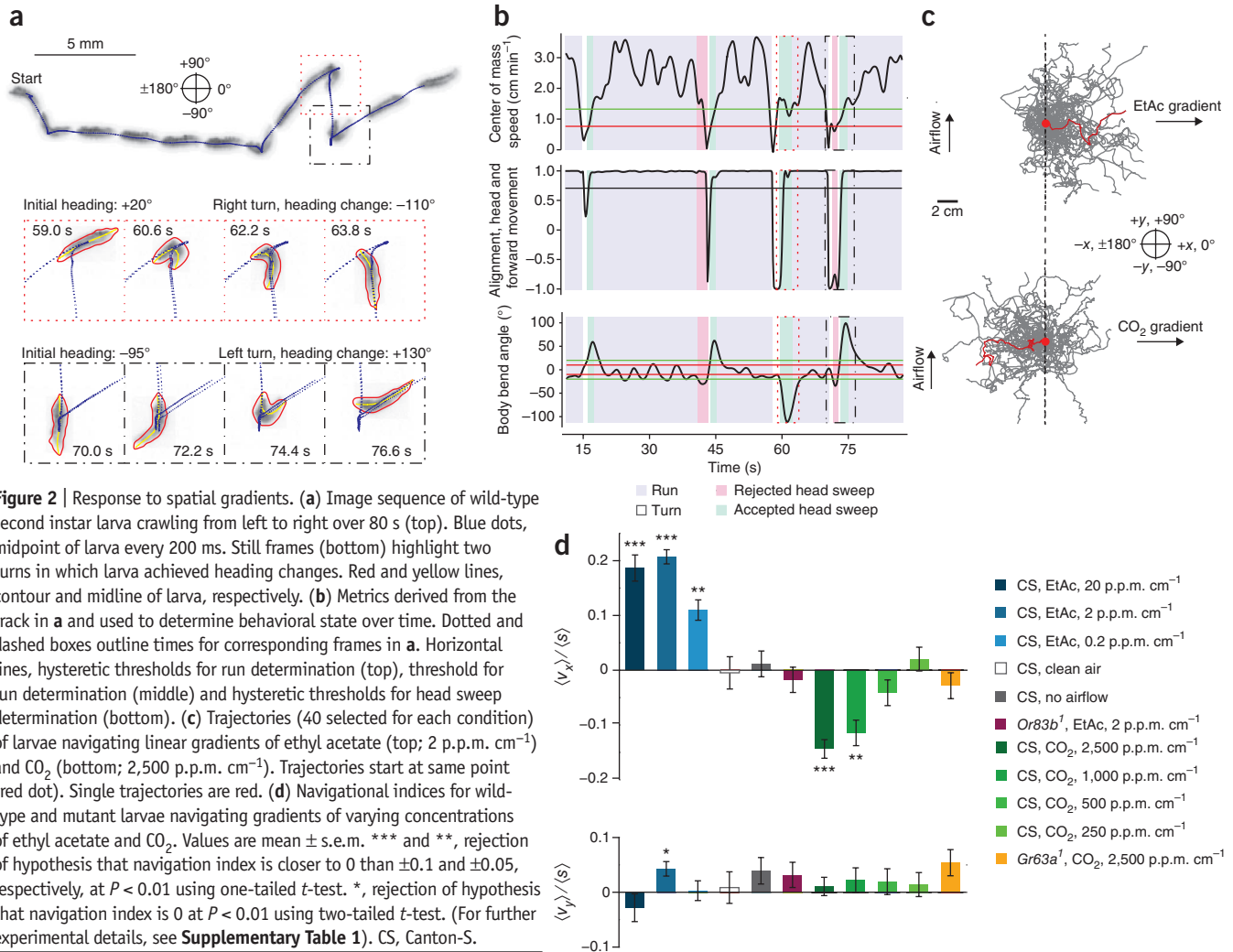
**Figure 1 |** Apparatus design and performance. **(a)** Schematic of the device (top). Clean airflow into the rear of the apparatus is regulated by a mass flow controller. For ethyl acetate experiments, a second mass flow controller controls airflow through a bubbler containing ethyl acetate. Odorized air is injected into points across the laminar airflow within a mixing block using a solenoid valve manifold. The laminar airflow odorized with a spatial gradient of ethyl acetate in the mixing block then passes into an observation chamber containing an experimental arena with transparent ceiling, allowing visualization of animal behavior inside the arena with a charge-coupled device (CCD) camera. Semitransparent isometric projection (bottom) of custom-machined components of the apparatus, including solenoid valve manifold, mixing block, experimental arena and observation chamber, and outlet. Direction of air flow (*y* axis) and gradient (*x* axis) are indicated. ‘Odor gradient’ arrow points to higher concentration in experiments described here. **(b,c)** Measurement of precision of linear spatial gradients of ethyl acetate (EtAc; **b**) or CO<sub>2</sub> (**c**) in the experimental arena. Gas concentration was measured at specific points in the experimental arena across the airflow (arena *x* axis) at indicated distances from the inlet (arena *y* axis). **(d)** CO<sub>2</sub> concentration at inlet and outlet during a 10-min temporal triangle ramp from 0% to 5% CO<sub>2</sub>.

its position along the *x* axis. With either ethyl acetate or CO<sub>2</sub> (**Fig. 1b,c**), we found that the deviation from linearity was <3% of the mean concentration in the region in which the behavioral experiments were done.

To generate temporal gradients, we mixed odor into the airstream before it entered the device, controlling the odor flow rate into the airstream while monitoring odor concentration at the chamber inlet and outlet (**Supplementary Note 2** and **Supplementary Fig. 2** and **Fig. 1d**). The concentration is constant along the *x* axis, as the odor is mixed into the airstream before entry into the flow tubes that are used to define a spatial gradient. Along the *y* axis, the concentration varies as the time-varying odor profile is pushed across the chamber by the moving air flow. We measured a time lag between the detection of an odor change in the inlet and the outlet that corresponds to the flow rate of the gas in the chamber. Thus, the concentration at any point in the chamber is given by  $C(y,t) = C_{\text{inlet}}(t - t_d - y/v_f)$ , where  $v_f$  is the flow speed in the chamber and  $t_d$  is the time it takes gas to flow from the inlet to the flow chamber entrance.

### Behavioral analysis

The trajectories of crawling *D. melanogaster* larvae are characterized by periods of forward movement (runs) that are interrupted by turns. We have previously used a high-resolution tracking microscope to follow individual *D. melanogaster* larvae on temperature gradients<sup>15</sup>. We have shown that a larva biases the frequency, direction and size of turns to move toward favorable temperatures. Here we sought to achieve the same resolution of behavioral analysis in a multianimal experiment. To do this, we developed the MAGAT analyzer software package to follow many larvae in parallel (**Supplementary Video 1**, **Supplementary Fig. 1** and **Supplementary Software 1**; software updates will be available at <https://github.com/samuellab/MAGATAnalyzer>) and determine the behavioral state of each larva (running, turning and sweeping the head) at all times (**Fig. 2a,b** and **Supplementary Note 3** and **Supplementary Videos 2–6**). The MAGAT analyzer quantifies the navigational performance of individual *D. melanogaster* larvae. By collecting navigational statistics across populations of *D. melanogaster* larvae, we uncovered behavioral strategies.



We characterized the navigational strategies of *D. melanogaster* larvae in response to ethyl acetate and CO<sub>2</sub> using defined spatial and temporal gradients. First, we examined the response to ethyl acetate, a volatile attractant<sup>16</sup>, in linear spatial gradients with defined steepness<sup>6</sup>. We placed second instar Canton-S larvae in the middle of each gradient and quantified the resulting trajectories (Fig. 2c). Throughout this study, we used a compass in which 0° indicates movement up the gradient (+x direction), 180° indicates movement down the gradient (-x direction), +90° indicates movement downwind, orthogonal to the gradient (+y direction) and -90° indicates movement upwind, orthogonal to the gradient (-y direction). To quantify the overall navigational response in each linear spatial gradient, we computed a navigational index by dividing the mean velocity of all larvae in the x direction,  $\langle v_x \rangle$ , by the mean crawling speed,  $\langle s \rangle$

$$\text{Index} = \langle v_x \rangle / \langle s \rangle \quad (1)$$

Hence, the navigational index was  $\pm 1$  if the larvae crawled uniformly straight up or down the gradient and 0 if the movement was unbiased. This index (Fig. 2d) was significantly greater than zero ( $P < 0.01$ ) across three ethyl acetate gradient steepnesses that we studied, indicating that chemotaxis toward ethyl acetate persists over two orders of magnitude in ethyl acetate concentration.

We did two control experiments without odorant, one in which the valves injected clean air into the laminar flow and one in which no laminar flow was provided (Fig. 2d). In both cases, the navigational index in the x direction was 0. We also tested *Orco*<sup>1</sup> larvae, which lack function in all olfactory neurons<sup>16,17</sup> and did not navigate ethyl acetate gradients (Fig. 2d).

Next, we examined the response to CO<sub>2</sub>, a gaseous repellent<sup>18</sup>, in linear spatial gradients with different steepnesses. The navigational indices were negative (indicating repulsion) and depended strongly on steepness (Fig. 2d). Reducing the steepness by 90% essentially abolished navigation away from CO<sub>2</sub>. We verified that a loss-of-function mutation in Gr63a, a required CO<sub>2</sub> chemosensory receptor<sup>13,18,19</sup>, disrupts CO<sub>2</sub> avoidance (Fig. 2d).

To assess whether the larvae responded to the laminar airflow itself (that is, exhibited rheotaxis), we computed the orthogonal navigational index, the mean velocity of all larvae in the y direction divided by the mean crawling speed (Fig. 2d). In all cases, orthogonal indices were ~0 and were not correlated with navigational indices in the gradient direction, indicating that airflow does not disrupt navigational response to the airborne cue.

### Navigation in spatial gradients

What biases in the sequence of runs and turns along each trajectory enable the larvae to ascend ethyl acetate gradients (Fig. 3)

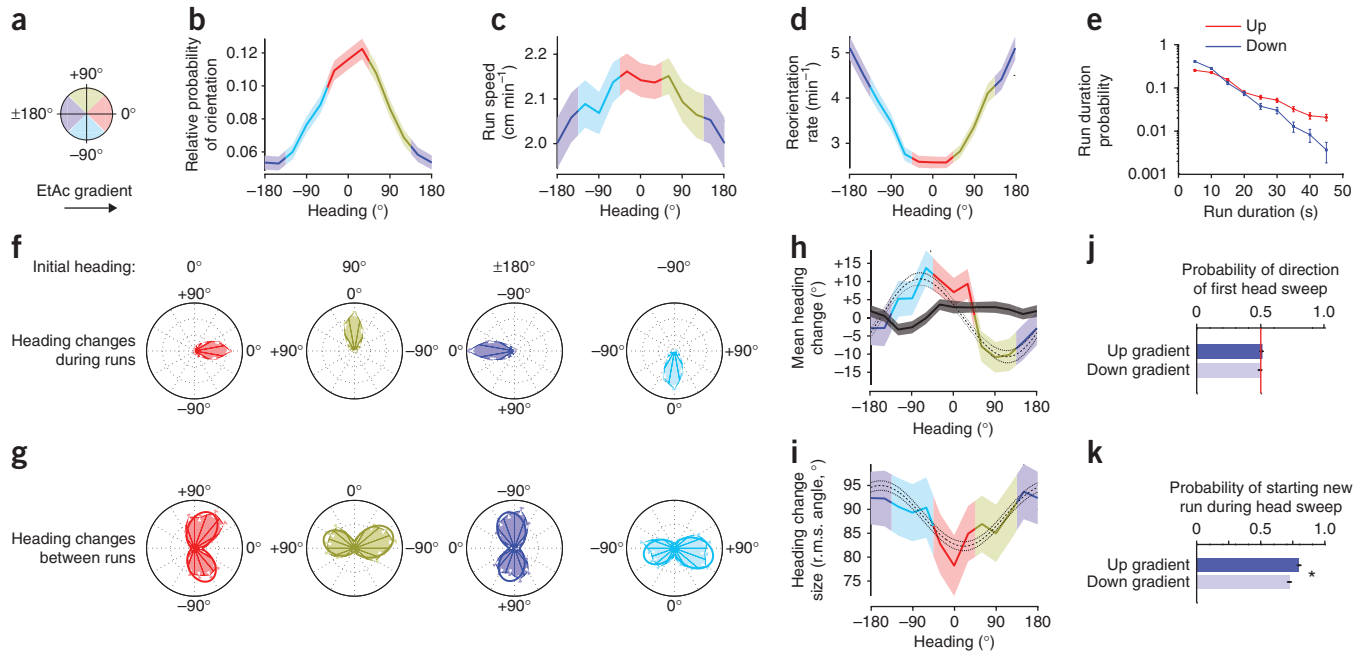


**Figure 3 |** Navigation of a 2 p.p.m.  $\text{cm}^{-1}$  ethyl acetate concentration gradient. (a) Schematic of heading angles; 0° is toward higher concentration. For data in this figure, ten experiments, 202 *D. melanogaster* larva and 29 h of behavior were analyzed. (b) Relative probability of headings during runs. (c) Speed versus heading during runs. (d) Turn rate versus heading. (e) Durations of runs headed up (1,537 runs) or down (1,091 runs) gradients. (f) Heading changes during runs sorted by initial heading: up gradients (red, 1,499 runs), orthogonal with higher concentration to right (gold, 1,354 runs), down gradients (blue, 1,062 runs) and orthogonal with higher concentration to left (cyan, 1,184 runs). (g) Heading changes achieved by turns, sorted as in f on the basis of heading immediately before the turn (0°, 1,201 reorientations; 90°, 1,214 reorientations; 180°, 1,105 reorientations; -90°, 1,049 reorientations). (h) Mean heading change achieved by runs (black line) versus initial heading and turns (colored line) versus heading before turn. Shaded regions indicate  $\pm$  s.e.m. (i) r.m.s. turn angle versus run heading before turn. Dashed and dotted lines in h,i represent prediction and 95% confidence interval of model (Online Methods). (j,k) Statistics of head sweeps during turns after runs headed orthogonal to concentration gradient. Probability of direction of first head sweep (j; 1,967 head sweeps) and probability that larva initiates a new run during head sweeps (k; 2,341 head sweeps). Asterisk, rejection of hypothesis that probabilities are the same at  $P < 0.01$  (Welch's  $t$ -test). Mean  $\pm$  s.e.m. calculated as described in Online Methods (b,c), mean  $\pm$  s.e.m. derived from counting statistics (d-g,j,k) and mean  $\pm$  s.e.m. (h,i).

and descend  $\text{CO}_2$  gradients (Fig. 4)? We describe the motion of larvae during runs by the magnitude (run speed) and direction (run heading) of the velocity vector. We calculated the fraction of time that larvae spent crawling in different directions on linear spatial gradients by making a histogram of run heading, and found that larvae spent the most time moving up ethyl acetate gradients and down  $\text{CO}_2$  gradients (Figs. 3b and 4b). Larvae also crawled slightly faster when heading up ethyl acetate gradients than down and crawled slightly slower when heading up  $\text{CO}_2$  gradients than down (Figs. 3c and 4c).

We examined the rate at which larvae initiated turns as a function of heading on linear spatial gradients, and found that the probability of larvae initiating a turn per unit time on linear gradients of ethyl acetate or  $\text{CO}_2$  (Figs. 3d and 4d) was a smoothly varying function of heading with maximum at 180° or 0°, respectively. Thus, larvae extended runs in favorable directions, up gradients of ethyl acetate and down gradients of  $\text{CO}_2$  (Figs. 3e and 4e). This strategy, termed the biased random walk, is also exhibited during *Escherichia coli* chemotaxis<sup>20</sup>.

*D. melanogaster* larvae have been proposed to directly orient toward higher attractant concentrations during periods of forward movement<sup>8</sup>. To investigate whether larvae steer within runs, we compared headings at the end and beginning of each run. If larvae were steering toward more favorable directions during runs, we would expect that, on average, runs would end with more favorable

headings than they began. We examined the angle change during runs (final heading minus initial heading) as a function of initial headings (Figs. 3f and 4f). The mean heading change (Figs. 3h and 4h) during runs was nearly zero regardless of initial heading, so larvae did not seem to orient themselves during runs.

To examine whether larvae modulate the size and direction of turns to augment the number of runs in a favorable direction, we examined the heading change effected by each turn (Supplementary Video 5). When larvae turned after a run up or down either ethyl acetate or  $\text{CO}_2$  gradients (Figs. 3g and 4g), the heading change distributions were bimodal and roughly symmetric but narrower when larvae were initially headed in the favorable direction. When larvae turned after a run oriented perpendicular to the gradient, they did so with the same distribution of angular sizes to the left or right, but made more turns toward the favorable direction. For any given initial heading, the angular distribution of heading changes after turns could be modeled as the sum of two skew-normal distributions (Online Methods).

To quantify how turns enhance orientation during navigation, we measured the moments of heading-change distributions as functions of initial heading. In contrast to the mean zero heading change achieved during runs, the mean heading change after turns (Figs. 3h and 4h) showed significant biases ( $P < 0.01$  using the model described in Online Methods) to orient the larvae toward higher concentration of ethyl acetate or lower concentration of

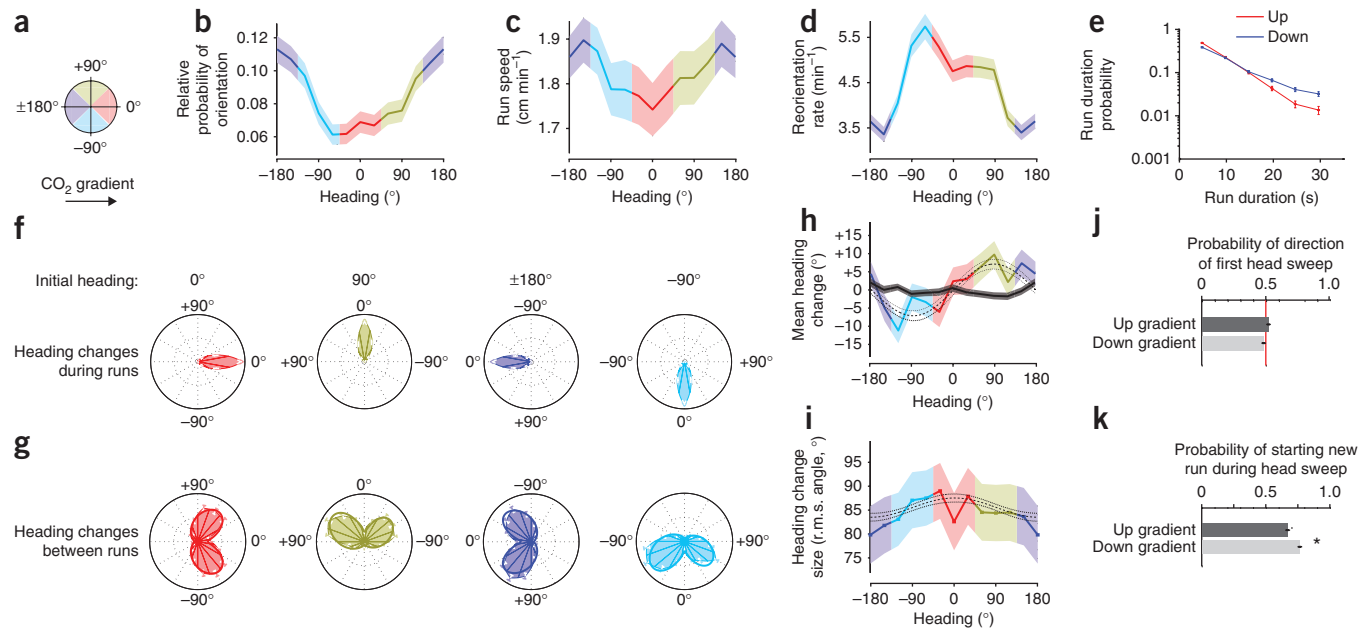


**Figure 4 |** Navigation of a 2,500 p.p.m.  $\text{cm}^{-1}$   $\text{CO}_2$  concentration gradient. **(a)** Schematic of heading angles; 0° is toward higher concentration. For data in this figure, 21 experiments, 168 *D. melanogaster* larva and 31 h of behavior were analyzed. **(b)** Relative probability of headings during runs. **(c)** Speed versus heading during runs. **(d)** Turn rate versus heading. **(e)** Durations of runs headed up (1,494 runs) or down (1,866 runs) gradients. **(f)** Heading changes during runs sorted by initial heading: up (red, 1,484 runs), down gradients (blue, 1,844 runs), orthogonal with higher concentration to right (gold, 1,651 runs) and orthogonal with higher concentration to left (cyan, 1,664 runs). **(g)** Heading changes achieved by turns, sorted as in **f** on the basis of heading immediately before the turn (0°, 1,196 reorientations; 180°, 1,336 reorientations; 90°, 1,306 reorientations; -90°, 1,375 reorientations). **(h)** Mean heading change achieved by runs (black line) versus initial heading and turns (colored line) versus heading before turn. **(i)** r.m.s. turn angle versus run heading before turn. Dashed and dotted lines in **h,i**, prediction and 95% confidence interval, respectively, of model described in Online Methods. **(j,k)** Statistics of head sweeps during turns after runs headed orthogonal to concentration gradient. Probability of direction of first head sweep (**j**; 2,497 head sweeps) and probability that the larva initiates a new run during head sweeps (**k**; 3,254 head sweeps). Asterisk, rejection of hypothesis that probabilities are the same at  $P < 0.01$  (Welch's  $t$ -test). Mean  $\pm$  s.e.m. calculated as described in Online Methods (**b,c**), mean  $\pm$  s.e.m. derived from counting statistics (**d-g,j,k**) and mean  $\pm$  s.e.m. (**h,i**).

$\text{CO}_2$  after orthogonal runs. The r.m.s. heading change (Figs. 3i and 4i) showed larger heading changes in turns after runs pointed toward lower ethyl acetate concentration or toward higher  $\text{CO}_2$  concentration.

During a turn, a larva sweeps its head to one side, after which it either starts a new run or initiates a new head sweep (Fig. 2 and Supplementary Video 6). To uncover bias in these detailed head sweeping movements, we analyzed the statistics of all head sweeps initiated by larvae after runs pointed orthogonal to ethyl acetate or  $\text{CO}_2$  gradients. In contrast to a recent report<sup>9</sup>, we found that the direction of the initial head sweep in each turn was unbiased by gradient direction (Figs. 3j and 4j). However, the larva more often initiated new runs during head sweeps that pointed in the favorable direction (Figs. 3k and 4k).

### Navigation in temporal gradients

The larva detects odors via the dorsal organ and  $\text{CO}_2$  via the terminal organ<sup>21</sup>. Because right and left dorsal and terminal organs are separated by only  $\sim 10 \mu\text{m}$ , the larva probably detects spatial gradients by making temporal comparisons during its movements rather than by directly comparing the activity of the two sensory organs. Indeed, larvae with unilateral olfactory function exhibited chemotaxis toward volatile attractants<sup>8</sup> nearly as well as larvae with bilateral olfactory function.

We used our system to determine whether patterns of behavior exhibited on spatial gas gradients could be driven with temporal

gradients of ethyl acetate or  $\text{CO}_2$  concentration that were spatially uniform along the  $x$  axis (Supplementary Fig. 2 and Fig. 1d). Triangular waveforms with linearly increasing and decreasing gas concentrations over time mimic the temporal stimulus experienced by a larva crawling in a straight line up or down a linear spatial gradient. When subjected to increasing concentration of  $\text{CO}_2$  over time, larvae reoriented more frequently, crawled more slowly and turned with larger angles (Fig. 5a) than when the concentration was decreasing, consistent with our observations of larvae on spatial gradients (Fig. 4c,d).

We also explored sensorimotor response to  $\text{CO}_2$  using step stimuli (Fig. 5b,c). We found that a small temporal step change (increase or decrease) in  $\text{CO}_2$  concentration produced a transient increase or decrease, respectively, in turning rate. Large steps in  $\text{CO}_2$  concentration were less adaptive, producing a sustained change in the turning rate. Very small concentration change (to 0.25%) did not affect turning rate but modulated crawling speed. Crawling speed was slow to adapt for small concentration changes and did not adapt at all for large concentration changes. The fact that turning rate adapted differently than crawling speed might indicate differences in the sensorimotor pathways between  $\text{CO}_2$  detection and the circuits that regulate crawling speed and turn initiation.

To verify lack of adaptation to changes in  $\text{CO}_2$ , we extended the step waveform period to 480 s and still saw no evidence for adaptation in response parameters (Fig. 5c). Mutants lacking the *Gr63a* sensor for  $\text{CO}_2$  modulated their behavior minimally in

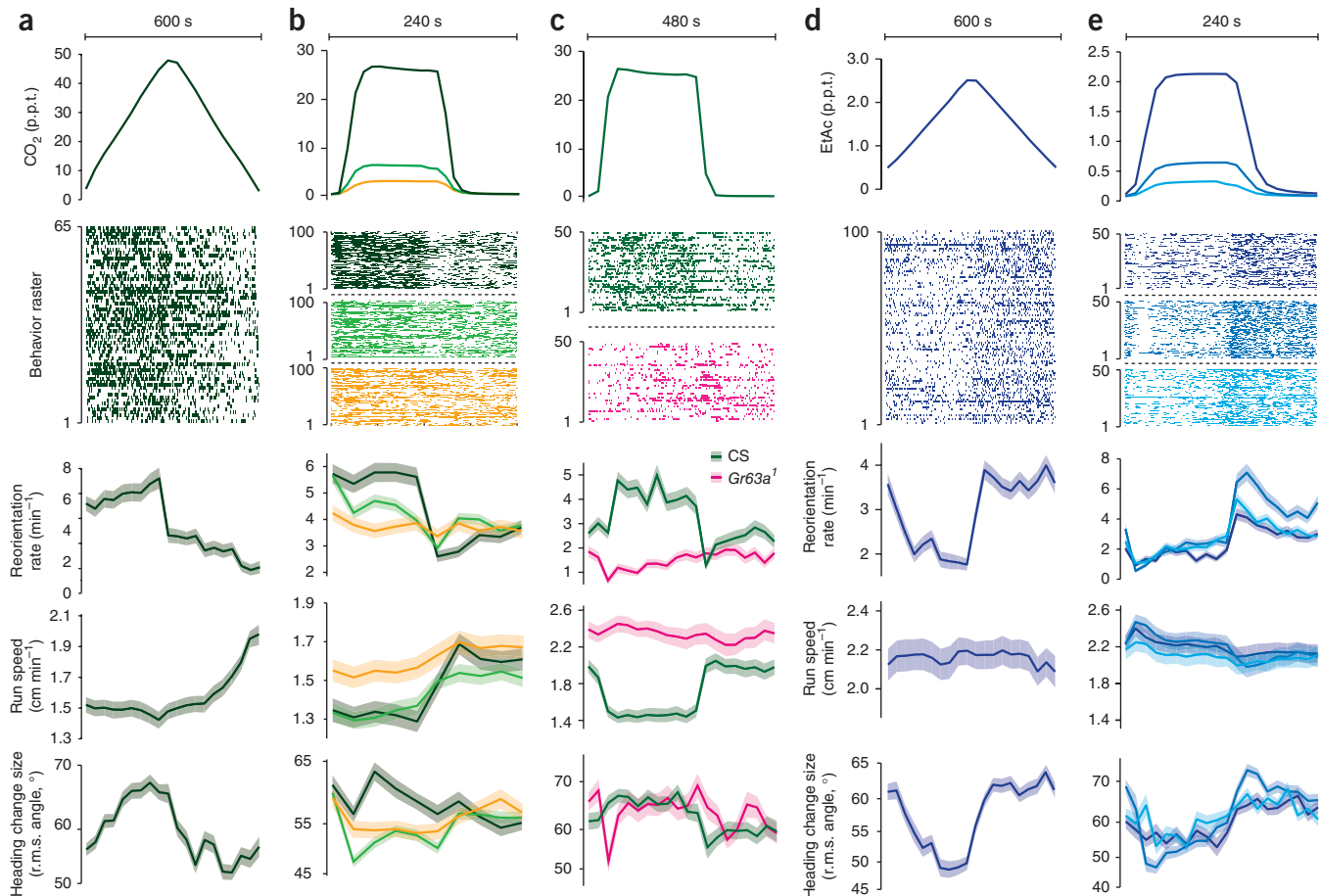


**Figure 5 |** Temporal  $\text{CO}_2$  and ethyl acetate gradients. **(a–e)** Statistics of turning decisions of larvae subjected to spatially uniform temporal gradients of  $\text{CO}_2$  delivered as repeating cycles of triangle waves **(a)** and steps **(b,c)** and of ethyl acetate delivered as triangle waves **(d)** and steps **(e)**. Top, one cycle of stimulus waveform. Raster plots, periods in which an individual larva was turning during the cycle; each row represents one larva tracked continuously through a cycle **(a, n = 65; b, n = 100 for each condition; c, n = 50 for each condition; d,e, n = 100 for each condition)**. Bottom, turning rate (mean  $\pm$  s.e.m.) derived from counting statistics, mean crawling speeds  $\pm$  s.e.m. calculated as described in Online Methods and root mean square heading change after turns  $\pm$  s.e.m. versus time within each cycle. Data from wild-type larvae (CS) are in **a,b,d,e**. Step response of wild-type larvae and  $\text{Gr}63\alpha^1$  mutant larvae are compared in **c**.

response to temporal changes in  $\text{CO}_2$  concentration (**Fig. 5c**). Thus,  $\text{CO}_2$ -evoked changes in turning behavior and crawling speed were due to active sensorimotor responses and not a metabolic consequence of higher  $\text{CO}_2$  concentration.

We examined larva behavior in temporal gradients of ethyl acetate. When larvae were subjected to a continuously increasing concentration of ethyl acetate over time, they reoriented less frequently and turned with smaller angles (**Fig. 5d**), consistent with their behavior on spatial gradients (**Fig. 3c,d**). Changes in crawling speed induced by linear ramps of ethyl acetate were not apparent (**Fig. 5d**). In contrast to the response to step changes in  $\text{CO}_2$  (**Fig. 5b,c**), the response to step changes in ethyl acetate was adaptive across a wide range of concentrations (**Fig. 5e**). A temporal step increase or decrease in ethyl acetate concentration produced, respectively, a transient decrease or increase in the rate of turn initiation, slightly higher or lower crawling speeds and a transient decrease or increase in the size of turns (**Fig. 5e**).

## DISCUSSION

Animals may sense the direction of a local gradient either directly, for example, by instantaneously comparing the activity of bilateral

sensory organs or by decoding temporal signals generated by moving their sensory organs through the gradient. Here we found evidence for the latter for both odor and  $\text{CO}_2$  gradients; larvae initiated turns more often when their forward movement caused an unfavorable change in concentration, and larvae based their turning decisions on the favorability of changes encountered during head sweeps, similar to our results in thermotaxis<sup>13</sup>. As in our studies of thermotaxis, we used time-varying spatially uniform signals to evoke behaviors observed in spatial gradients. We did not see signs of direct gradient measurement; specifically, larvae did not steer during runs and did not favor the preferred direction in the first head sweep of a turn.

In experiments involving odor and agar substrates, some odorant can be absorbed into the gel. Substantial odorant absorption into the substrate could affect stimulus presentation during temporal gradients, but as *D. melanogaster* larva responded consistently to abrupt changes in odor concentration over the course of our experiments, any effect of odorant absorption was modest. Our ability to present rapid changes in odor concentration was slightly compromised by the design of the reservoirs in the apparatus, but the 10–90% rise time for a step change (20.8 s) was smaller

than the bin sizes in **Figure 5 (Supplementary Note 3)**. The rise time can be decreased by redesigning the reservoirs or increasing the flow rate. In experiments in which we suddenly reversed the direction of the gradient (data not shown), larvae followed the new gradient direction rather than the old, also indicating that odorant absorption does not confound airborne navigation.

In navigation experiments, asymmetry with respect to the arena boundary can confound the results. For example, without stimulus, larvae placed at the left edge of a plate will show a navigational bias to the right because they are physically constrained from moving left. For this reason, we began each experiment with the larvae placed roughly in the center of the arena. Otherwise, as the spatial odor gradient in our apparatus is linear in the *x* direction, constant in the *y* direction and steady in time, experiments in our apparatus are less sensitive to initial placement of the larvae than droplet-based assays.

Our apparatus flexibly and accurately provided airborne stimulants to freely moving larva. Using this apparatus and machine-vision analysis that is sensitive to time-varying position and posture of each larva, we analyzed the algorithmic structure of navigational behavior with precision. We determined the navigational strategies of larvae in response to ethyl acetate and CO<sub>2</sub>, showed internal consistency between their behavioral response to spatial gradients and temporal gradients, and uncovered a nonadaptive response for temporal changes in CO<sub>2</sub>. The marked similarities between the algorithmic structure of navigational strategies during chemotaxis and thermotaxis suggest that homologous sensorimotor circuits might be used to encode larval navigation in response to diverse sensory inputs<sup>15</sup>.

## METHODS

Methods and any associated references are available in the online version of the paper at <http://www.nature.com/naturemethods/>.

*Note: Supplementary information is available on the Nature Methods website.*

## ACKNOWLEDGMENTS

We thank E. Soucy and J. Greenwood for engineering advice and suggestions. This work was supported by a US National Institutes of Health (NIH) Pioneer award to A.D.T.S., NIH grants to J.R.C. and an NIH National Research Service award to E.A.K.

## AUTHOR CONTRIBUTIONS

M.G. designed and constructed the linear and dynamic gaseous gradient apparatus, designed and wrote MAGAT analyzer software, designed and carried out experiments, analyzed all data and assembled figures. M.B. designed and carried out experiments. D.M. and L.L. designed and carried out preliminary experiments. E.A.K. designed experiments. J.R.C. and A.D.T.S. supervised the project and designed experiments. M.G., E.A.K. and A.D.T.S. wrote the manuscript.

## COMPETING FINANCIAL INTERESTS

The authors declare no competing financial interests.

Published online at <http://www.nature.com/naturemethods/>. Reprints and permissions information is available online at <http://www.nature.com/reprints/index.html>.

1. Brody, C.D. & Hopfield, J.J. Simple networks for spike-timing-based computation, with application to olfactory processing. *Neuron* **37**, 843–852 (2003).
2. Cleland, T.A. & Linster, C. Computation in the olfactory system. *Chem. Senses* **30**, 801–813 (2005).
3. Hopfield, J.J. Olfactory computation and object perception. *Proc. Natl. Acad. Sci. USA* **88**, 6462–6466 (1991).
4. Chalasani, S.H. et al. Dissecting a circuit for olfactory behaviour in *Caenorhabditis elegans*. *Nature* **450**, 63–70 (2007).
5. Masse, N.Y., Turner, G.C. & Jefferis, G.S. Olfactory information processing in *Drosophila*. *Curr. Biol.* **19**, R700–R713 (2009).
6. Bargmann, C.I., Hartwig, E. & Horvitz, H.R. Odorant-selective genes and neurons mediate olfaction in *C. elegans*. *Cell* **74**, 515–527 (1993).
7. Kreher, S.A., Mathew, D., Kim, J. & Carlson, J.R. Translation of sensory input into behavioral output via an olfactory system. *Neuron* **59**, 110–124 (2008).
8. Louis, M., Huber, T., Benton, R., Sakmar, T.P. & Vosshall, L.B. Bilateral olfactory sensory input enhances chemotaxis behavior. *Nat. Neurosci.* **11**, 187–199 (2008).
9. Gomez-Marin, A., Stephens, G.J. & Louis, M. Active sampling and decision making in *Drosophila* chemotaxis. *Nat. Commun.* **2**, 441 (2011).
10. Chronis, N., Zimmer, M. & Bargmann, C.I. Microfluidics for *in vivo* imaging of neuronal and behavioral activity in *Caenorhabditis elegans*. *Nat. Methods* **4**, 727–731 (2007).
11. Lockery, S.R. et al. Artificial dirt: microfluidic substrates for nematode neurobiology and behavior. *J. Neurophysiol.* **99**, 3136–3143 (2008).
12. Albrecht, D.R. & Bargmann, C.I. High-content behavioral analysis of *Caenorhabditis elegans* in precise spatiotemporal chemical environments. *Nat. Methods* **8**, 599–605 (2011).
13. Jones, W.D., Cayirlioglu, P., Kadow, I.G. & Vosshall, L.B. Two chemosensory receptors together mediate carbon dioxide detection in *Drosophila*. *Nature* **445**, 86–90 (2007).
14. Cayirlioglu, P. et al. Hybrid neurons in a microRNA mutant are putative evolutionary intermediates in insect CO<sub>2</sub> sensory systems. *Science* **319**, 1256–1260 (2008).
15. Luo, L. et al. Navigational decision making in *Drosophila* thermotaxis. *J. Neurosci.* **30**, 4261–4272 (2010).
16. Larsson, M.C. et al. Or83b encodes a broadly expressed odorant receptor essential for *Drosophila* olfaction. *Neuron* **43**, 703–714 (2004).
17. Vosshall, L.B. & Hansson, B.S. A unified nomenclature system for the insect olfactory coreceptor. *Chem. Senses* **36**, 497–498. (2011).
18. Faucher, C., Forstreuter, M., Hilker, M. & de Bruyne, M. Behavioral responses of *Drosophila* to biogenic levels of carbon dioxide depend on life-stage, sex and olfactory context. *J. Exp. Biol.* **209**, 2739–2748 (2006).
19. Kwon, J.Y., Dahanukar, A., Weiss, L.A. & Carlson, J.R. The molecular basis of CO<sub>2</sub> reception in *Drosophila*. *Proc. Natl. Acad. Sci. USA* **104**, 3574–3578 (2007).
20. Berg, H.C. & Brown, D.A. Chemotaxis in *Escherichia coli* analysed by three-dimensional tracking. *Nature* **239**, 500–504 (1972).
21. Vosshall, L.B. & Stocker, R.F. Molecular architecture of smell and taste in *Drosophila*. *Annu. Rev. Neurosci.* **30**, 505–533 (2007).

## ONLINE METHODS

**Strains.** Wild-type larvae were Canton-S (CS). *Gr63a*<sup>1</sup> (Bloomington stock 9941) and *Orco*<sup>1</sup> (Bloomington stock 23129) flies were obtained from the Bloomington stock center. *Orco* represents the new gene name for *Or83b*<sup>17</sup>. All behavioral experiments were done on second instar larvae. Adult flies were allowed to lay eggs on grape-juice agar growth plates with yeast for 3 h. After egg laying, plates were kept at 22 °C on a 12 h day-night cycle. Experiments were carried out at 22 °C during the day cycle or early hours of the night cycle. Time since egg laying was used to roughly stage larvae, and actual stage was verified by examining spiracle morphology.

**Odor gradient apparatus.** The odor gradient apparatus (**Fig. 1a**) comprises a controlled clean air source, an odor source, an array of microcontroller-activated valves, a mixing flow block and a laminar flow chamber. Compressed air was regulated to 140 kPa and cleaned with a charcoal filter (Agilent HT200-4) before delivery to a computer-controllable mass-flow controller (MFC; Aalborg GFC 17). A second MFC was used to inject airborne chemical stimulants into the laminar airflow. For ethyl acetate experiments, the second MFC injected air into a bubbler made up of a 250-ml glass bottle with a stainless steel cap and frit, containing ethyl acetate (Mallinckrodt) either pure or diluted in deionized water. This generated an odorized air stream with the concentration of ethyl acetate in the air determined by the concentration of ethyl acetate in the bubbler. The water-ethyl acetate mixture does not obey Raoult's Law, so the ethyl acetate vapor pressure of the mixture was measured directly using a photoionization detector (PID; Baseline-Mocon Pidtech Plus). For CO<sub>2</sub> experiments, pure CO<sub>2</sub> was metered using an MFC calibrated for CO<sub>2</sub>.

The carrier air was injected into the rear of the mixing flow block. For temporally varying, spatially uniform stimuli (**Fig. 1d** and **Supplementary Fig. 2**), the outlet of the odor source was connected to the inlet of the mixing block at the same location as the carrier air. The total amount of odor in the chamber was set by adjusting the flow rate of odor while holding the carrier flow rate constant (generally 2 l min<sup>-1</sup>). The odor concentration was monitored during each experiment at the inlet using either a PID or a nondispersive infrared CO<sub>2</sub> sensor (<http://www.co2meter.com/>, GSS C20).

For spatially varying, temporally uniform stimuli (**Fig. 1b,c**), the outlet of the odor source was connected to the inlet of the valve manifold. Compact solenoid valves (Lee, LHDA1221111H) were used to meter odor through a section of teflon tubing into each flow tube in the mixing block. The valves were controlled by a custom circuit board based on SpokePOV (Adafruit Industries) and were programmed to open for linearly increasing amounts of time over a period of ~1.5 s (**Supplementary Software 2**). The valves were operated in a pattern that kept exactly half open at any time, presenting a constant impedance to the MFC (**Supplementary Fig. 3**). The minimum continuous time a valve was opened or closed was therefore ~50 ms, whereas the valve switching time was 3 ms. The mean concentration of the gradient was set by varying the ratio of odor flow to carrier air flow and was monitored at the outlet of the flow chamber by the appropriate gas sensor.

Diffusion smooths odor profiles generated by the valves. Between the outlet of the mixing block and the start of the experimental arena, diffusion smooths the profile with a length scale

of 1.2 cm for ethyl acetate and 1.7 cm for CO<sub>2</sub>. By the far edge of the experimental arena, the smoothing length scale is 1.8 cm and 2.5 cm for ethyl acetate and CO<sub>2</sub>, respectively. Thus, spatial irregularities owing to the discrete injection points are relaxed by the time the laminar airflow enters the arena, but the gradient itself is not dissipated before the airflow exits the arena.

The laminar airflow containing spatial or temporal gradients of ethyl acetate or CO<sub>2</sub> passed through an experimental arena made from a solid piece of black anodized aluminum. A glass lid provided a viewing window for observing behavior. A hinged, pneumatic compressor was used to press the glass ring against an O-ring, creating a reliable seal. The integrity of all O-ring seals (at the inlet, outlet and glass lid) was continuously verified by monitoring the airflow rate at the outlet.

Video microscopy of larvae within the experimental arena was done using dark-field illumination with red LEDs (624 nm, outside the range of larval phototaxis) that were mounted at the perimeter of the experimental arena. Video was recorded at 5 frames s<sup>-1</sup> using a 5-megapixel USB camera (Mightex BCE-B050-U) and an 18-mm focal-length C-mount lens (Edmund Optics NT54-857). Each pixel in the captured images corresponded to a 0.063 mm × 0.063 mm square of the experimental arena.

**Behavior experiments.** Before each experiment, larvae were staged, washed in phosphate-buffered saline and placed on 10-cm Petri dish containing clean 1% (wt/vol) Bacto agar medium for at least 5 min to allow the larvae to adapt to the medium used in the experiments and shed any residual odorous contaminants. After each behavioral experiment, all larvae were discarded.

The substrate for the behavioral experiments was a ~4-mm-thick Bacto agar gel (1% wt/vol) on top of square, flat, black, anodized aluminum plates (24 cm × 24 cm). Each plate with the gel on top could be placed in the experimental arena, providing a large uniform substrate for the larvae to navigate without edges to impede or distort airflow. Larvae were transferred from 10-cm Petri dishes to experimental arena using a paintbrush, the chamber was pneumatically sealed and the entire apparatus was enclosed in a light-tight box. After the chamber was pneumatically sealed, it took ~30 s for the laminar airflow to fully purge the chamber and establish a defined spatial gradient. We discarded the first 2 min of recorded behavior during analysis. We recorded behavior for 25–30 min per experiment; for experiments involving spatial gradients, we analyzed the first 15 min (after the discarded 2 min), after which larvae started nearing the edges of the gradients.

**Behavioral analysis.** The MAGAT analyzer software package is available as **Supplementary Software 1** or the latest version, with example video recordings, is available at <https://github.com/samuellab/MAGATAnalyzer>.

Larval positions and postures were extracted from video records using custom machine vision software written in C++ and based on OpenCV, an open-source computer vision software suite. With similar features to software that has been written to automatically follow *C. elegans* behavior<sup>22–25</sup>, our software tracks each larva throughout the arena and records an image of the larva, the position of center of mass, the outline of the body, the position of the head and tail and a midline running down the center of the larva (**Fig. 2a** and **Supplementary Fig. 1** and **Supplementary Note 3**). Using data analysis software written in MATLAB (MathWorks),

we analyzed navigational statistics such as path curvature, speed, heading and angle of head relative to body (**Fig. 2b**). These were used to segment trajectories into an alternating sequence of runs and turns.

To calculate statistics involving center-of-mass movement along larval trajectories (for example, distributions of instantaneous heading and speed in **Figs. 3b,c** and **4b,c** and navigational indices in **Fig. 2d**) we needed to estimate the number of independent observations of quantities of center-of-mass movement along each larval trajectory. To do this, we calculated the autocorrelation function of the direction of motion,

$$C(\tau) = \langle \hat{v}(t) \cdot \hat{v}(t + \tau) \rangle_t \quad (2)$$

and extracted the time constant,  $T$ , of its component of exponential decay,

$$C(\tau) \approx e^{-\tau/T} \quad (3)$$

This correlation time constant was typically  $\sim 20$  s. To calculate the s.e.m. of center-of-mass motion statistics, we estimated the number of independent observations as the total observation time for each measurement divided by twice the correlation time constant<sup>23</sup>.

To calculate statistics of decision making along trajectories, trajectories were segmented into a sequence of alternating runs and turns. Runs (**Supplementary Video 4**) were defined as continuous periods of forward movement with head direction aligned with direction of forward travel (**Fig. 2b**). A hysteretic threshold for run speed was determined on an individual *D. melanogaster* larva basis by examining the speed near points of high curvature in the path; the speed to begin a run was higher than the speed to end one. The head was considered aligned with the direction of forward motion if the angle between the mid-head vector and the heading was  $<37^\circ$ . Turns separated successive runs. The initiation of each head sweep (**Supplementary Video 6**) during a turn was flagged when the body bend angle between the anterior and posterior of the *D. melanogaster* larva was  $>20^\circ$  (**Fig. 2b**). Each head sweep ended when the body bend angle was  $<10^\circ$  or changed sign (head swept to other side of body) or when a new run began. Each turn ended at the start of a new run. Thus, each turn could involve zero or more head sweeps. Turns with zero head sweeps (pauses) were excluded from the statistics of reorientation after turns. Rare head sweeps in which the body bend angle was so extreme that the head touched the tail created difficulty during feature extraction because the tracker could no longer effectively distinguish head from tail. These head sweeps were also excluded from statistical analysis.

Video records of each larva along its trajectory could be played back, overlaid by extracted contour, head and tail locations, and path with annotations noting runs, turns and head sweeps (**Supplementary Videos 2 and 3**). A subset of these videos was examined visually to verify the performance of automated segmentation and analysis of larval trajectories.

**Statistical model for heading change distributions after turns.** To describe the distribution of heading changes after turns, we developed a statistical model to represent our observation that heading changes,  $\Delta\theta$ , are biased in size and direction by head sweeping movements and contingent on the initial heading on spatial gradients before each turn,  $\theta_i$ . In this model, the magnitude of heading change is drawn from skew-normal distributions whose mean and skewness depend on  $\theta_i$ , thereby allowing the size of turns to depend on initial heading on spatial gradients as observed. The direction of heading change (to the left ( $\Delta\theta > 0$ ) or right ( $\Delta\theta < 0$ )) is determined by a biased coin-flip distribution whose mean depends on  $\theta_i$ , thus biasing the likelihood of initiating new runs to the left or right

$$\begin{aligned} P(\Delta\theta|\theta_i) = & \left( \frac{1}{2} - A \sin(\theta_i - \theta_0) \right) \times SN(\Delta\theta, \mu - B \cos(\theta_i - \theta_0), \\ & \sigma, \alpha - C \cos(\theta_i - \theta_0)) + \left( \frac{1}{2} + A \sin(\theta_i - \theta_0) \right) \\ & \times SN(-\Delta\theta, \mu - B \cos(\theta_i - \theta_0), \sigma, \alpha - C \cos(\theta_i - \theta_0)) \end{aligned} \quad (4)$$

where

$$SN(x, \mu, \sigma, \alpha) = \frac{e^{-\frac{(x-\mu)^2}{2\sigma^2}}}{\sigma\sqrt{2\pi}} \operatorname{Erfc}\left(\frac{-\alpha(x-\mu)}{\sigma\sqrt{2}}\right) \quad (5)$$

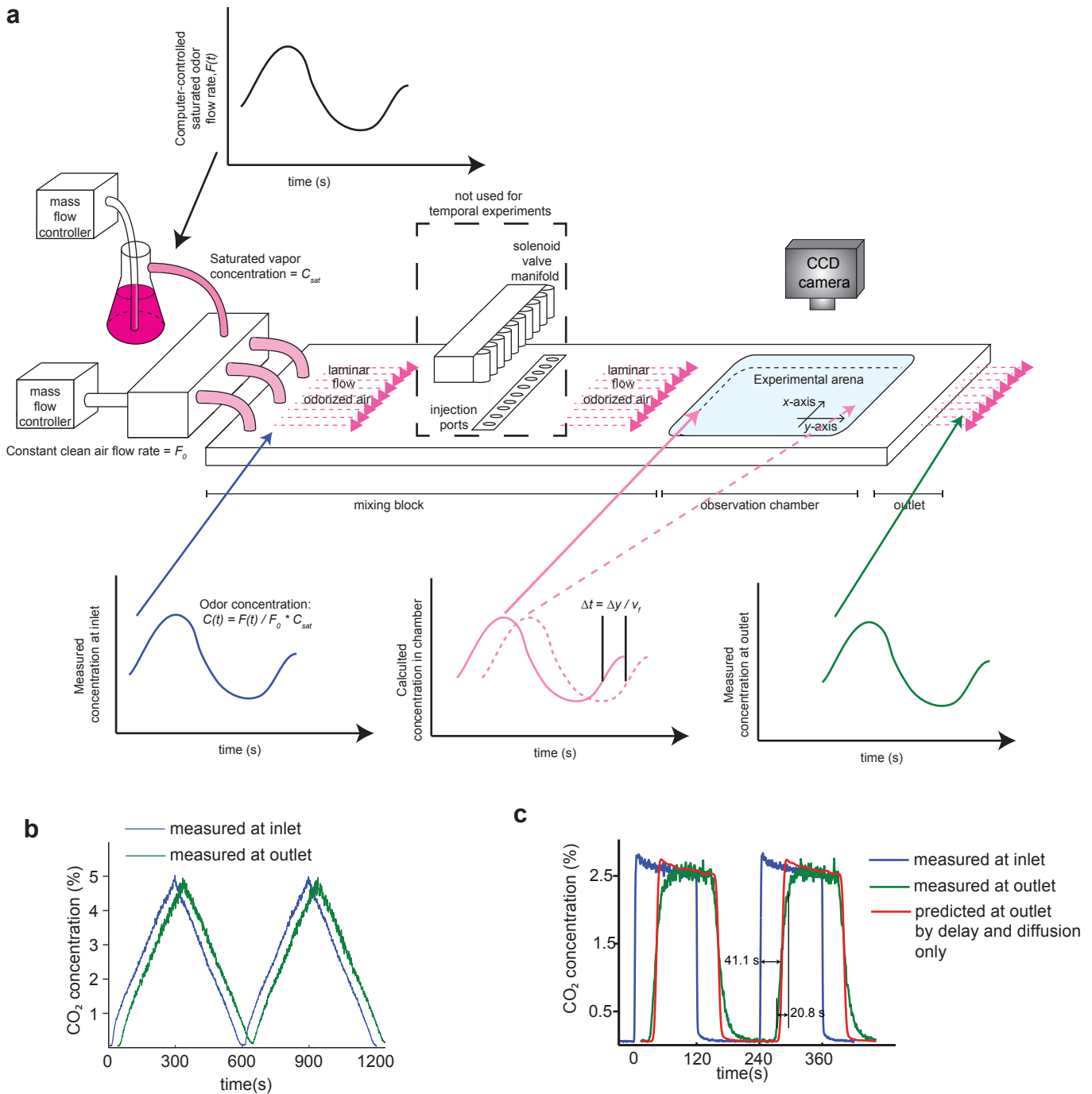
We adjusted the parameters of the model ( $A, B, C, \mu, \sigma, \alpha$  and  $\theta_0$ ) to maximize the likelihood of the observed initial heading-heading change pairs. The solid lines overlaying the histograms in **Figures 3h** and **4h** and dashed lines overlaying the plots of heading change magnitude and direction in **Figures 3e,f** and **4e,f** represent predictions of the model fit (equations (4) and (5)) to the experimental data.

For both ethyl acetate and  $\text{CO}_2$ , we assessed the statistical model represented by equations (4) and (5) by also calculating the maximum likelihood of observed data given null models that eliminated certain features from the full statistical model by setting one or more parameters to zero. We computed the logarithm of the ratios of maximum likelihood for the null model and full statistical model. These results are summarized in **Supplementary Table 2**. All null models could be rejected in favor of the full statistical model at  $P < 0.01$ .

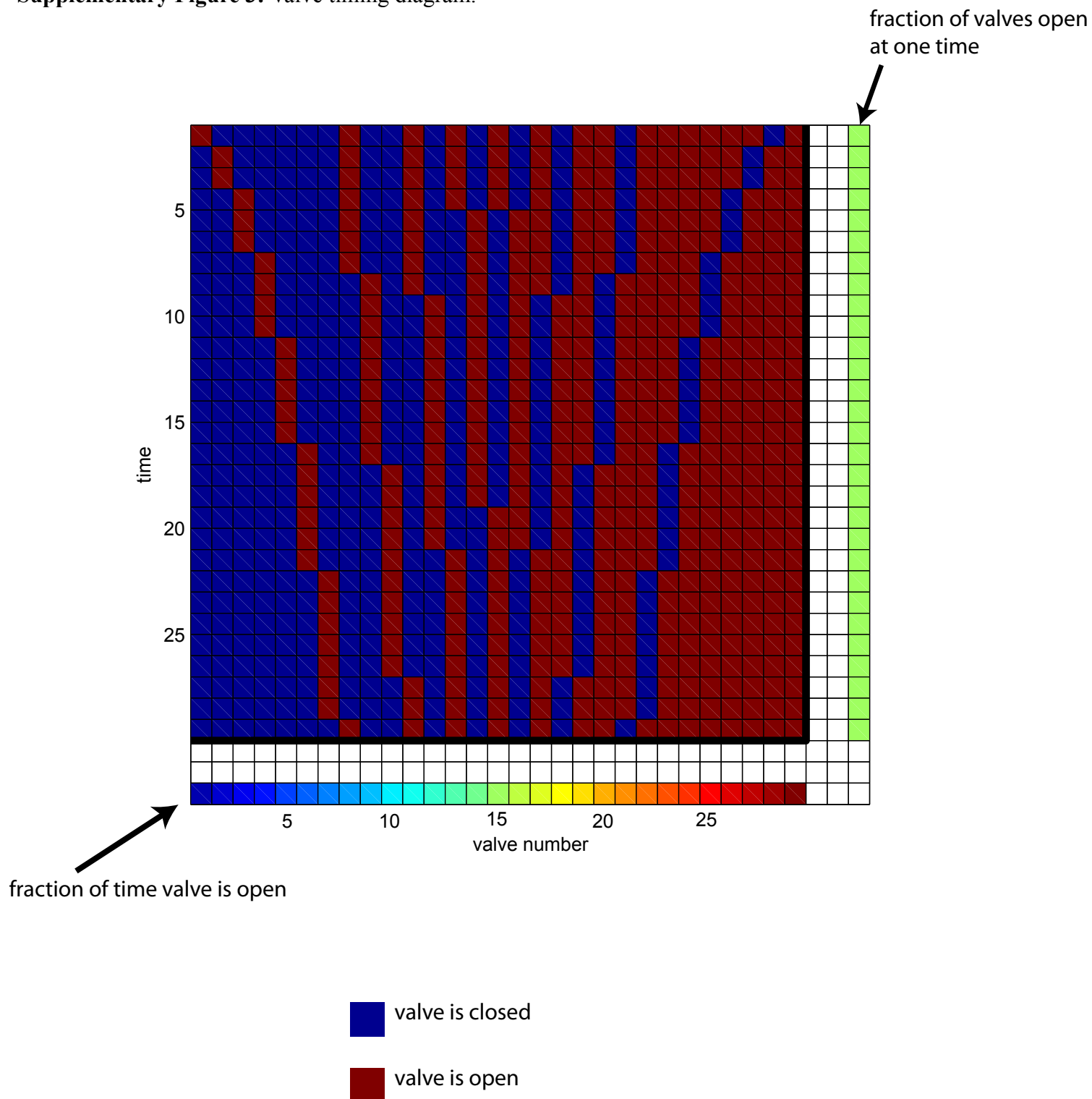
- 22. Baek, J.H., Cosman, P., Feng, Z., Silver, J. & Schafer, W.R. Using machine vision to analyze and classify *Caenorhabditis elegans* behavioral phenotypes quantitatively. *J. Neurosci. Methods* **118**, 9–21 (2002).
- 23. Cronin, C.J., Feng, Z. & Schafer, W.R. Automated imaging of *C. elegans* behavior. *Methods Mol. Biol.* **351**, 241–251 (2006).
- 24. Swierczek, N.A., Giles, A.C., Rankin, C.H. & Kerr, R.A. High-throughput behavioral analysis in *C. elegans*. *Nat. Methods* **8**, 592–598 (2011).
- 25. Ramot, D., Johnson, B.E., Berry, T.L.J., Carnell, L. & Goodman, M.B. The Parallel Worm Tracker: a platform for measuring average speed and drug-induced paralysis in nematodes. *PLoS ONE* **3**, e2208 (2008).

## Supplementary Figure 2: Temporal Gradients

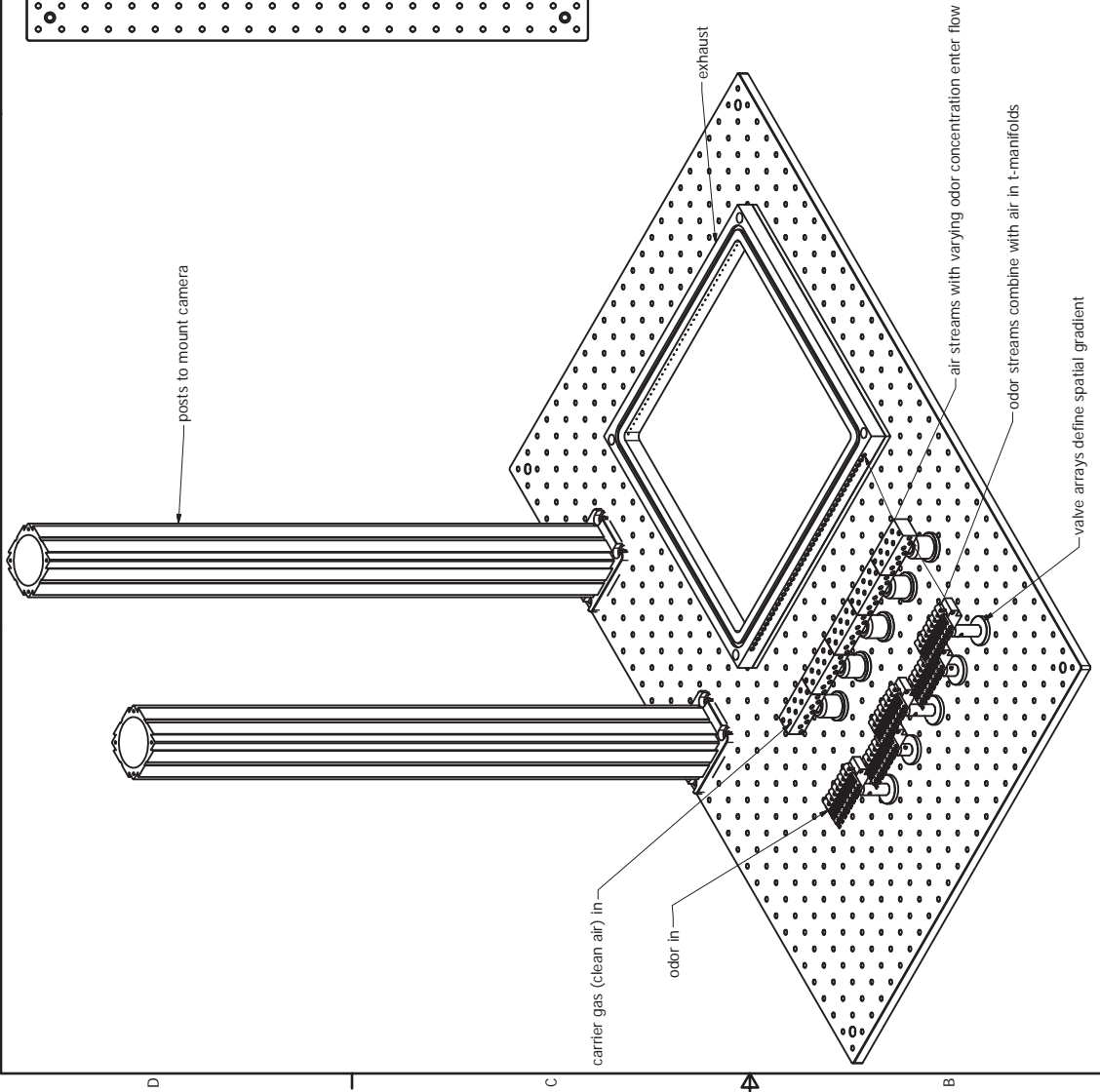
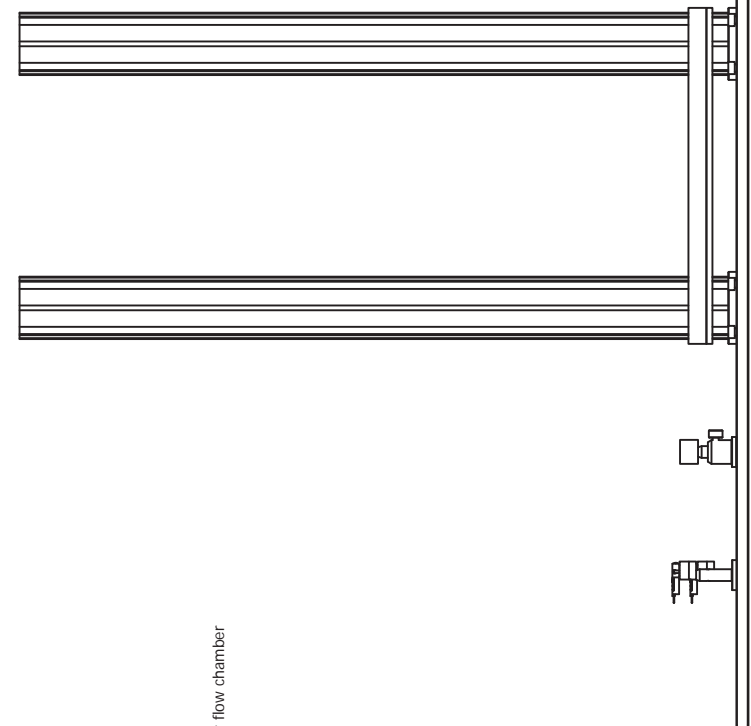
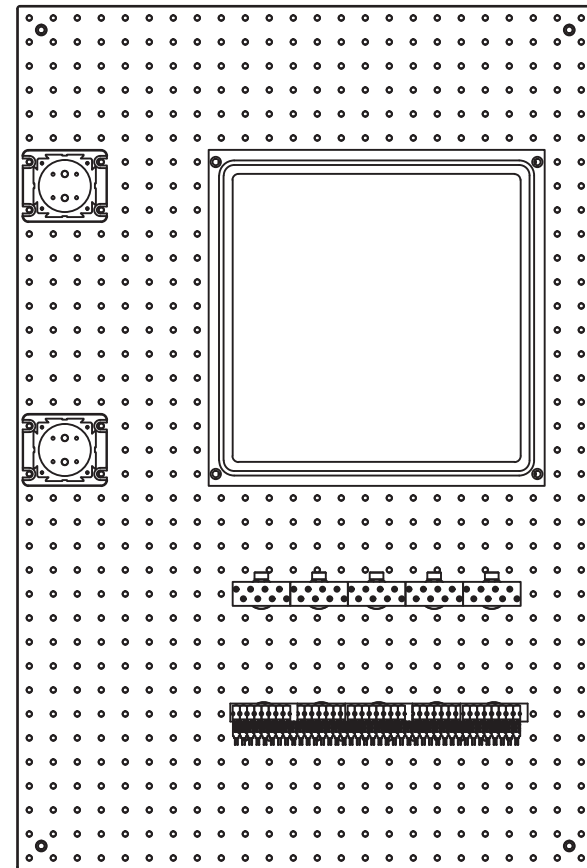
Pg 10



**Supplementary Figure 2: Temporal Gradients.** (a) Schematic of setup for temporal gradient experiments. The valve array is bypassed. Odor/gas is combined with clean air prior to the device inlet. Gas concentration is manipulated by setting the flow rate of odor/gas relative to the flow rate of clean air. The concentration in the chamber is constant in the x-direction and varies in the y-direction as the temporal waveform flows across the chamber. The concentration at any point in the chamber can be calculated using the measured inlet concentration, the y-position and the gas flow rate ( $v_f$ ). (b) Carbon dioxide concentration during triangle wave (same conditions as Figure 5a, reproduced from Figure 1). (c) Carbon dioxide concentration measured during square wave (same conditions as Figure 5b). 2 complete periods are shown. Blue line – concentration measured immediately upstream of the mixing block inlet . Green line – concentration measured immediately downstream of flow chamber outlet; Orange line – expected measurement at outlet taking into account diffusion and flow time from inlet to outlet. The time delay (41.1 s) agrees with the prediction obtained by dividing the chamber volume by the gas flow rate. The rise time (20.8 s) is longer than that predicted by diffusion.

**Supplementary Figure 3:** Valve timing diagram.

**Supplementary Figure 3:** Valve timing diagram. Time in the cycle progresses vertically from top to bottom, valve number increments horizontally from left to right. Blue squares indicate the valve is closed at a particular time in the cycle, red squares that the valve is open.

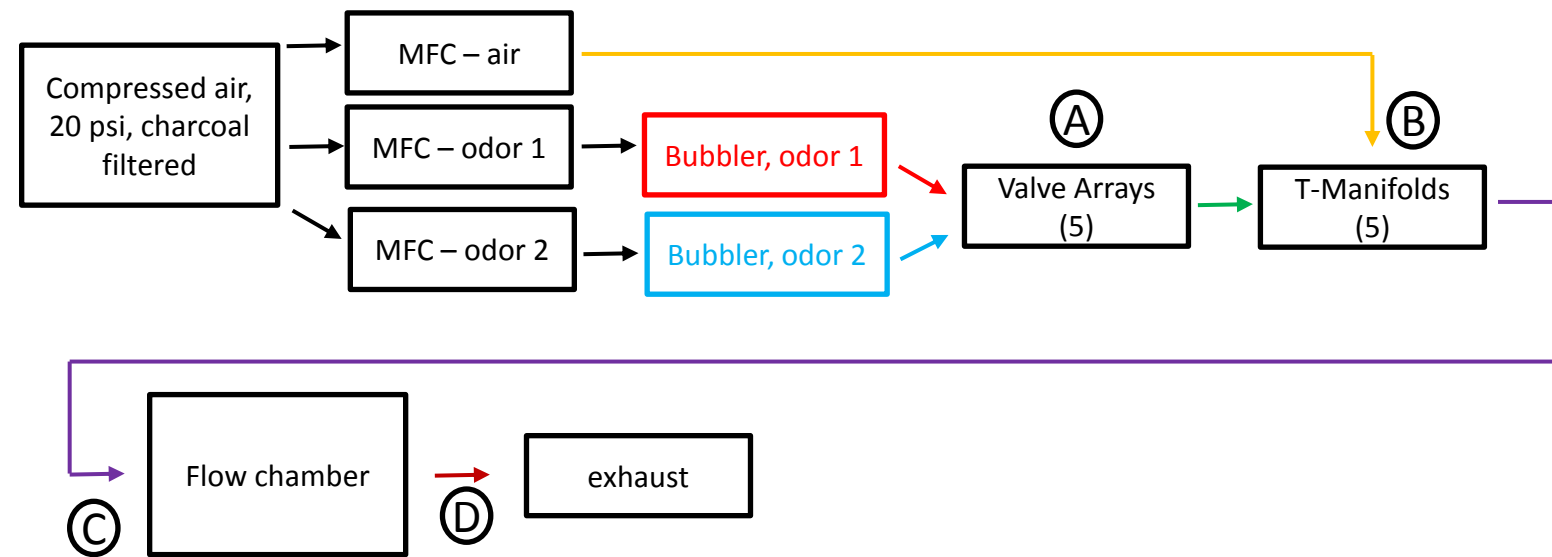


not pictured:  
tubing fittings, and manifolds to source odor & air and connect components  
gas handling (air source, regulator, exhaust, flow meter)  
Mass Flow Controllers, bubbler  
pneumatic hinge and lip plate to seal flow chamber  
electronics (valve controller, lights)  
camera, lenses, filters, channelmodispin stimulating light source

## LADY GAGA V2 Basic flow scheme

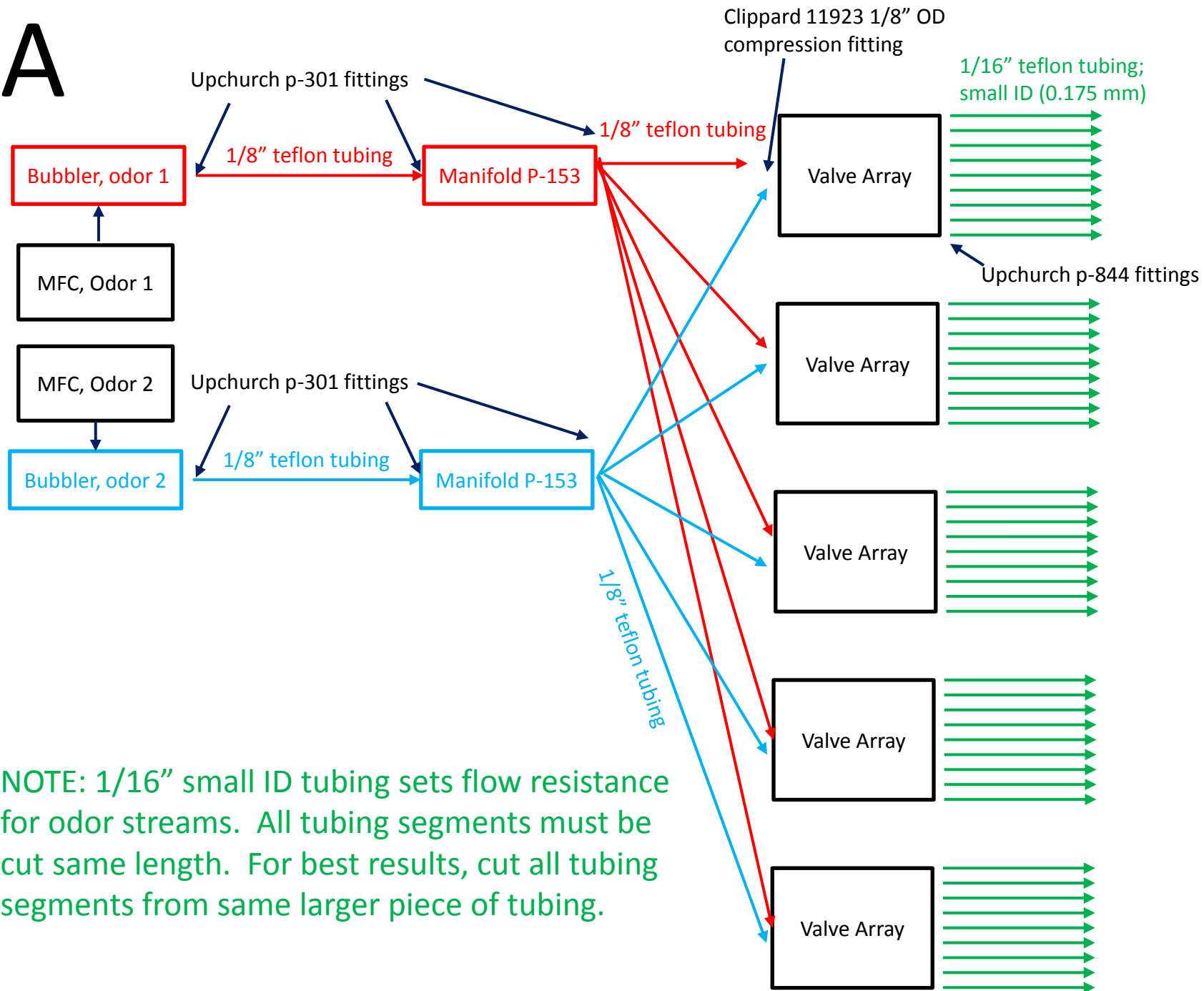
arrow indicates air flows between components in indicated direction.

Letters indicate details follow on subsequent pages.



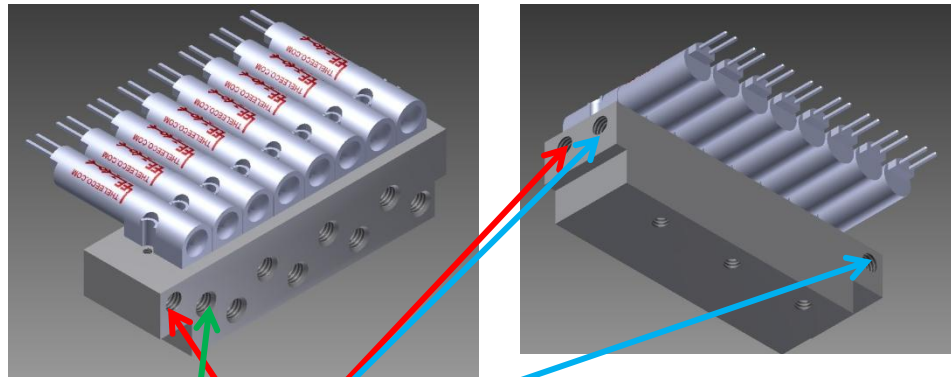
Note: all clippard fittings require that the buna-n gasket (default) be replaced by epdm

A



# A

## Manifold with valves

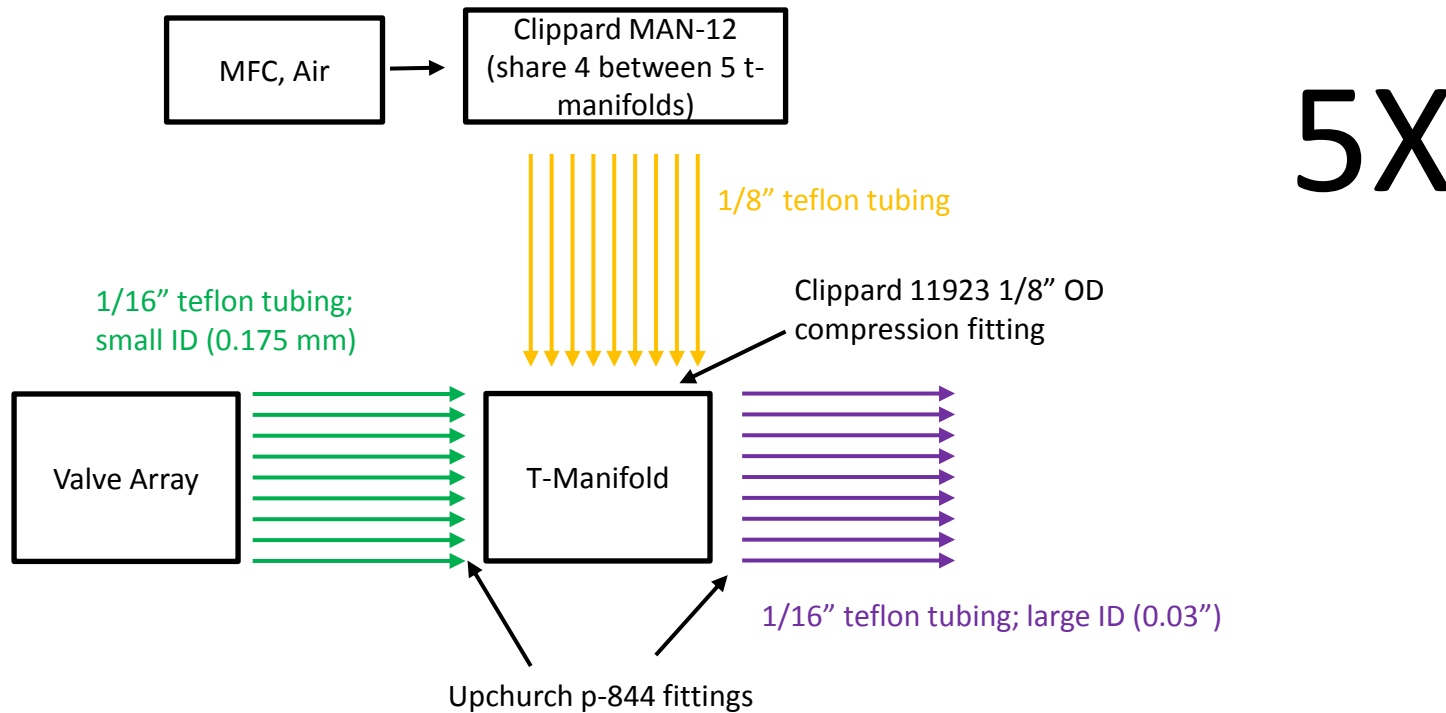


**Odor 1 (NO) inlet, Odor 2 (NC) inlet:** connect with clippard 10-32 to 1/8" compression fitting and 1/8" OD teflon tubing or seal with clippard 10-32 plug

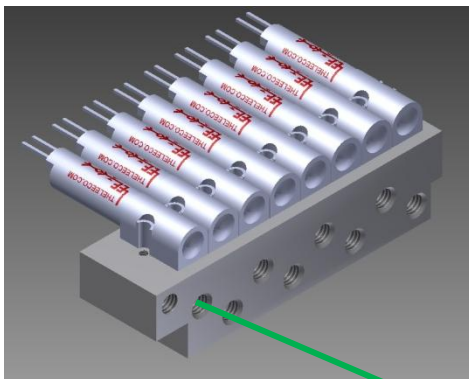
**Valve common (outlet), 8X:** connect with upchurch 10-32 flat bottom vacutight fitting to 1/16" OD, 175 um ID

To distribute odor to 5 valve manifolds, use upchurch p-153, 6-port manifold for 1/8" OD tubing

B



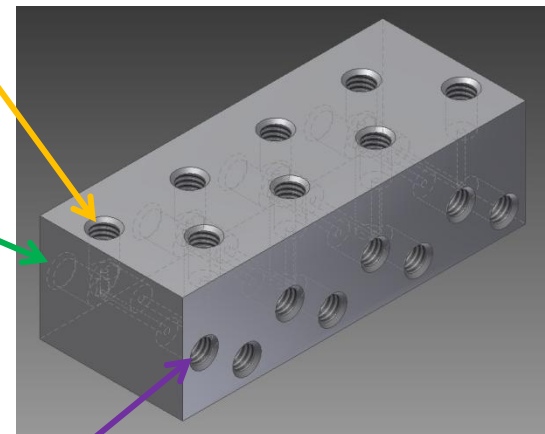
NOTE: 1/16" large ID tubing sets flow resistance for air streams. All tubing segments must be cut same length. For best results, cut all tubing segments from same larger piece of tubing.



**Odor flows** from valve manifold to t-manifold through 1/16" OD 175 um ID teflon tubing (connect at both ends with 10-32 vacutight fittings) (8x)

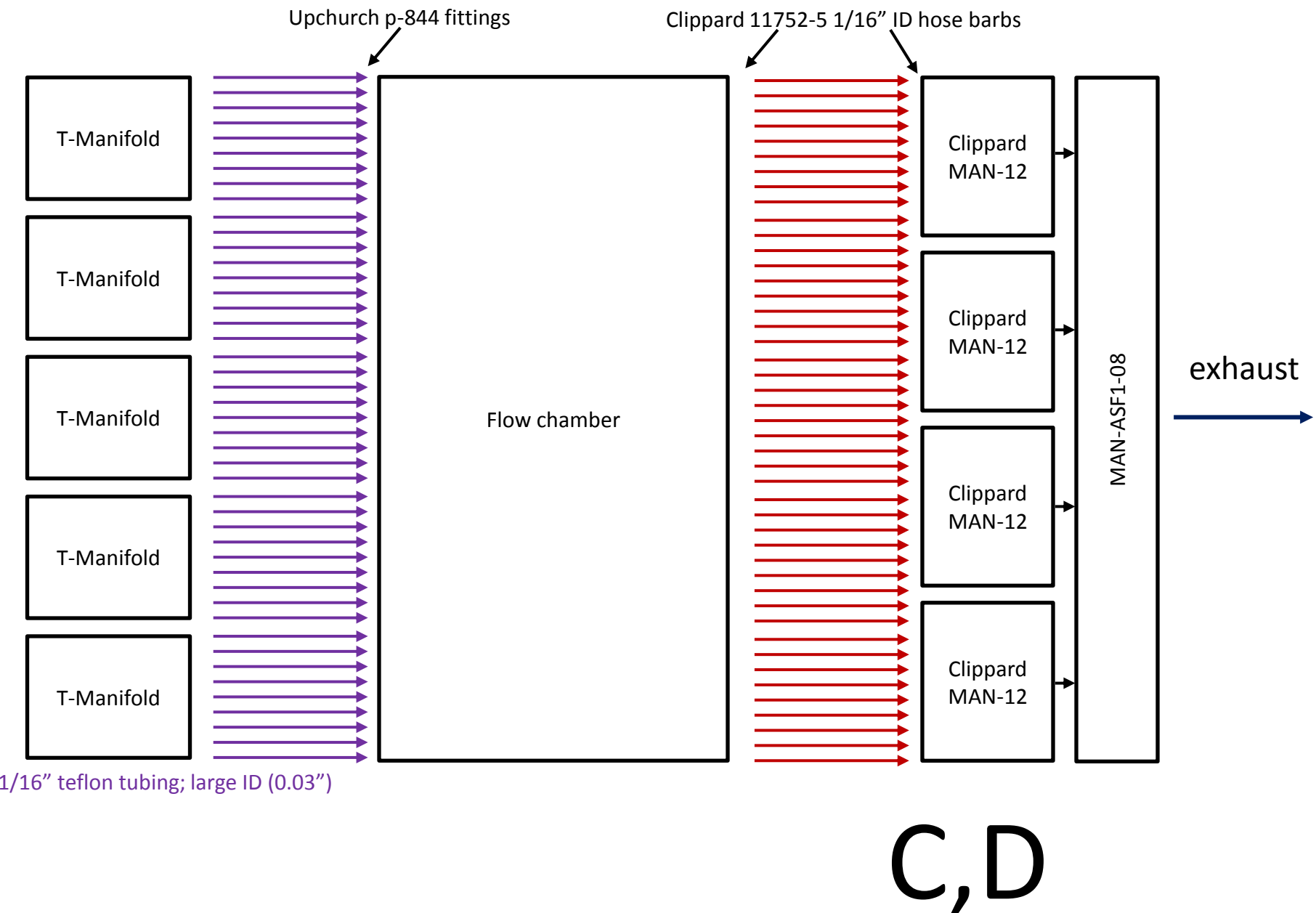
**Air inlet 8x.** Connect with 10-32 clippard compression fittings to 1/8" OD teflon tubing.

**B**



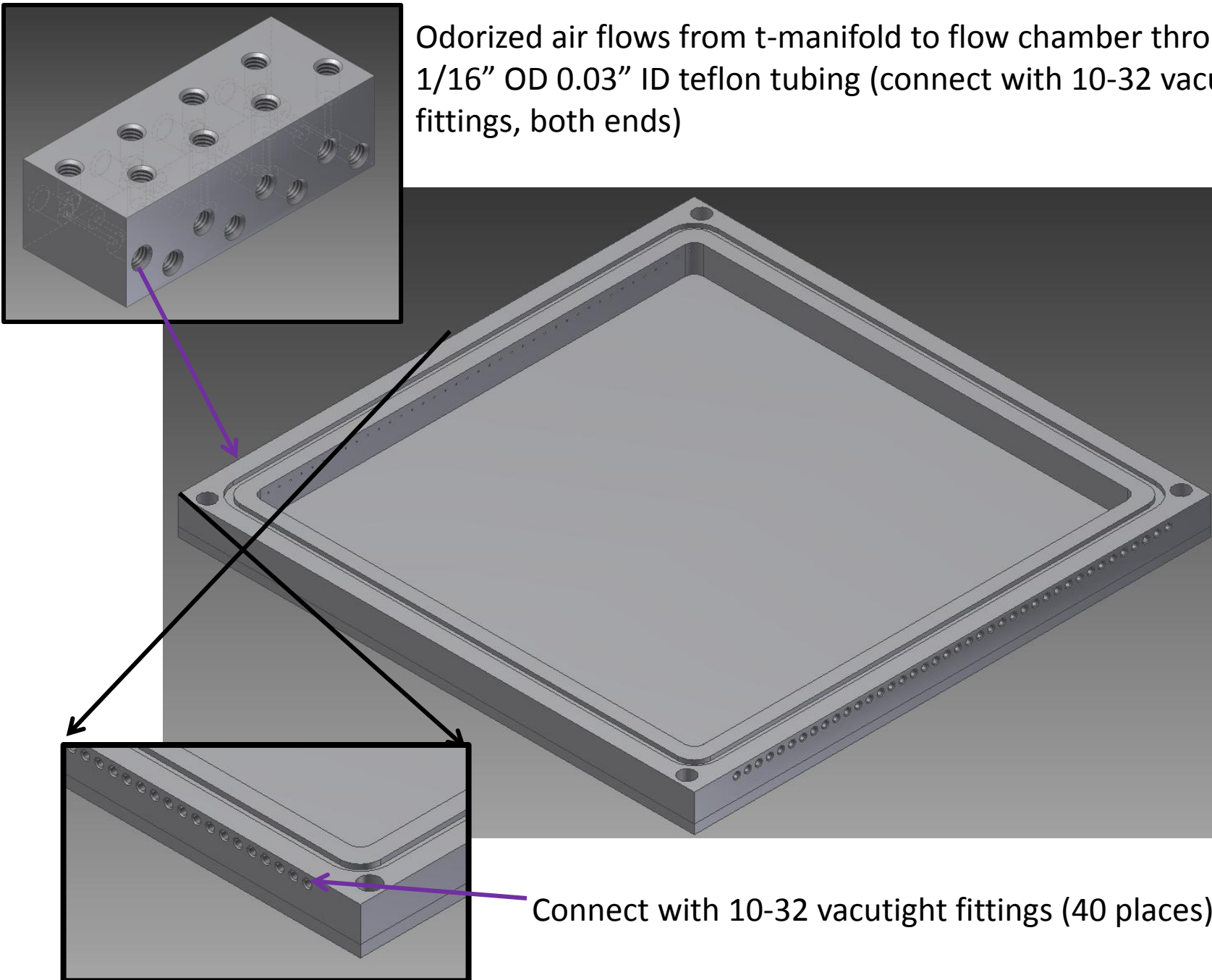
**Combined air and odor outlet, 8x.** Connect with 10-32 vacutight fittings and 1/16" OD, 0.03" ID teflon tubing.

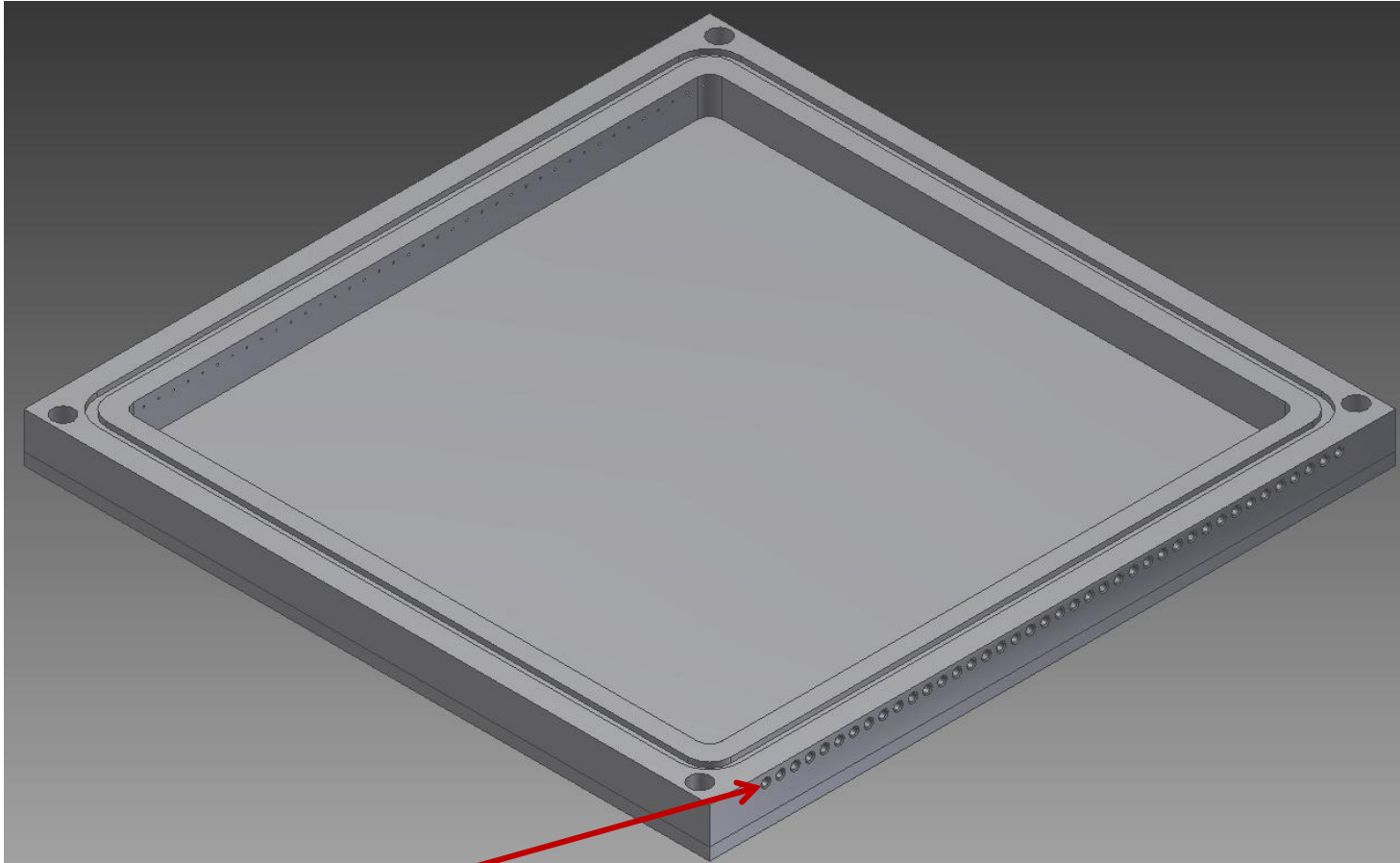
Notes: to combine multiple valve arrays, use t-manifolds in series, connected with 1/16" OD 0.03" ID tubing. Air inlet should be last connection.  
To distribute air to each inlet, use clippard MAN-12 and NPT tees.



Odorized air flows from t-manifold to flow chamber through 1/16" OD 0.03" ID teflon tubing (connect with 10-32 vacutight fittings, both ends)

C

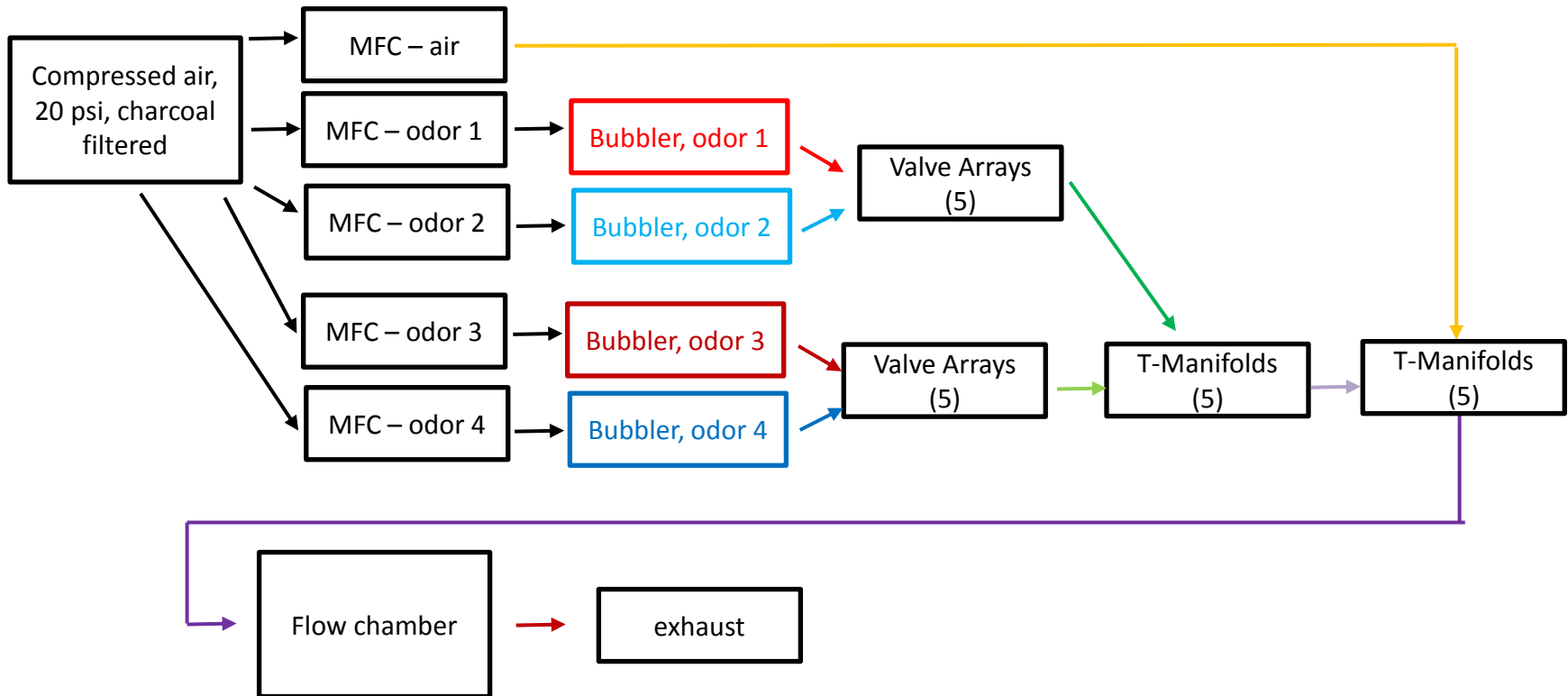


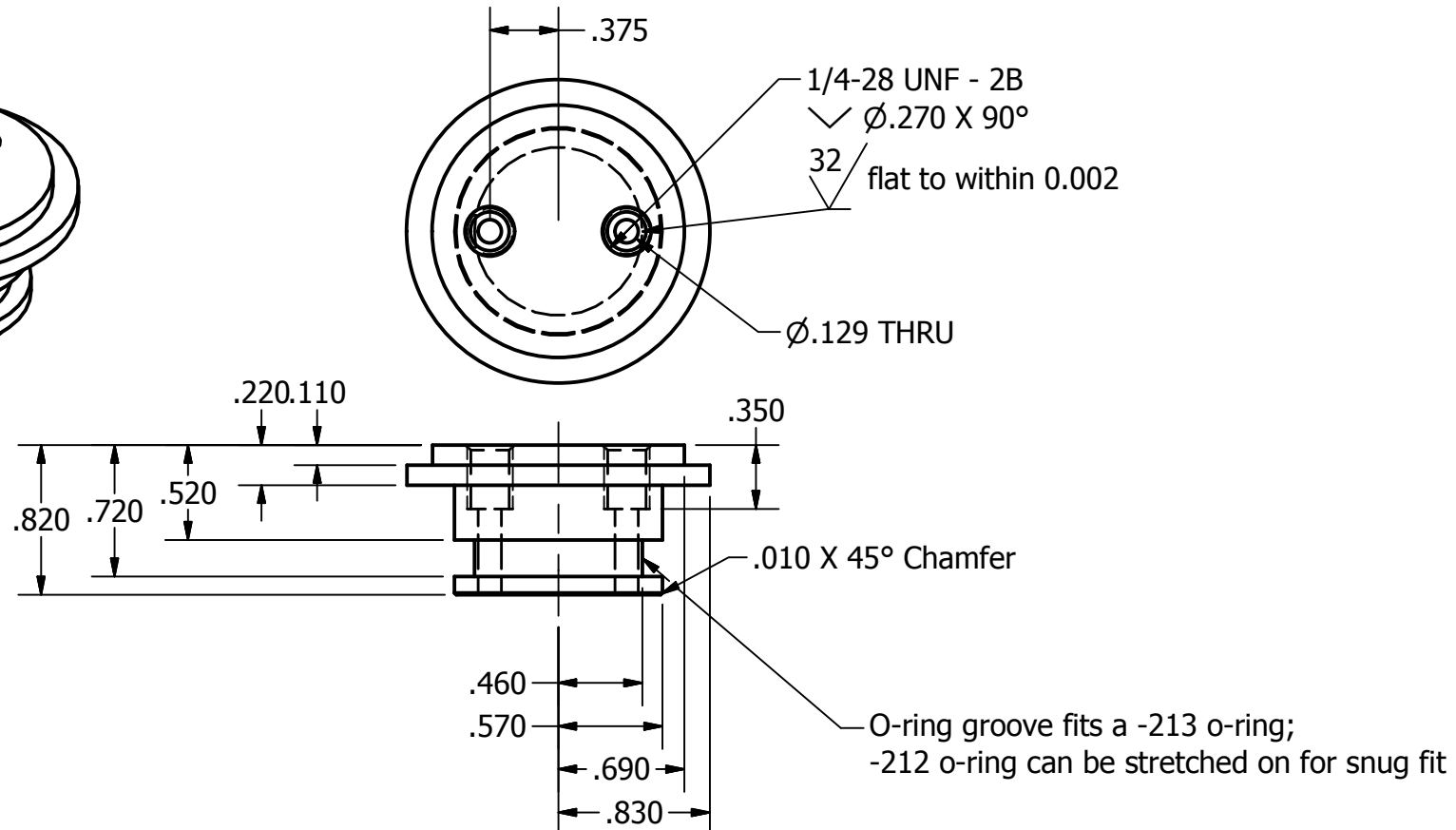
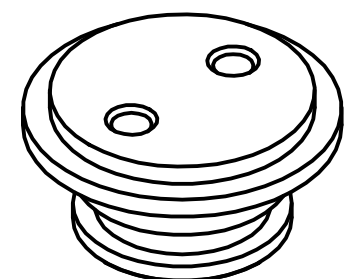


D

**Flow chamber outlet:** connect with clippard 10-32 to 1/16" ID hose barbs to 1/8" OD, 1/16" ID fep lined tygon tubing (40 x). Connect other end to clippard MAN-12 using clippard barbs. Connect all MAN-12s to MAN-ASF1-08 (use NPT plugs to fill empty connections). connect MAN-ASF1-08 to tubing (this is the outlet, which should run through a flow meter and then into whatever venting system you decide to use)

## Alternate connection scheme for multiple independent valve arrays



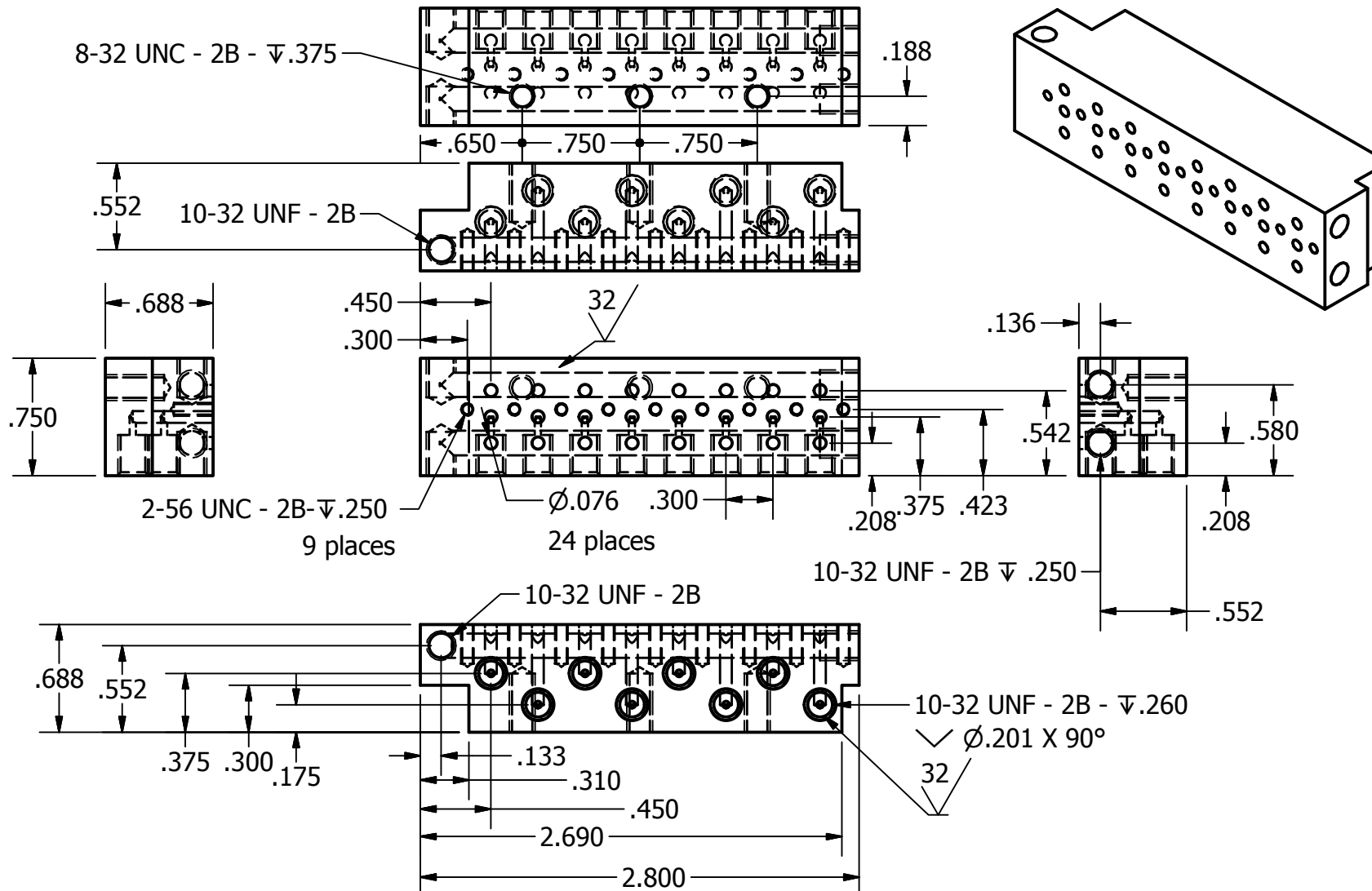


DRAWN Marc Gershaw	3/19/2012	LADY GAGA V. 2 (Marc Gershaw, Samuel Lab, Harvard)		
CHECKED		TITLE		
QA		GL45 bottle - 1/428 flat bottom adapter		
MFG				
APPROVED		SIZE A	DWG NO GL45 - 1/4 28	REV
		SCALE		SHEET 1 OF 1

2

1

Pg 23



DRAWN	Marc Gershaw	3/19/2012	LADY GAGA V. 2 (Marc Gershaw, Samuel Lab, Harvard)	
CHECKED				
QA			TITLE	
MFG			Valve Manifold with 10-32 flat bottom fittings; shared nc and nc	
APPROVED				
			SIZE	REV
			A	00
			SCALE	
			SHEET 1 OF 1	

2

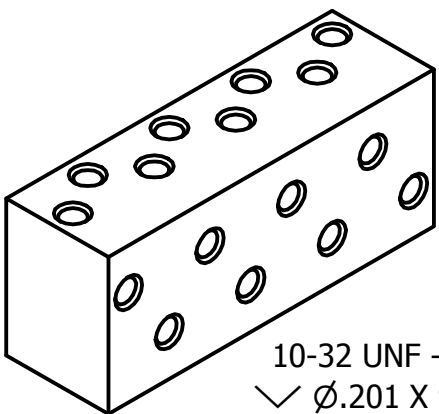
1

4

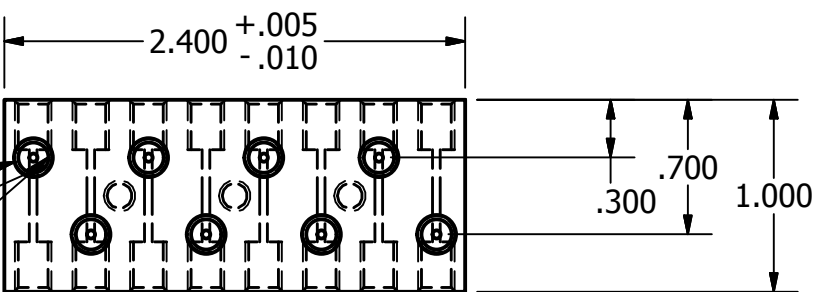
A

2

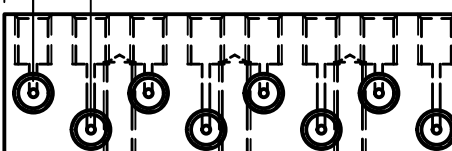
1



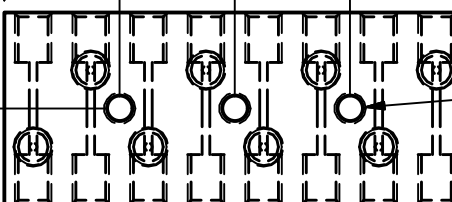
10-32 UNF - 2B  
 $\checkmark \quad \phi .201 \times 90^\circ$   
 32  
 Flat to within 0.002  
 0.26" deep 24 places



.300  
 .150



.600  
 .500



8-32 UNC - 2B 0.5" depth 3 places

PRODUCED BY AN AUTODESK EDUCATIONAL PRODUCT

PRODUCED BY AN AUTODESK EDUCATIONAL PRODUCT

DRAWN	Marc Gershaw	3/19/2012	LADY GAGA V. 2 (Marc Gershaw, Samuel Lab, Harvard)		
CHECKED					
QA			TITLE		
MFG			T-Manifold		
APPROVED			SIZE	DWG NO	REV
			A	t-manifold	00
			SCALE	1:1	SHEET 1 OF 1

2

1

2

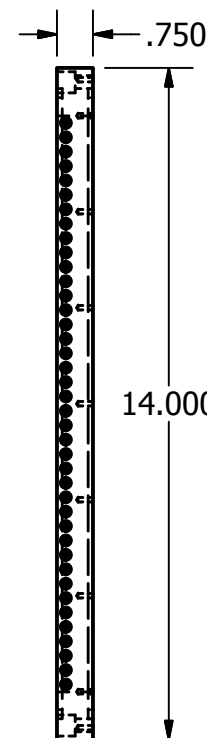
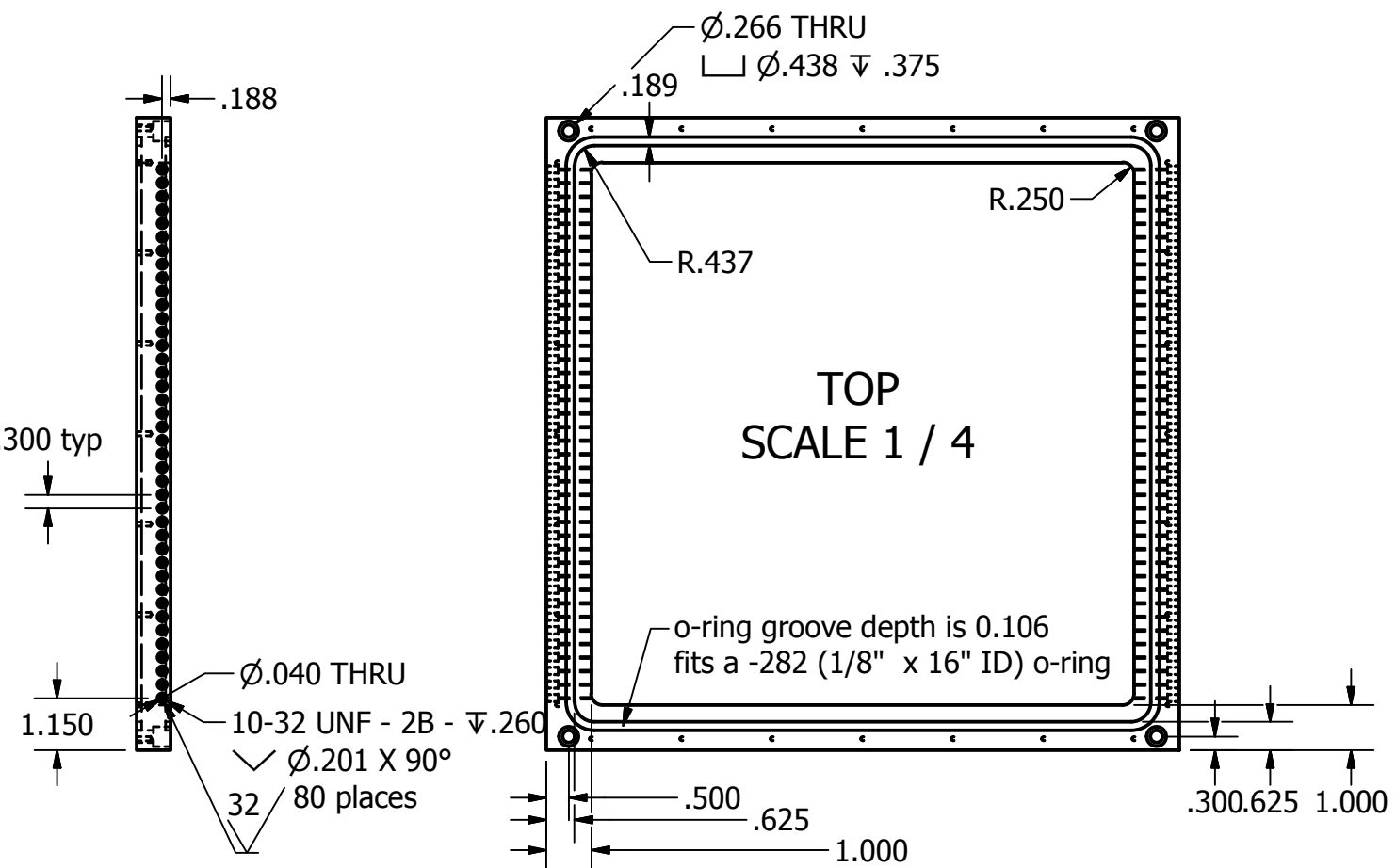
1

Pg 25

PRODUCED BY AN AUTODESK EDUCATIONAL PRODUCT



A



PRODUCED BY AN AUTODESK EDUCATIONAL PRODUCT



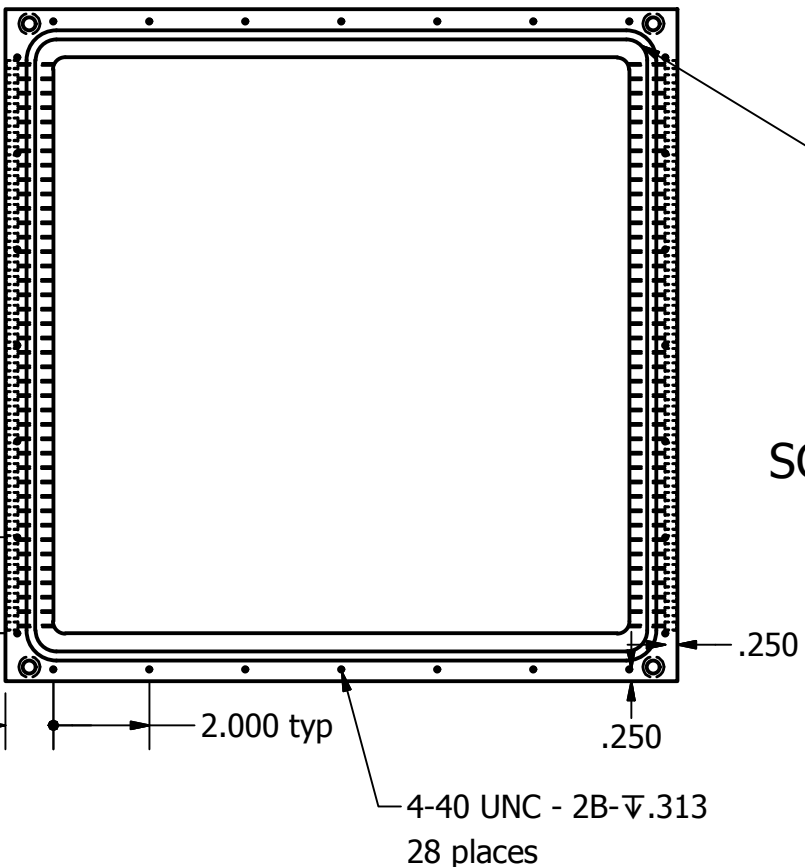
A

DRAWN	Marc Gershaw	3/19/2012	LADY GAGA V. 2 (Marc Gershaw, Samuel Lab, Harvard)		
CHECKED			TITLE		
QA			Flow Chamber Walls		
MFG					
APPROVED			SIZE	DWG NO	REV
			A	FlowChamberWalls	00
			SCALE		
				SHEET 1 OF 2	

2

1





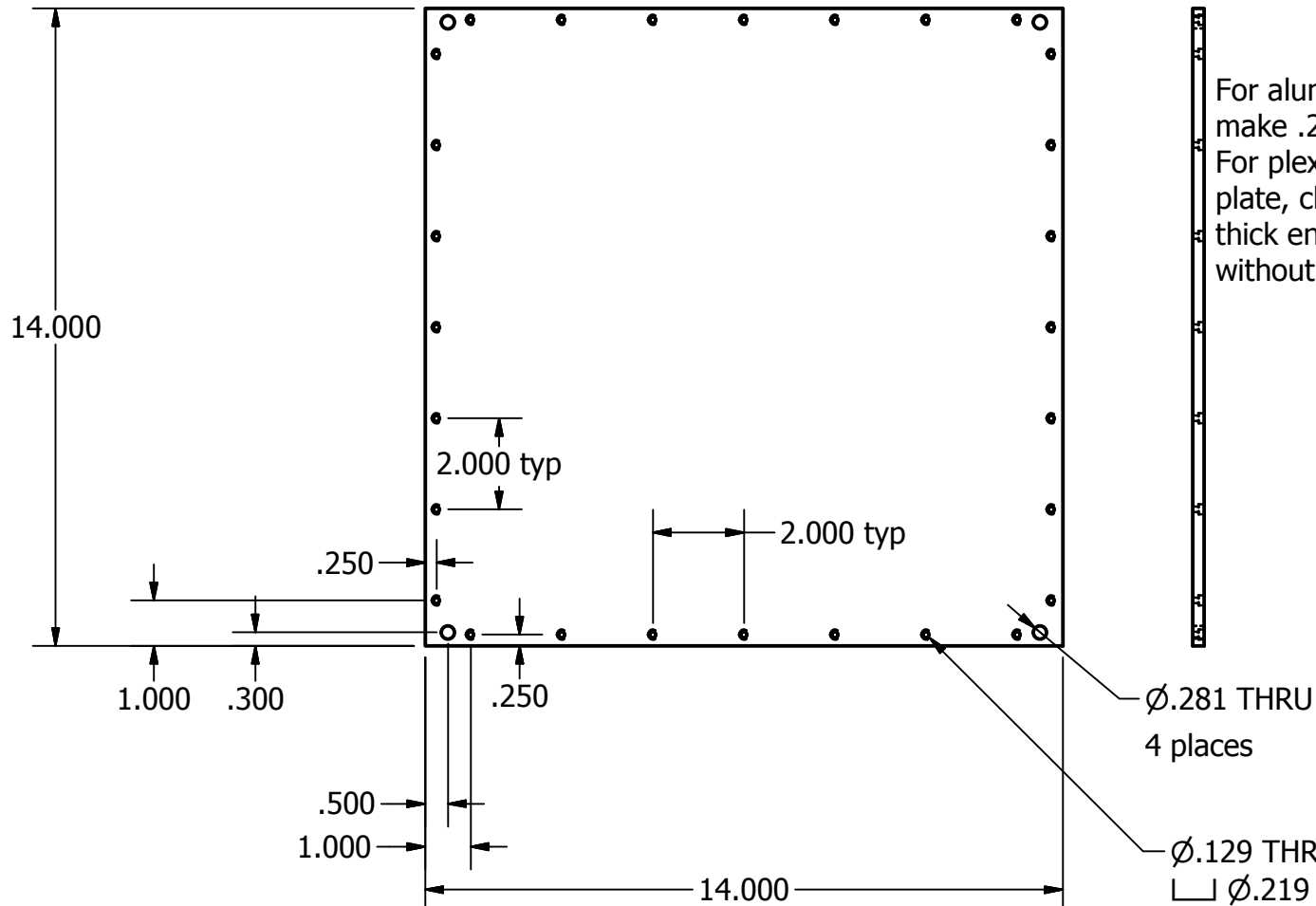
Bottom  
SCALE 1 / 4

DRAWN	Marc Gershon	3/19/2012	LADY GAGA V. 2 (Marc Gershon, Samuel Lab, Harvard)		
CHECKED			TITLE		
QA			Flow Chamber Walls		
MFG					
APPROVED			SIZE	DWG NO	REV
			A	FlowChamberWalls	00
			SCALE		SHEET 2 OF 2

2

1

PRODUCED BY AN AUTODESK EDUCATIONAL PRODUCT



.250

 $\varnothing .281$  THRU  
4 places $\varnothing .129$  THRU  
 $\varnothing .219 \downarrow .125$   
28 places

DRAWN	Marc Gershaw	3/19/2012	LADY GAGA V. 2 (Marc Gershaw, Samuel Lab, Harvard)		
CHECKED			TITLE		
QA			Solid Base Plate For Flow Chamber		
MFG					
APPROVED			SIZE	DWG NO	REV
			A	FlowChamberBase	00
			SCALE		SHEET 1 OF 1

2

1

PRODUCED BY AN AUTODESK EDUCATIONAL PRODUCT

A

B

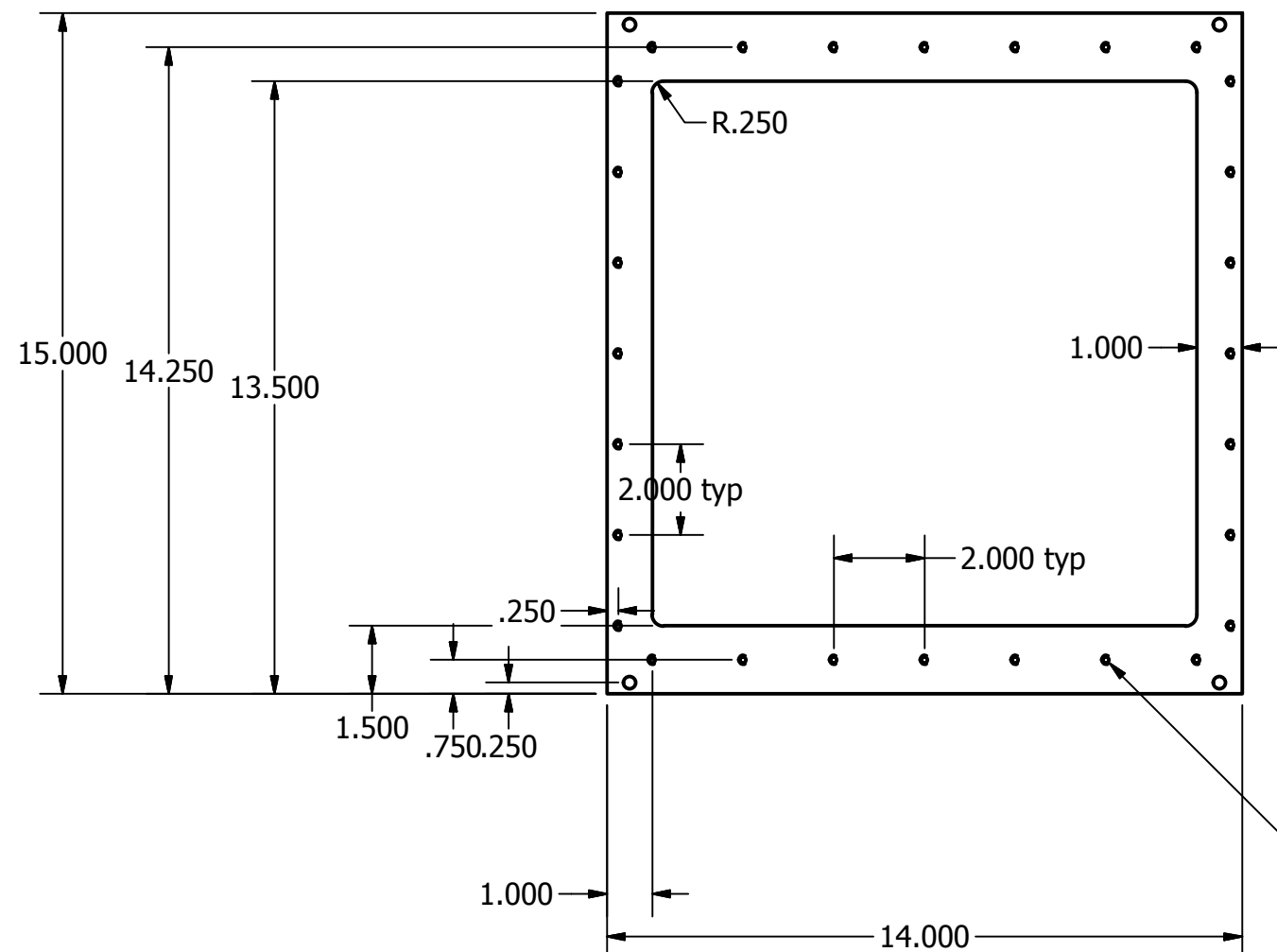
2

1

Pg 28

PRODUCED BY AN AUTODESK EDUCATIONAL PRODUCT

B



.250

1.000

R.250

2.000 typ

2.000 typ

1.500  
.750  
.250

1.000

14.000

$\varnothing$ .129 THRU  
└  $\varnothing$ .219  $\downarrow$  .125  
28 places

DRAWN	Marc Gershon	3/19/2012	LADY GAGA V. 2 (Marc Gershon, Samuel Lab, Harvard)		
CHECKED			TITLE		
QA			Flow Chamber Clamp for Glass Bottom		
MFG			SIZE		
APPROVED			A	DWG NO	
				FlowChamberBase for Glass	
			SCALE		REV
					00
				SHEET 1 OF 1	

2

1

B

PRODUCED BY AN AUTODESK EDUCATIONAL PRODUCT

4

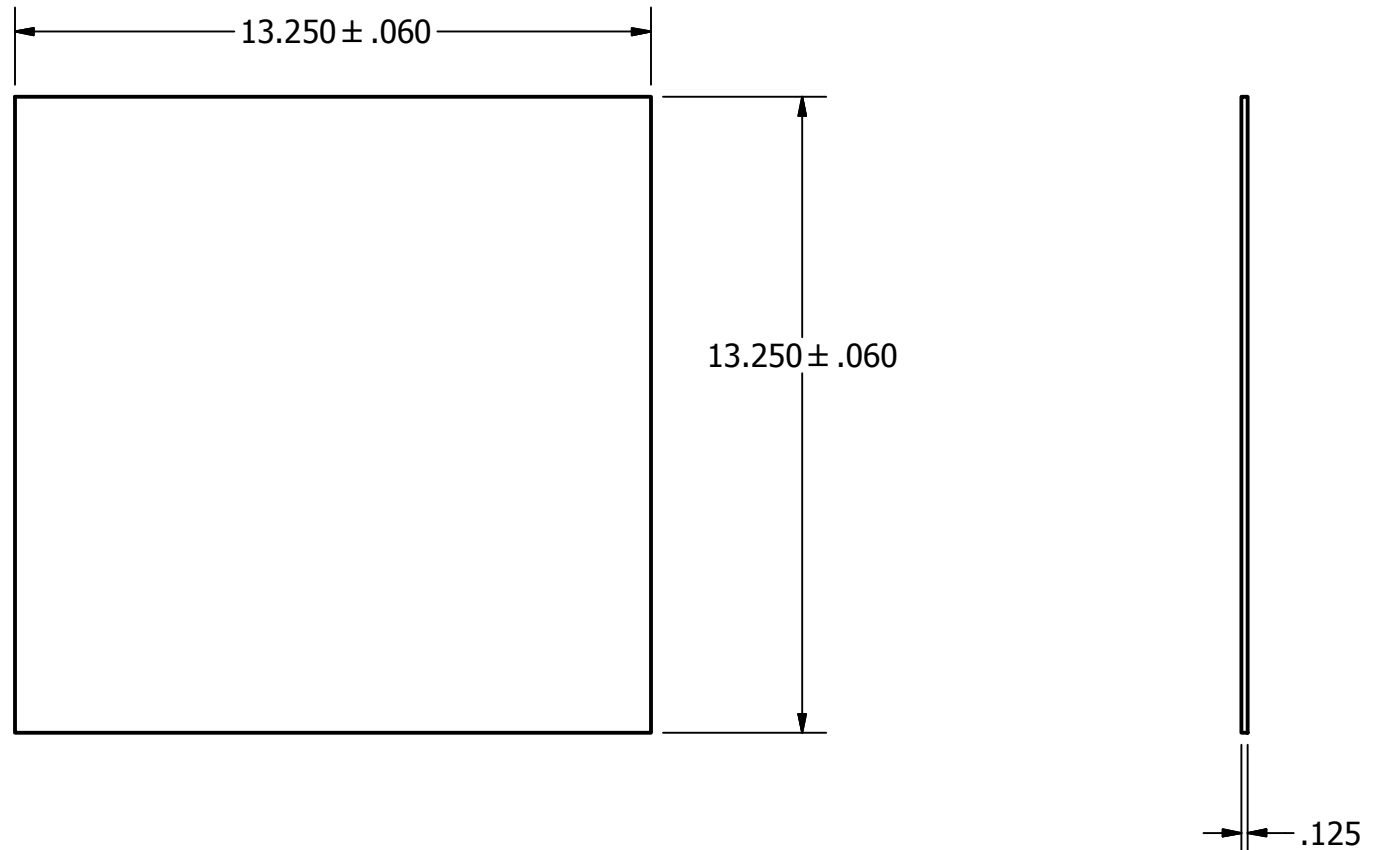
2

1



B

B

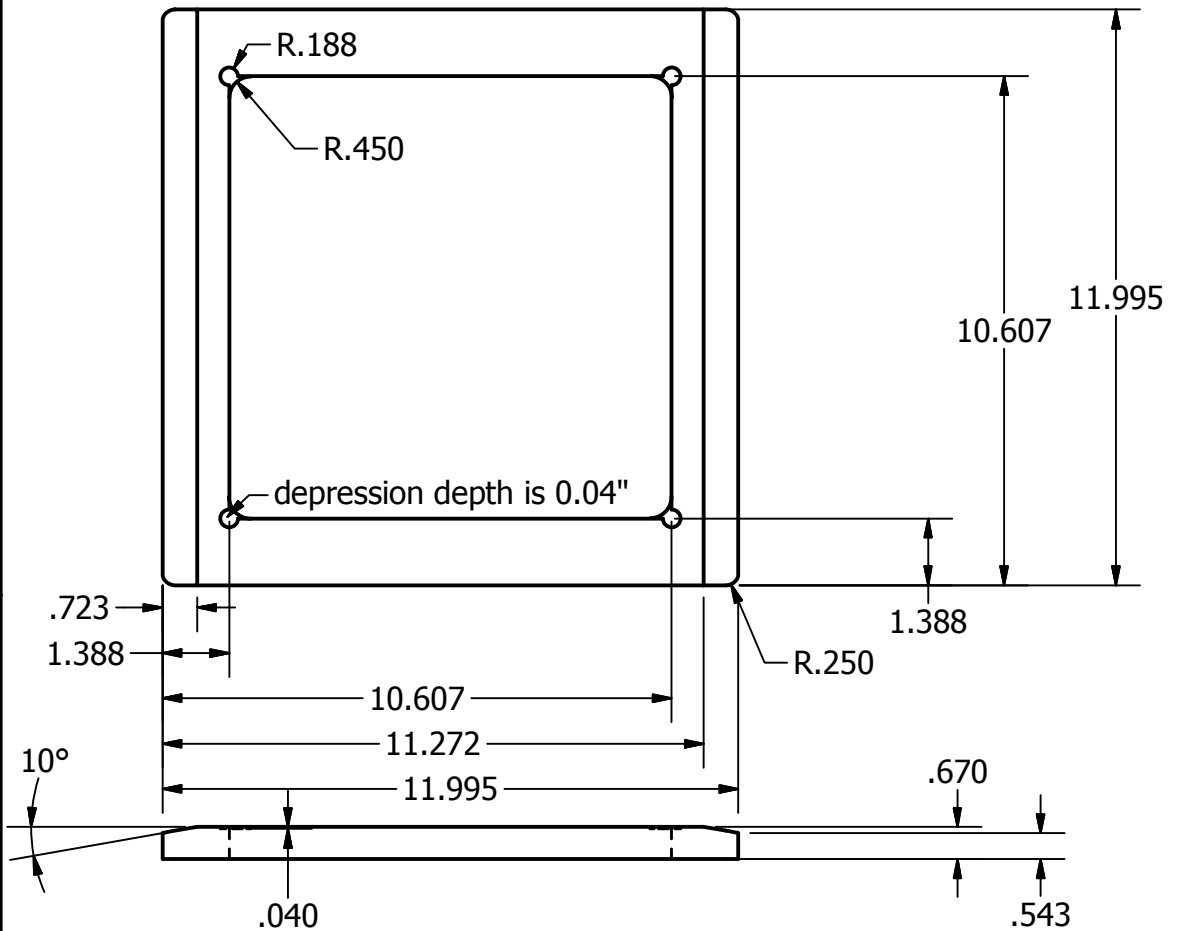


DRAWN	Marc Gershon	3/19/2012	LADY GAGA V2 (Marc Gershon, Samuel Lab, Harvard)		
CHECKED			TITLE		
QA			Bottom Glass Plate		
MFG					
APPROVED			SIZE	DWG NO	REV
			A	Bottom Glass Plate	00
			SCALE		SHEET 1 OF 1

2

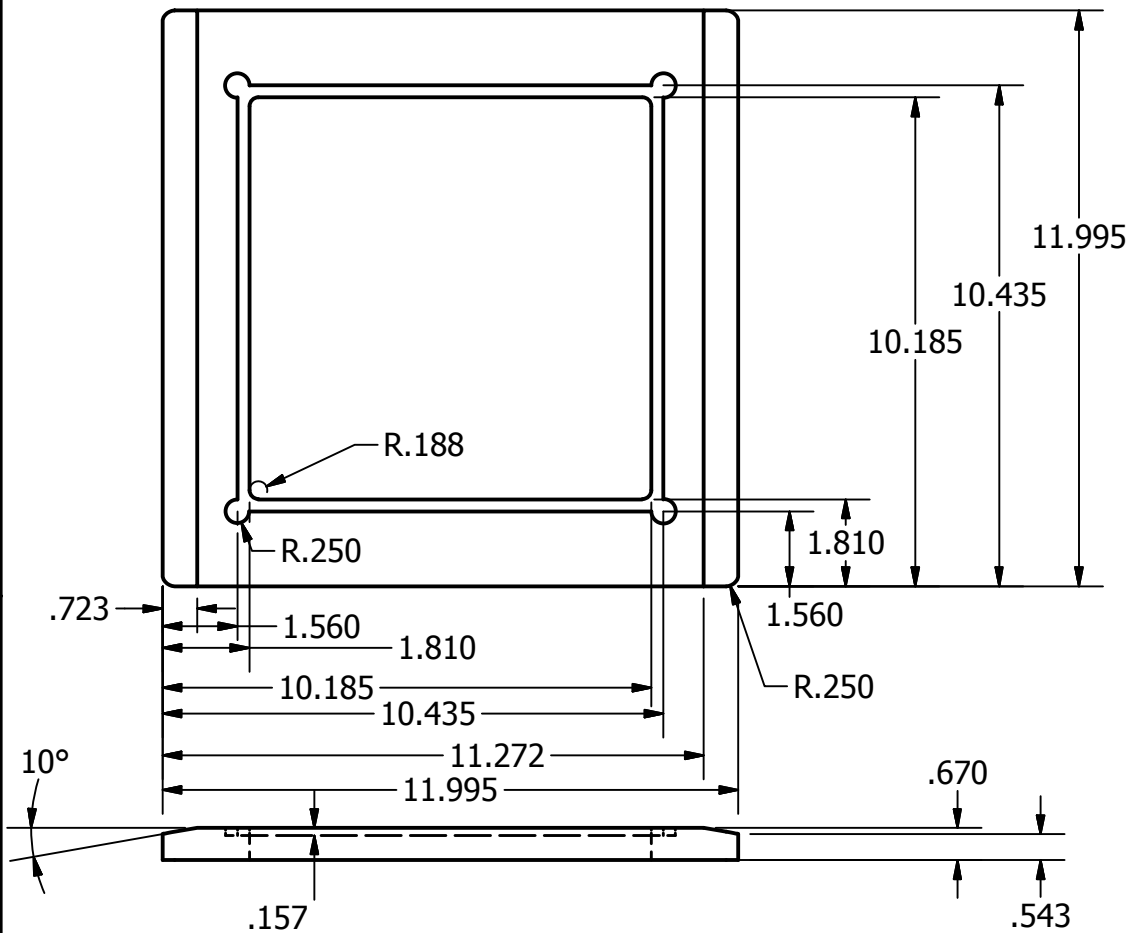
1





Insert should slip fit into flow chamber  
 BD Biodish-XL should slip fit into center  
 of insert  
 Insert height should match top edge of  
 BD Biodish-XL when both are placed on  
 same flat surface

DRAWN	Marc Gershaw	3/19/2012	LADY GAGA V. 2 (Marc Gershaw, Samuel Lab, Harvard)		
CHECKED			TITLE		
QA			Insert to hold BD Biodish XL		
MFG					
APPROVED			SIZE	DWG NO	REV
			A	FlowChamberInsert_BiodishXL	00
			SCALE		
				SHEET 1 OF 1	



Insert should slip fit into flow chamber  
 Central Depression dimensions are  
 approximate and will depend on size of  
 clear plate with agar provided by JFRC.  
 Actual Central Depression must be  
 designed to hold clear plate with gel so  
 that top of agar surface is flush with top  
 of insert.

DRAWN	Marc Gershaw	3/19/2012	LADY GAGA V. 2 (Marc Gershaw, Samuel Lab, Harvard)		
CHECKED					
QA			TITLE		
MFG			Insert to hold agar plate		
APPROVED			SIZE	DWG NO	REV
			A	FlowChamberInsert_Plate	00
			SCALE		
				SHEET 1 OF 1	

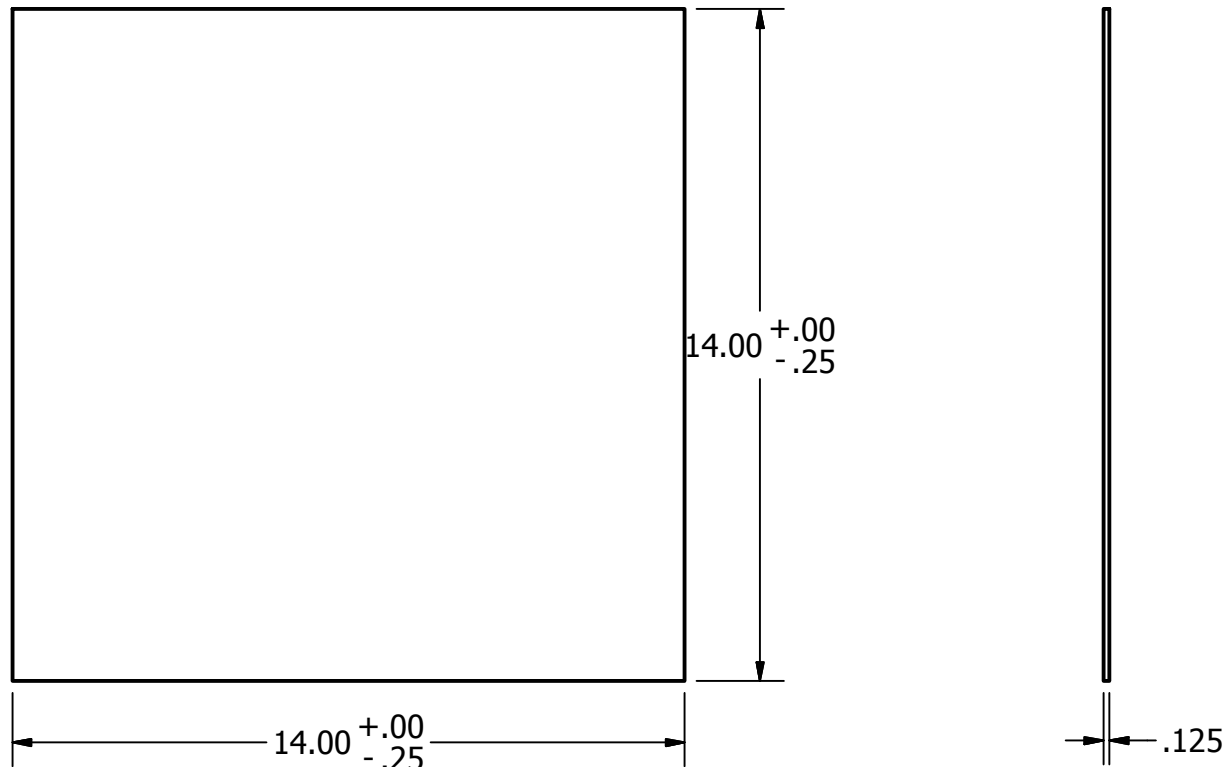


2

1

Pg 32

PRODUCED BY AN AUTODESK EDUCATIONAL PRODUCT



B

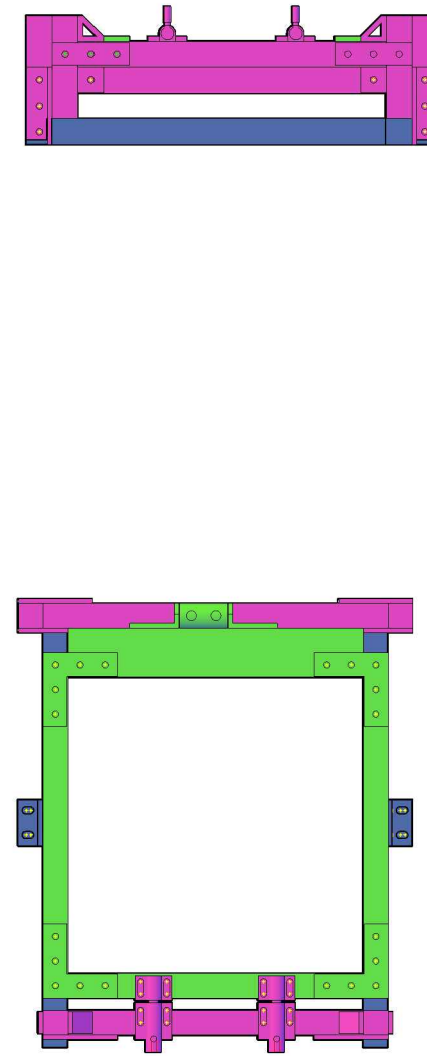
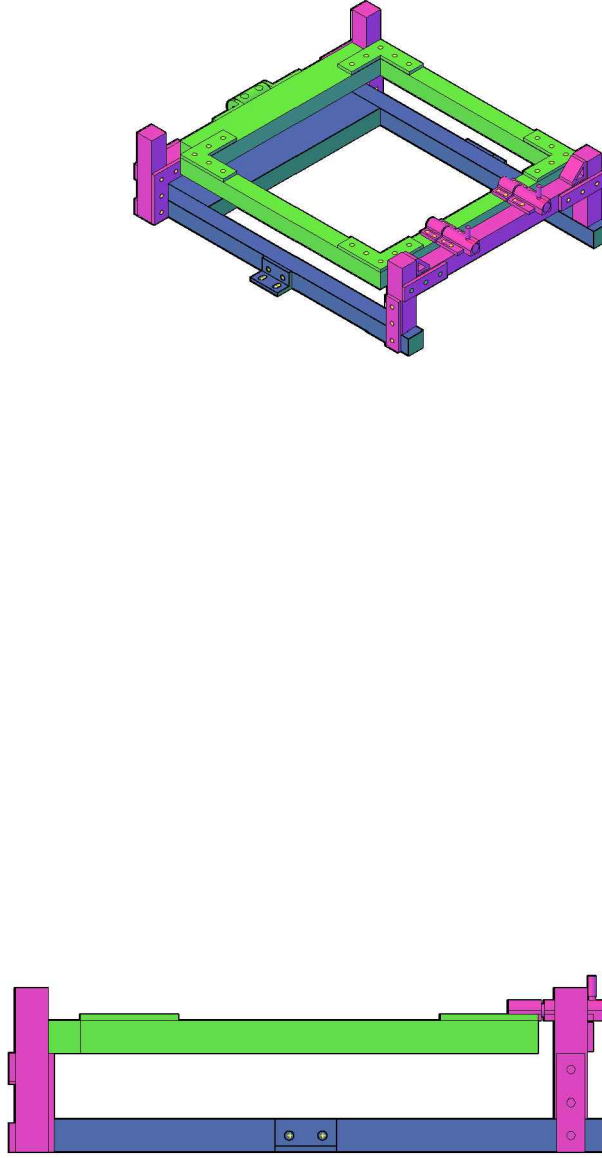
PRODUCED BY AN AUTODESK EDUCATIONAL PRODUCT

DRAWN	Marc Gershaw	3/19/2012	LADY GAGA V. 2 (Marc Gershaw, Samuel Lab, Harvard)		
CHECKED			TITLE		
QA			Glass Plate for Top of Flow Chamber		
MFG					
APPROVED			SIZE	DWG NO	REV
			A	Top Glass Plate	00
			SCALE		SHEET 1 OF 1

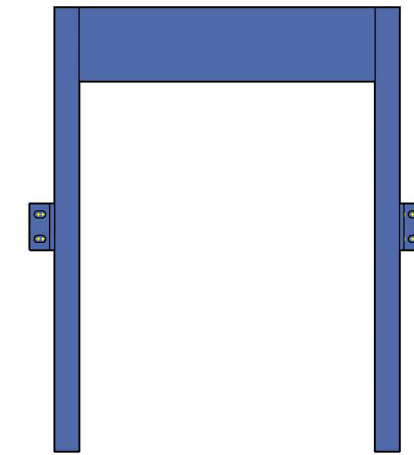
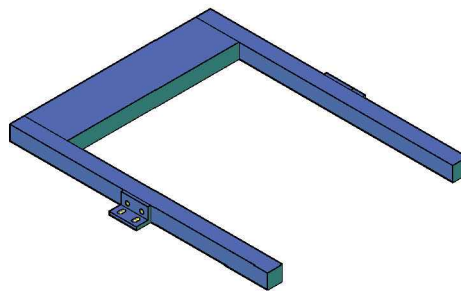
A

2

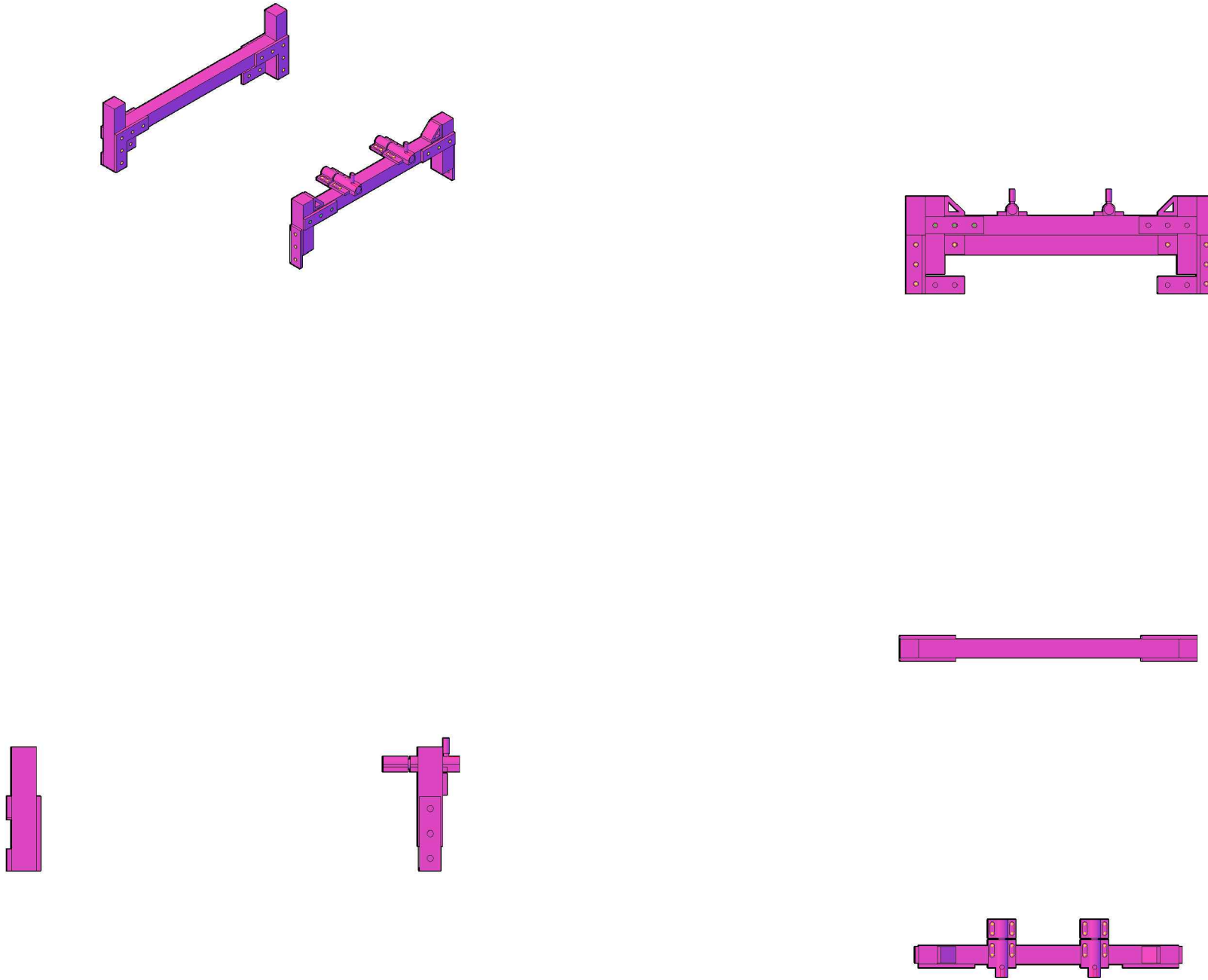
1



PRODUCED BY AN AUTODESK EDUCATIONAL PRODUCT

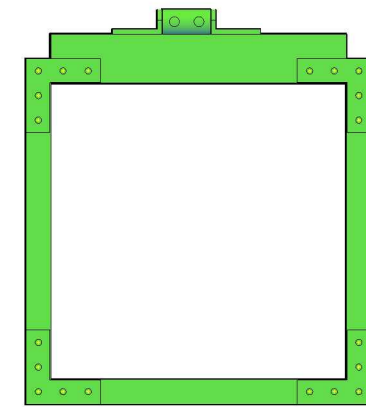
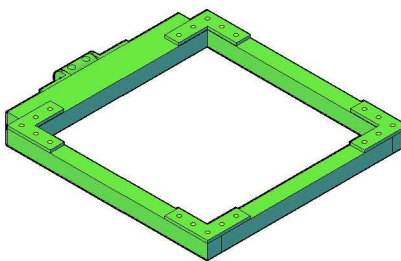


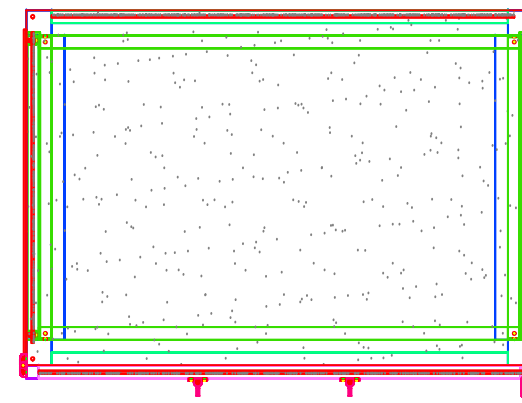
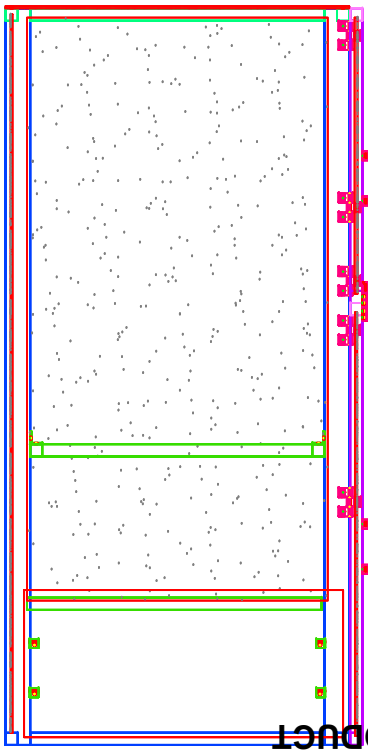
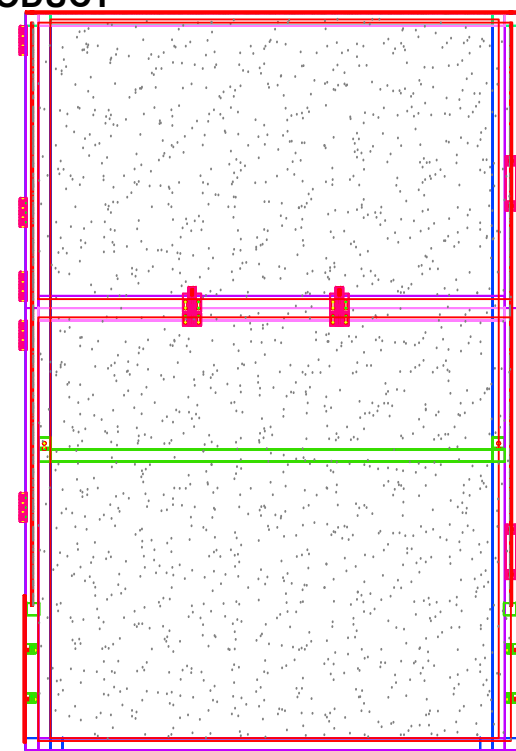
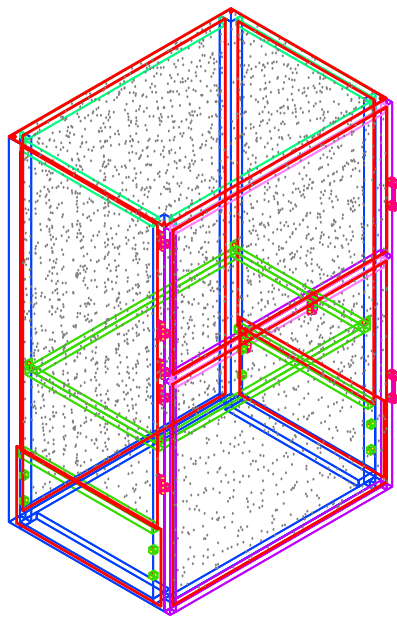
PRODUCED BY AN AUTODESK EDUCATIONAL PRODUCT



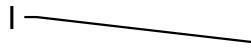
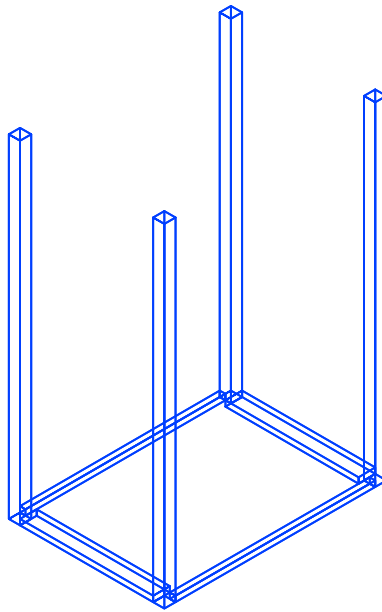
PRODUCED BY AN AUTODESK EDUCATIONAL PRODUCT

PRODUCED BY AN AUTODESK EDUCATIONAL PRODUCT

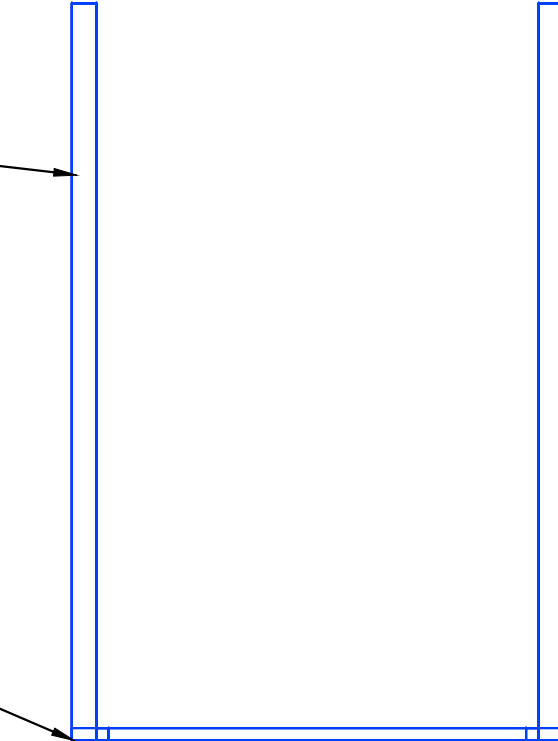




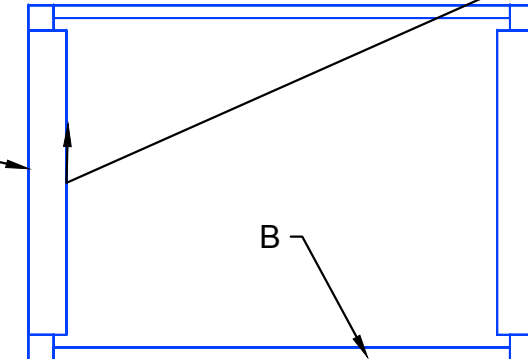
assembly instructions for lady gaga enclosure  
(is it really that much worse than IKEA?)  
Letters indicate line on BOM



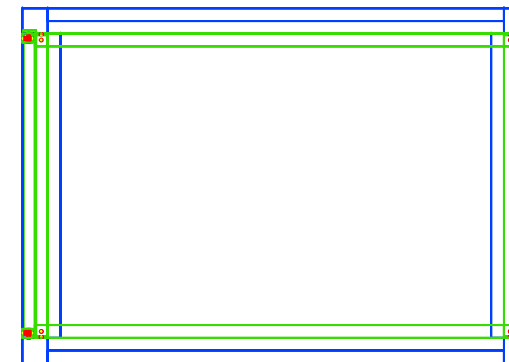
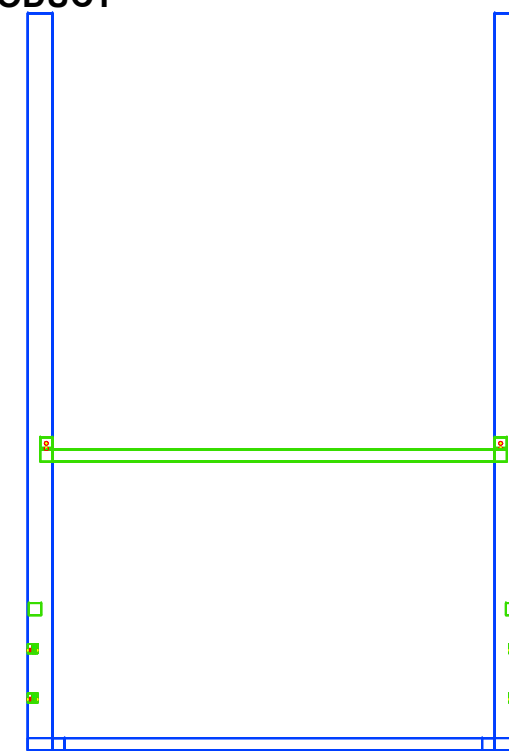
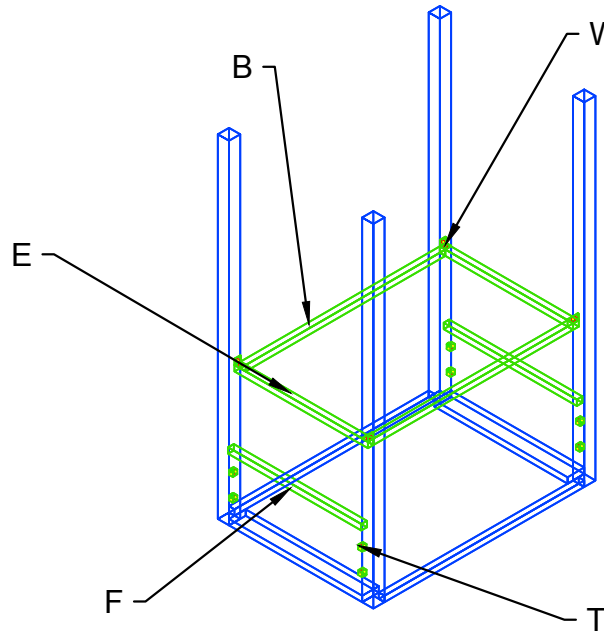
Anchor fastener goes on bottom of box



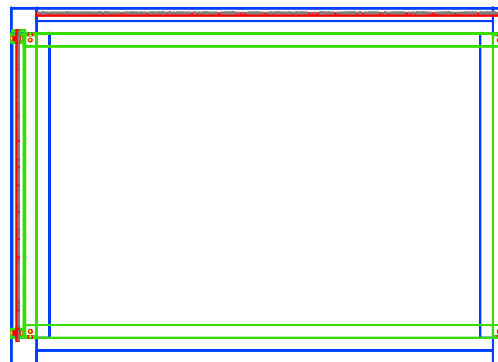
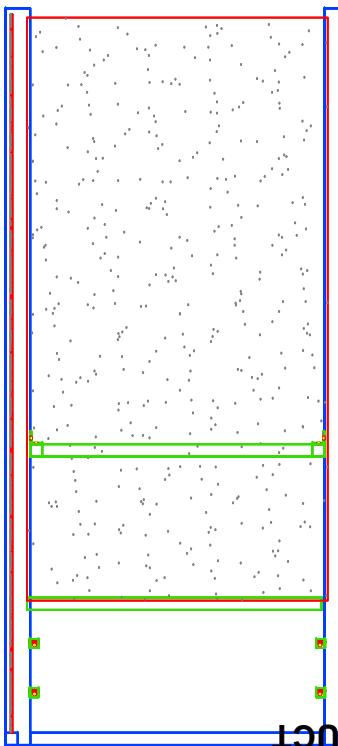
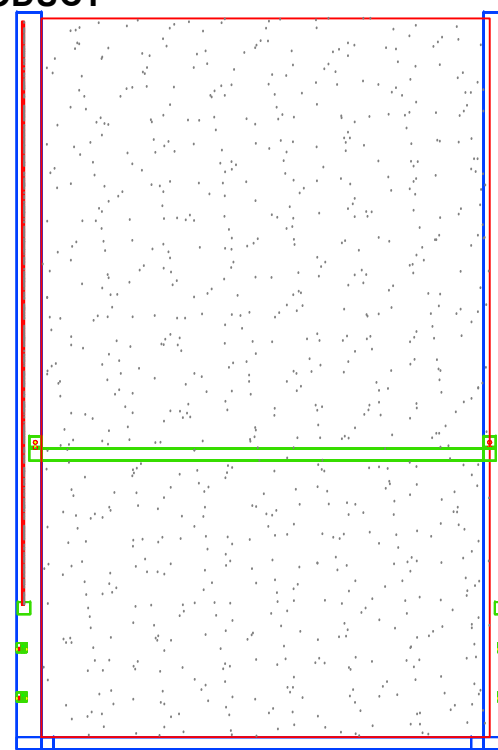
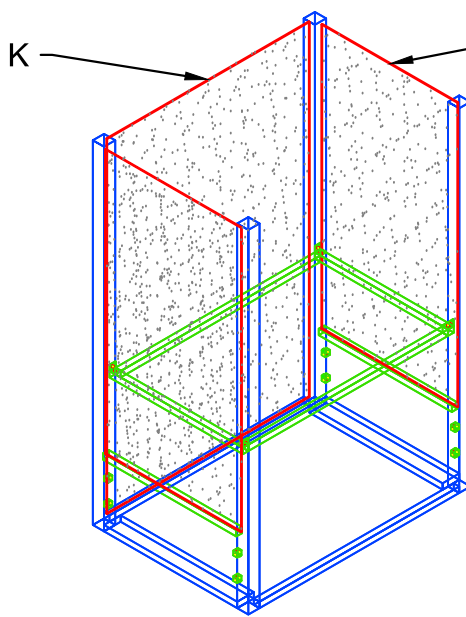
Place a 1/4-20 double economy t-nut in top middle t-slot before assembling (both sides)



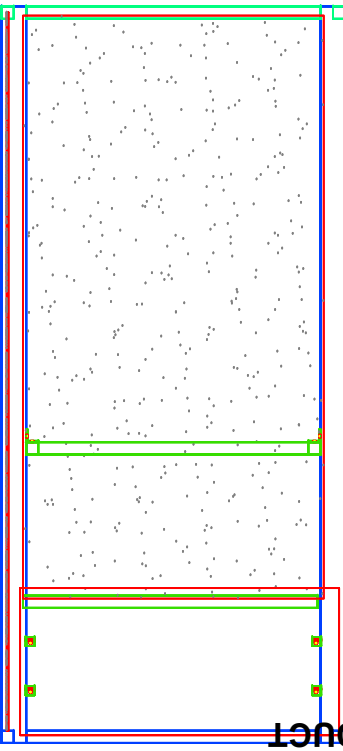
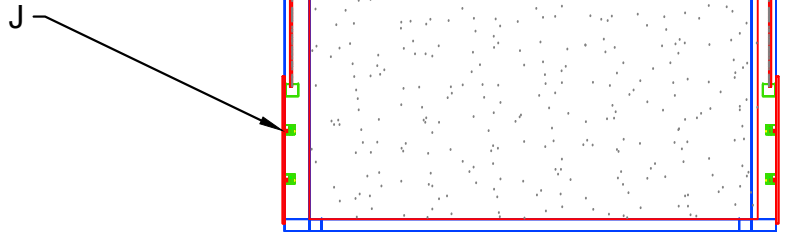
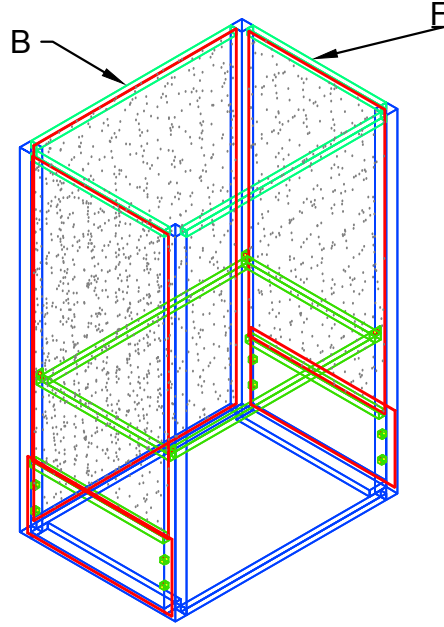
connect side posts (2x2x60) to bottoms (1x3x24 and 1x1x36). All parts should line up on the outside of the box. Make sure anchor fasteners face down.



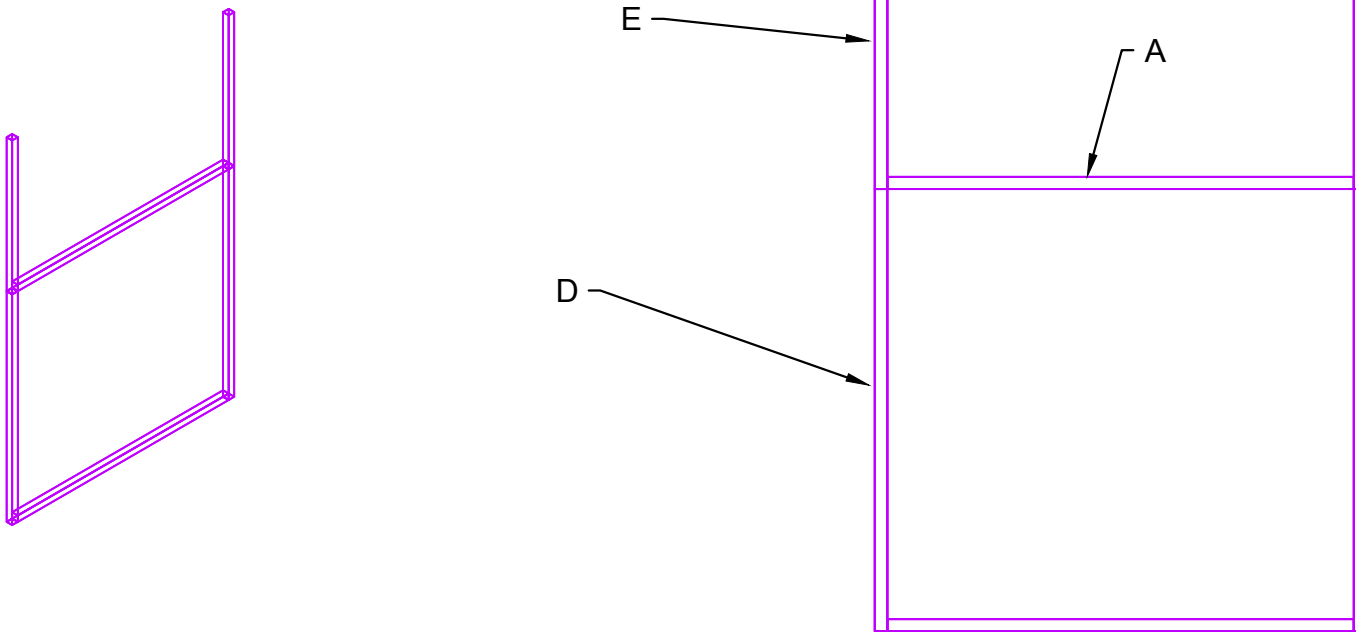
insert panel mount blocks and panel divider (1x1x24 with anchor fasteners at either end) into outer t-slots.  
Insert accessory support frame into inner t-slots.



insert panels into t-slots. back panel is 36.5x58.5. side panels are 24.5 x 47.5. face textured surface in.

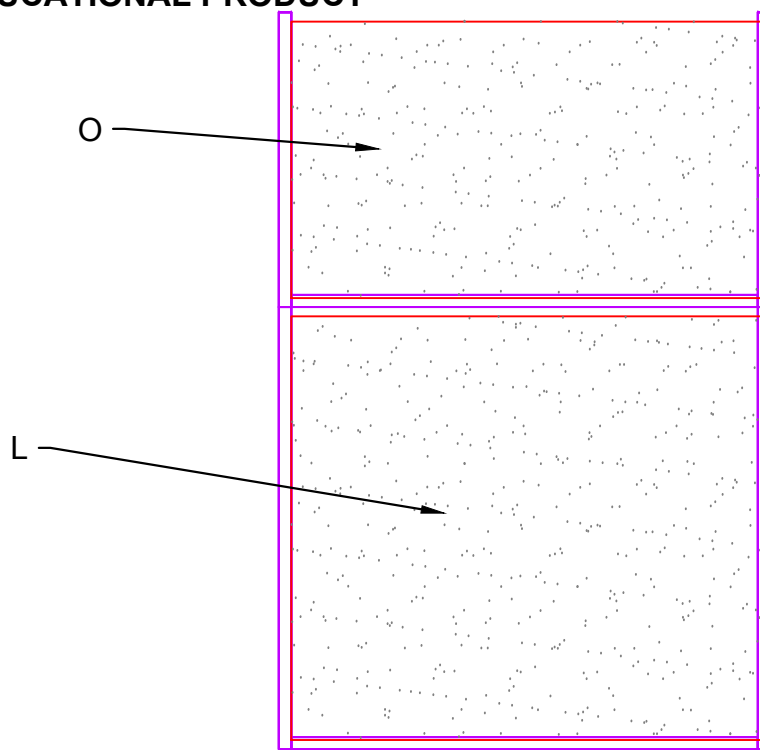
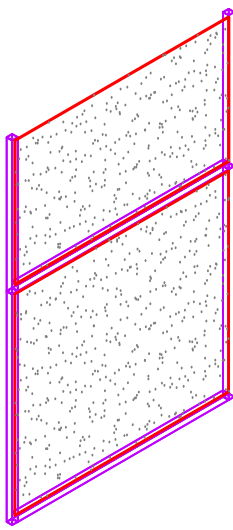


Place extrusion on top of frame to secure panels. Anchor fasteners should face up. Use 2 1x1x24 extrusions and 2 1x1x36 extrusions with anchor fasteners in both sides. Attach feedthrough panels to panel mount blocks.



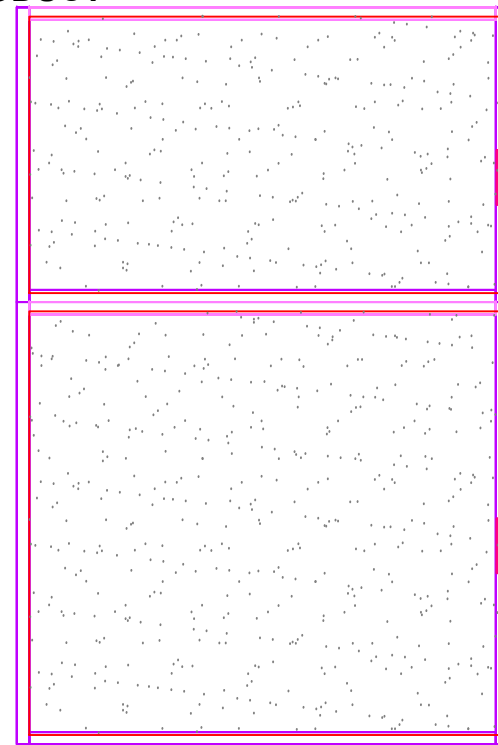
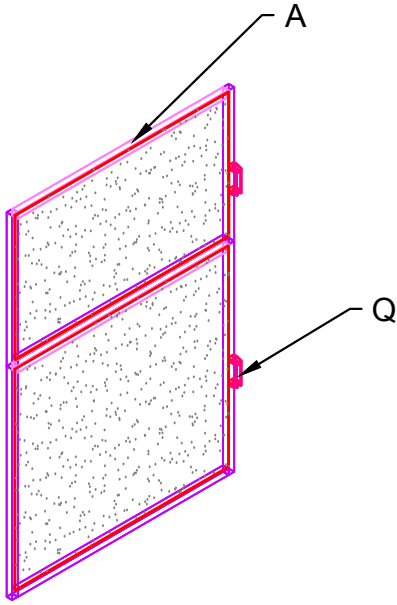
assemble doors. Although drawn together here, doors are separate and are not screwed together. Start by assembling sides (1x1x24 x 2 pieces top; 1x1x36 x 2 pieces bottom) and bottoms (1x1x38 with anchor fasteners in either end). Face anchor fasteners down.





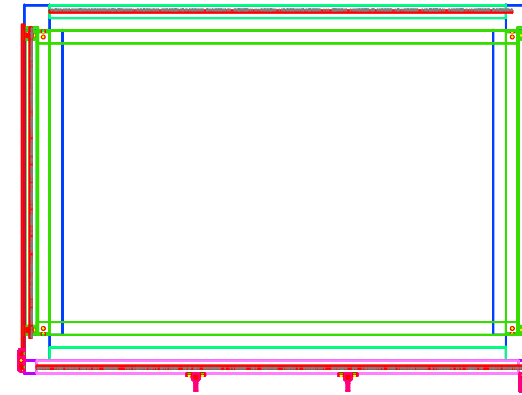
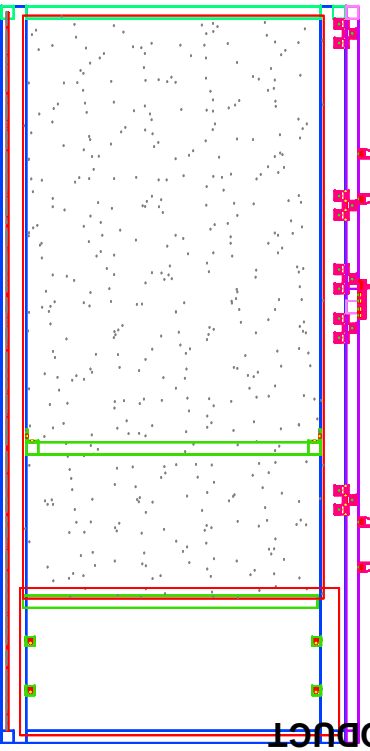
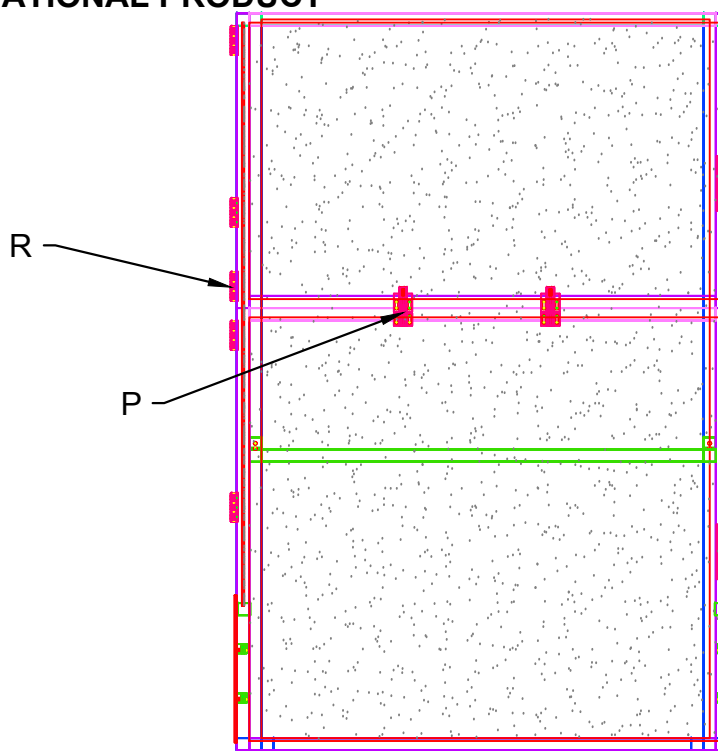
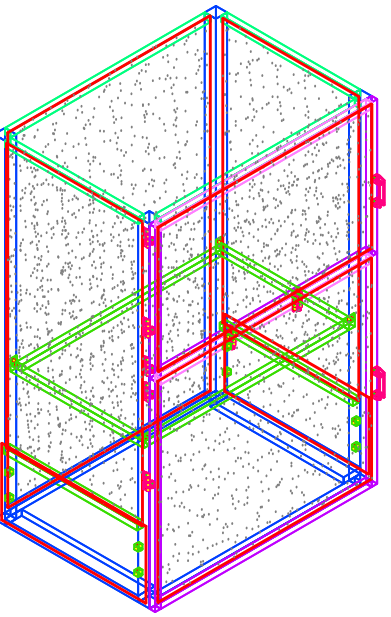
insert panels (38.5 x 22.5 top; 38.5x34.5 bottom) into doors.



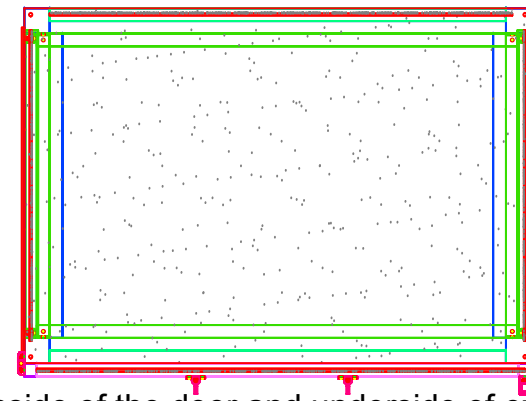
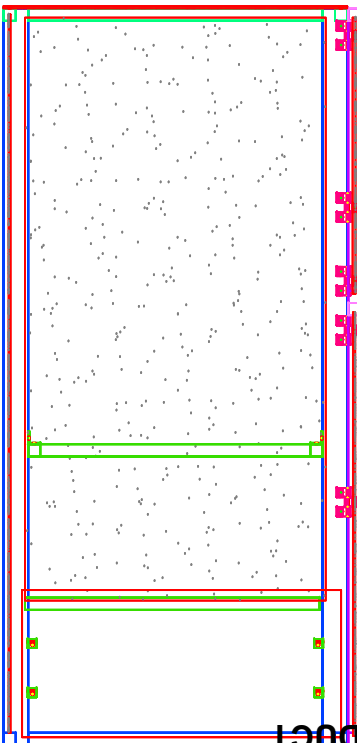
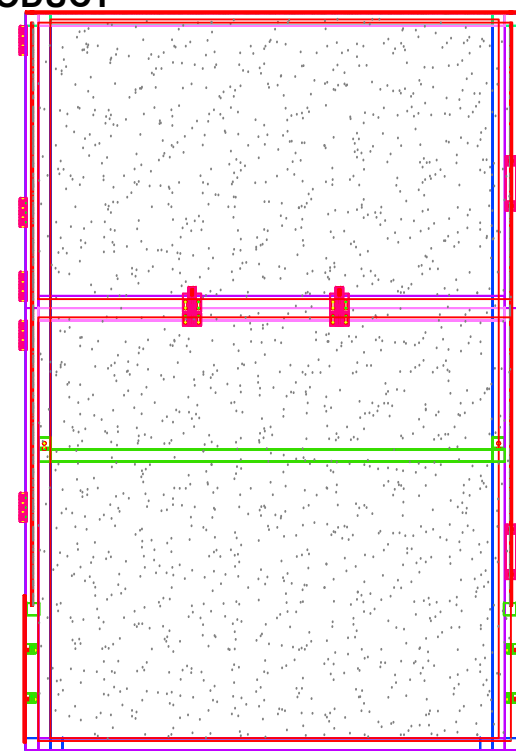
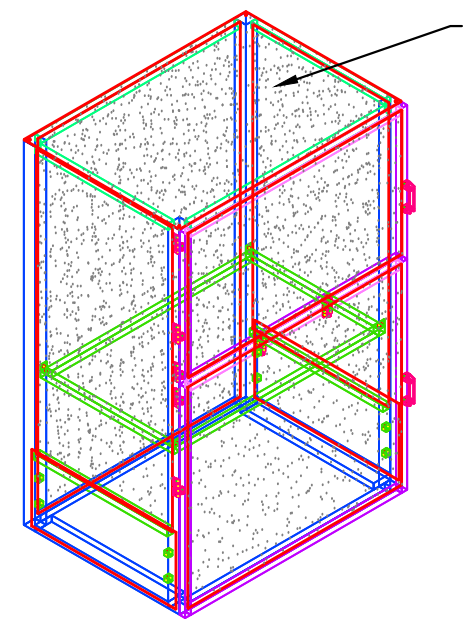


add top extrusion to secure panel (1x1x38 with anchor fasteners both sides). anchor fasteners face up



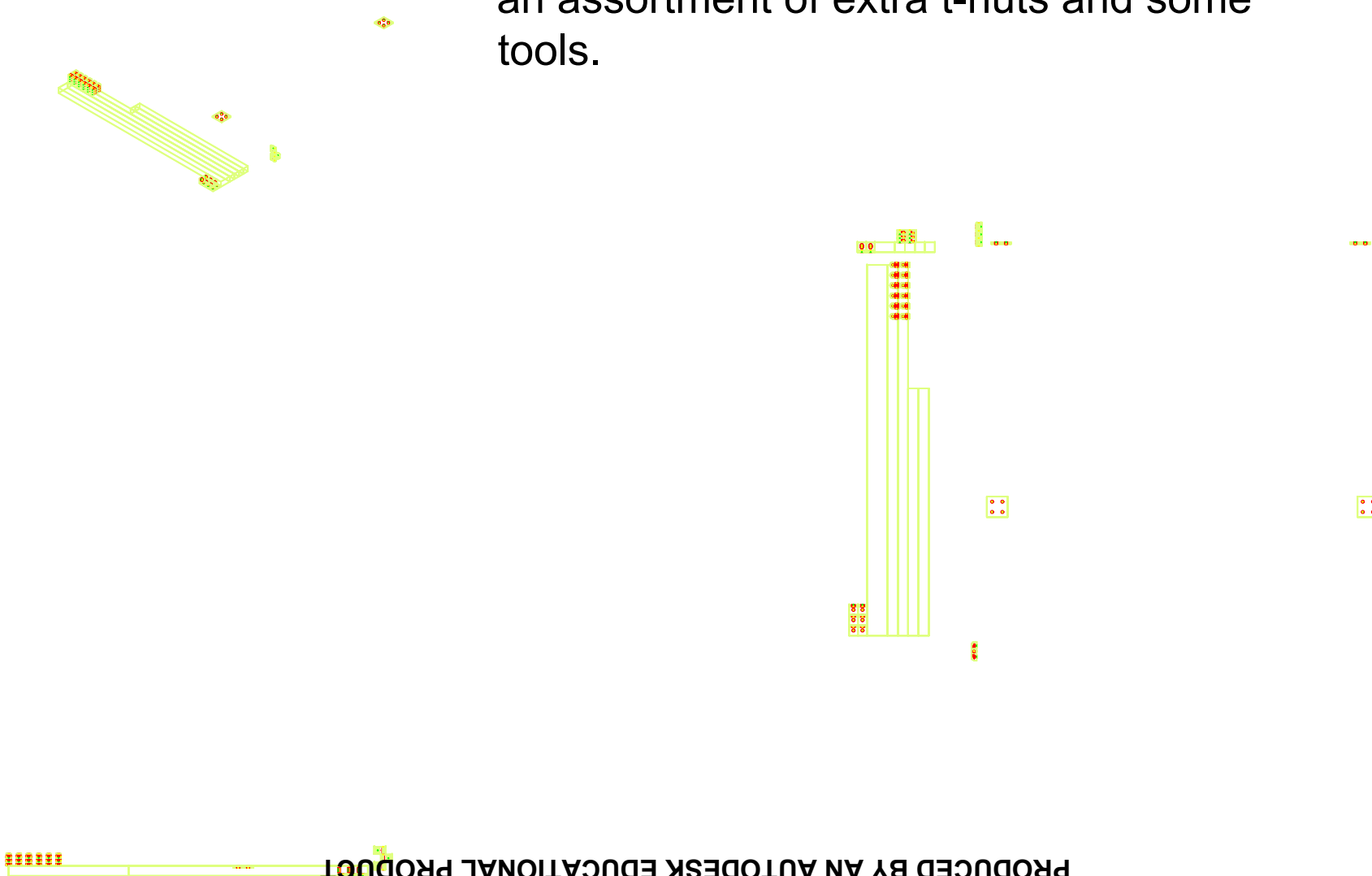


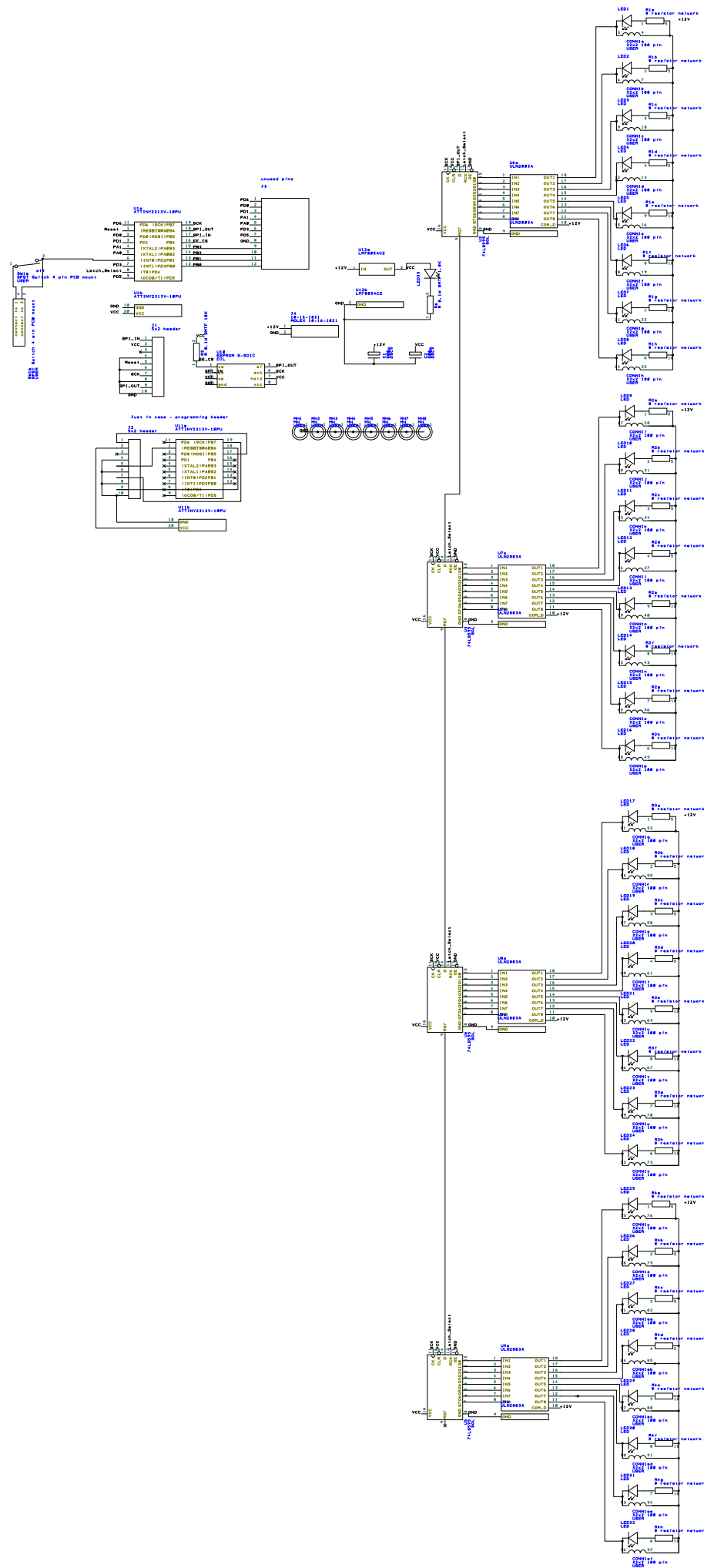
mount doors to box using hinges. doors should sit on top of one another. when you are satisfied with door placement, connect them with deadbolt latch

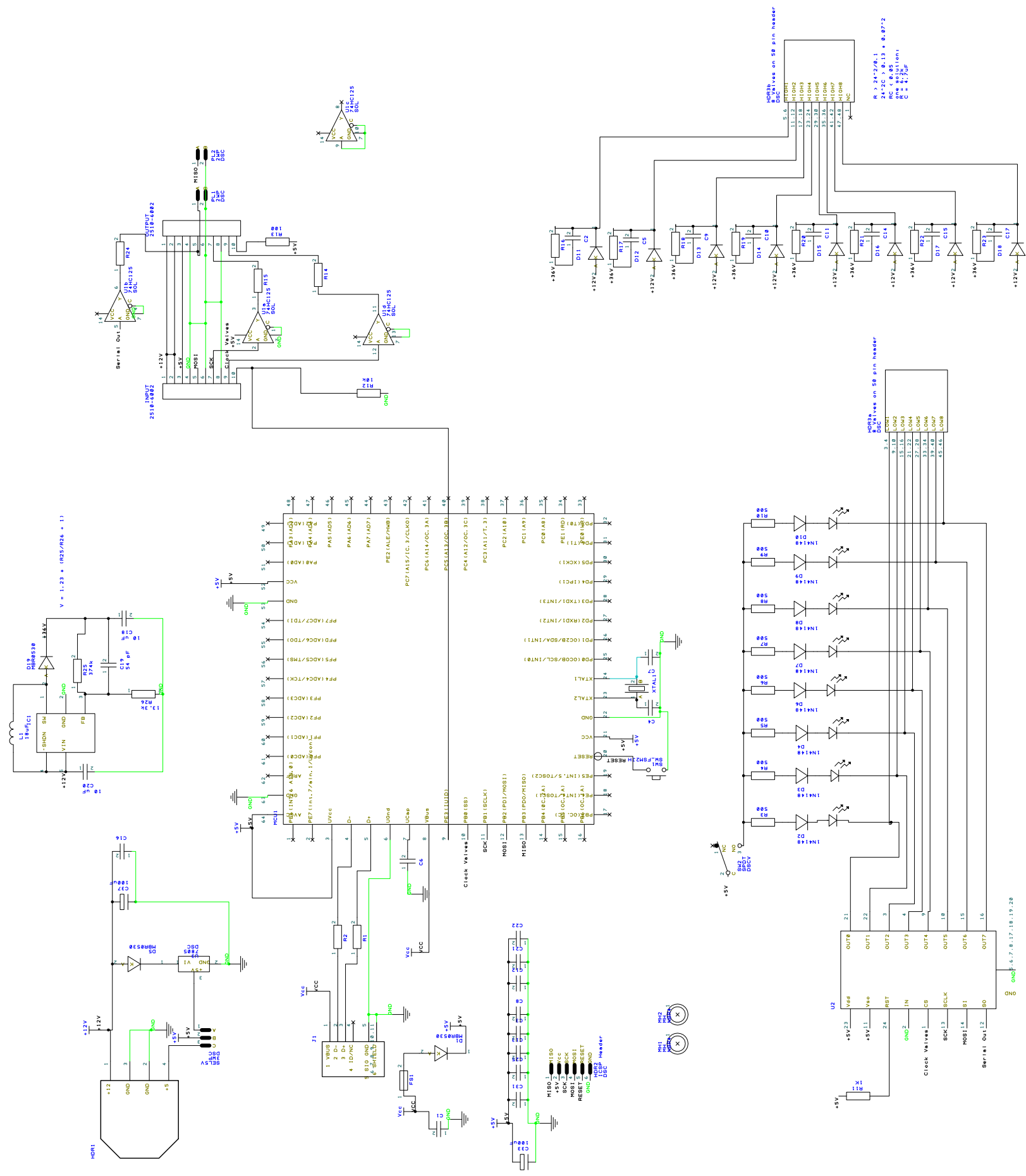


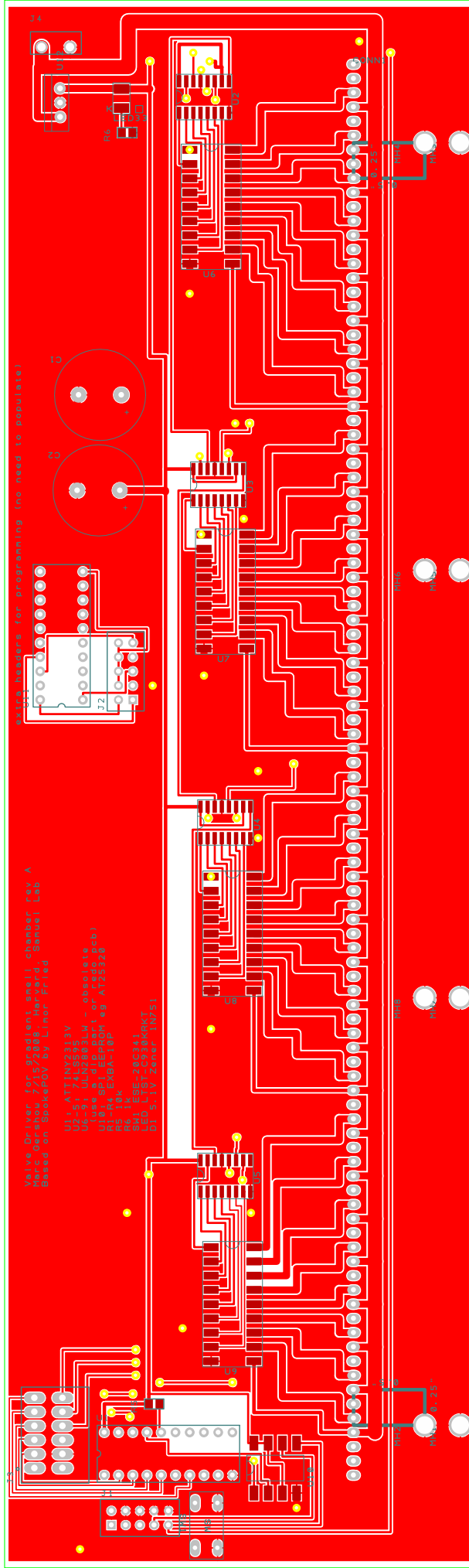
gasket the panels (using panel gasket strip) inside of the door and underside of exterior feedthrough panels (using  $\frac{1}{16}$ " adhesive gasket from mcmaster). install draw latches (mcmaster carr) using 8-32 t-nuts (you may have to drill out clearance on latch slightly). screw on the top with  $\frac{1}{4}$ -20 screws. Have a beer! You're done

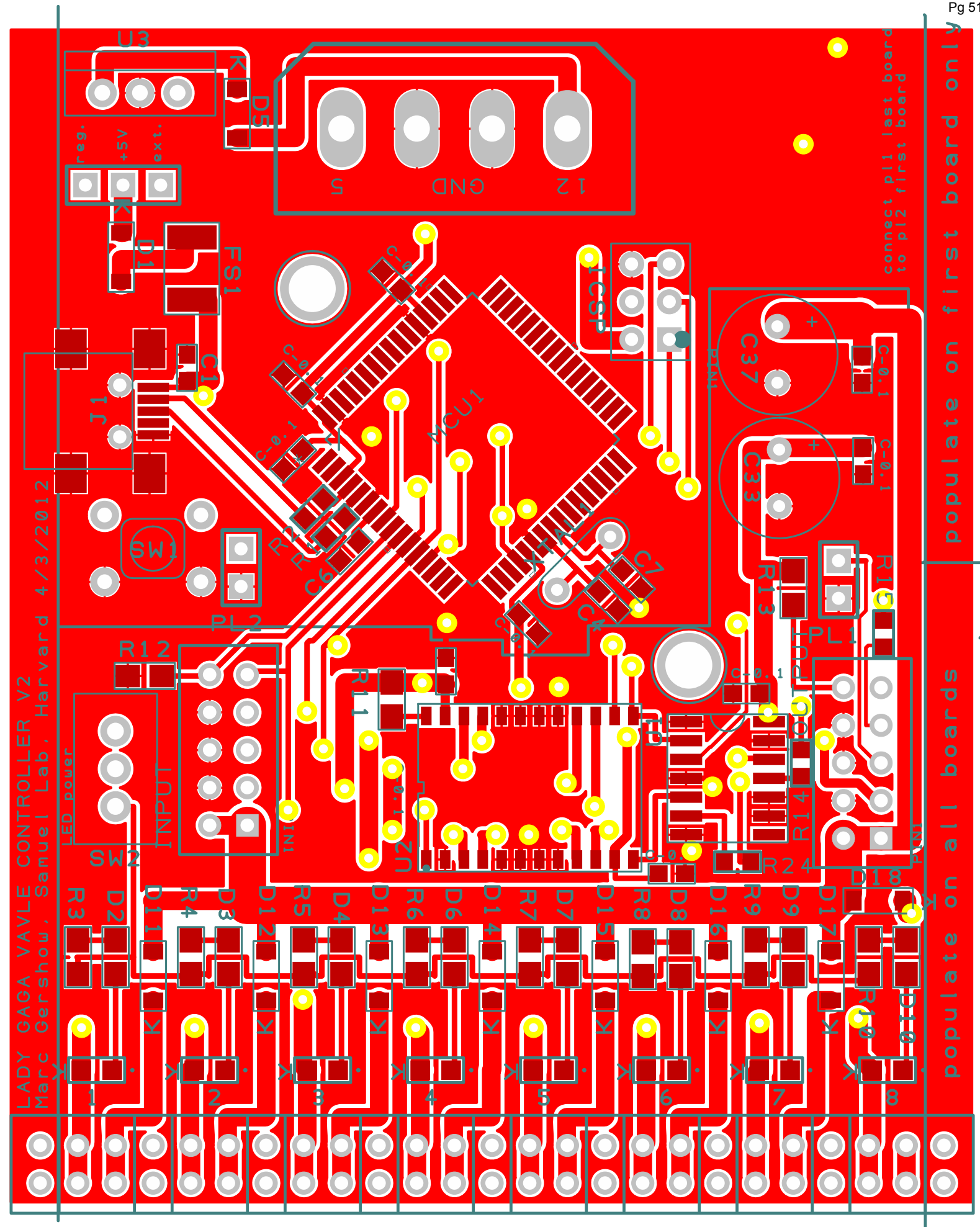
extra hardware (really just to confuse you, but also possibly useful). Extra extrusion to construct interior scaffolding; tubing supports; extra I-brackets. 4 hole plates to attach breadboard to frame. Also included an assortment of extra t-nuts and some tools.

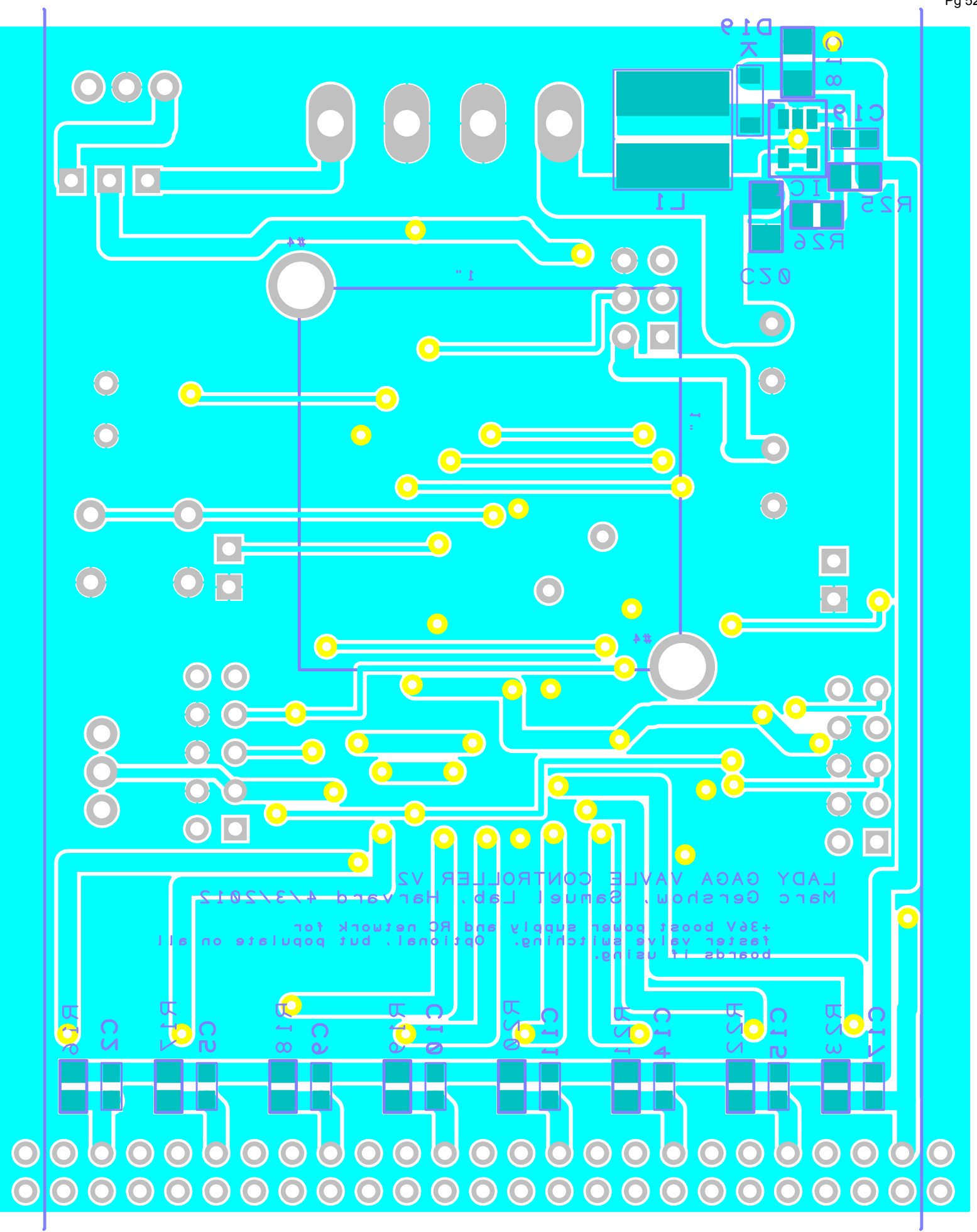


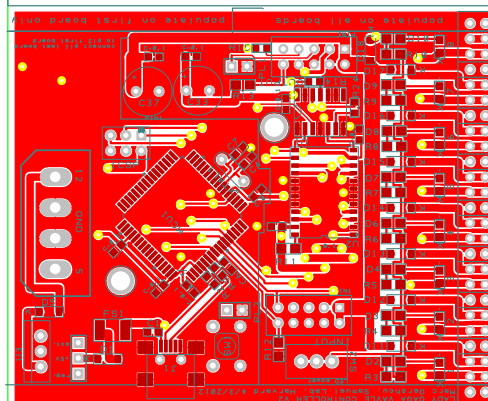
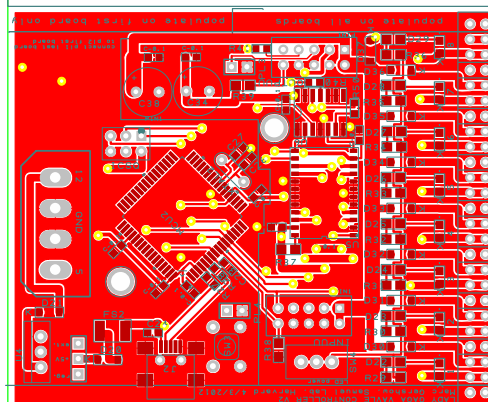
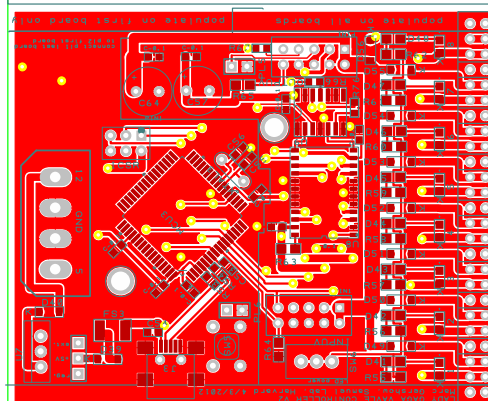
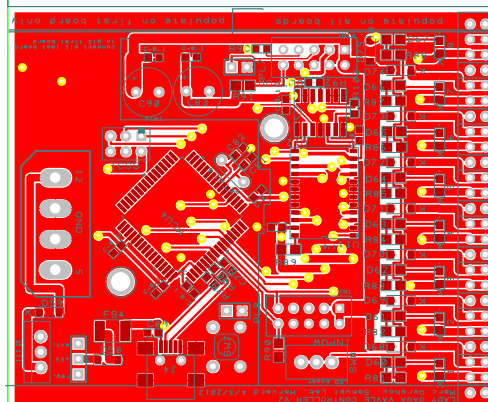
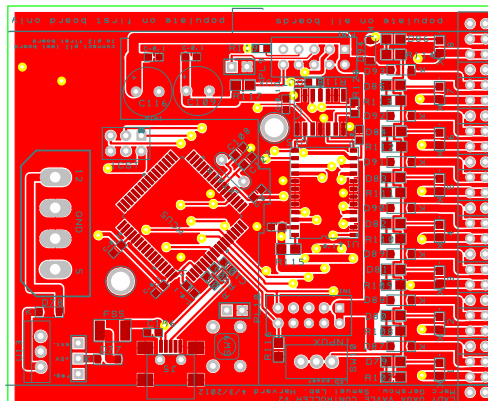


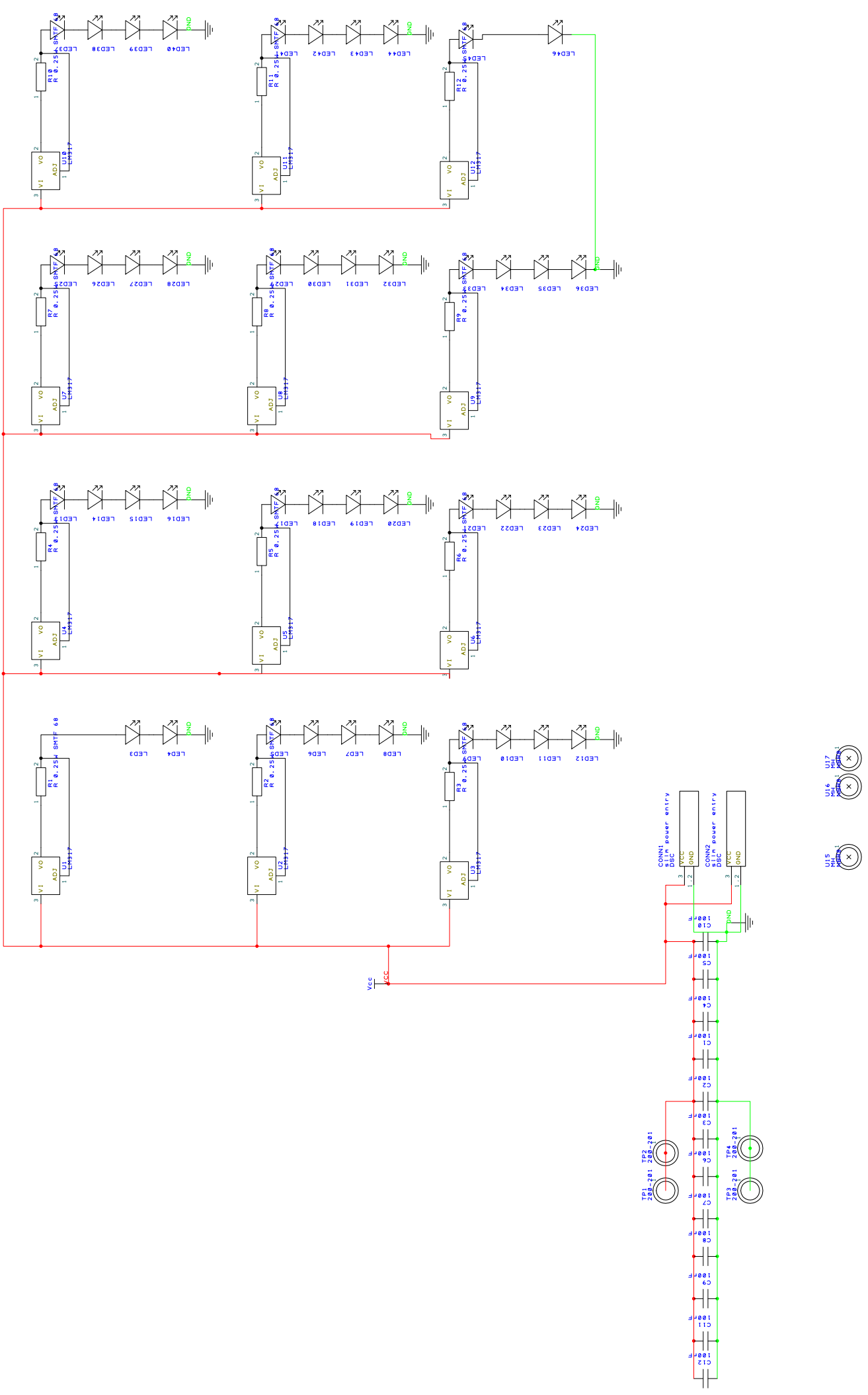


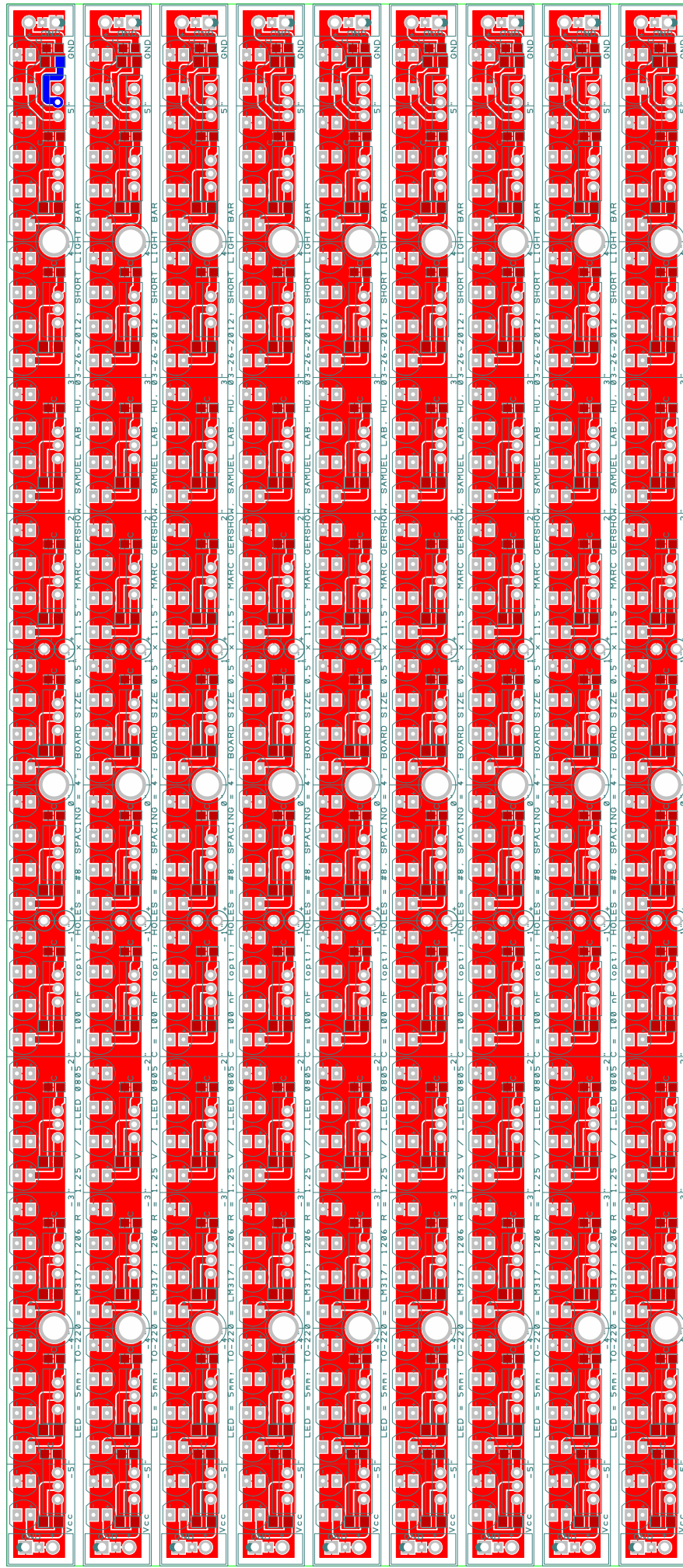












## Custom Machined Components

Description	File Name	Material	Qty Needed	Qty Spare	Qty	Notes
Flow Chamber Walls	FlowChamberWalls	Aluminum, anodized black	1	0	1	
Flow Chamber Clamp for Glass Base	FlowChamberBase For Glass Plate	Aluminum, anodized black	1	0	1	Several Base Options
Glass Base For Flow Chamber	Bottom Glass Plate	Glass	1	2	3	Clear Glass, Clear Polycarb/Acryl
Polycarbonate/Aluminum Base For Flow Chambe	FlowChamberBase	Polycarb or Aluminum(black)	1	0	1	Or Anodized Aluminum (black)
Insert to hold BD biodish XL	FlowChamberInsert_BiodishXL	Aluminum, anodized black	1	0	1	
Insert to hold clear agar plate	FlowChamberInsert_Plate	Aluminum, anodized black	1	0	1	
Glass Plate to Seal Flow Chamber	Top Glass Plate	Glass	1	4	5	
post mountable 10-32 t-manifold	t-manifold	stainless steel	5	1	6	
post mountable valve manifold	ValveManifold shared no and nc individu	stainless steel	5	1	6	for lee lhda hdi face mount valve
GL45 bottle to 1/4-28 flat bottom adapter	GL45 bottle cap insert with qtr28 flat bot	stainless steel	3	3	6	used to make bubbler for odor
Top Plate for Gradient measurement	top plate for gradient measurement	Aluminum (anodization option	1	0	1	
Clamp for Pidtech plus	simple clamp block for pidtech plus	Aluminum (anodization option	2	1	3	
flow block for draw sampling	flow block for measuring concentration i	Aluminum (anodization option	2	1	3	

## Thorlabs

Description	Part #	Cost	Qty Needed	Qty Spare	Qty	Total
Aluminum Breadboard, 24" x 36" x 1/2", 1/4"-20 MB2436		690	1	0	1	690
Ø1/2" x 3/4" Stainless Steel Optical Post	TR075	4.74	5	0	5	23.7
Ø1/2" x 1" Stainless Steel Optical Post	TR1	4.74	2	1	3	14.22
Ø1/2" x 1.5" Stainless Steel Optical Post	TR1.5	4.97	3	0	3	14.91
1" Post holder	PH1	7.03	5	0	5	35.15
Pedestal Base Adapter	BE1	9.1	15	0	15	136.5
Small Clamping Fork	CF125	8.75	15	0	15	131.25
8-32 drop in t-nut box of 10	XE25T4	23	0	1	1	23
XE25 rail table clamp	XE25CL2	11.3	0	1	1	11.3
1/4-20 cap screw and hardware kit	HW-KIT2	106.1	0	1	1	106.1
66 mm construction rail, L = 75 cm	XT66-750	82	2	0	2	164
Vertical Mounting Plate for 66 mm rail	XT66P1	34	2	0	2	68

additional components required to mount camera; see bruno afonso setup

additional components required to filter out channelrhodopsin stimulating light

## Index/Upchurch

Description	Part #	Cost	Qty Needed	Qty Spare	Qty	Total
headless vacutight nut, 10-32 w/ ferrule 10 pk	P-844x	46.82	20	2	22	1030.04
vacutight ferrule 10 pk	P-840x	46.76	0	4	4	187.04
teflon fep tubing, yellow 175 um ID x 1/16" OD	1477-20	96.48	1	0	1	96.48
teflon fep tubing, natural 0.030" ID x 1/16" OD	1520L	85	1	0	1	85
peek tubing 1/16" ID x 1/8" OD		85.19	1	0	1	85.19
flangeless ferrule 1/8" yellow	P-300x	11.91	1	1	2	23.82
flangless nut 1/4-28 for 1/8" tubing	P-301x	11.91	1	0	1	11.91
6-port manifold for 1/8" OD tubing	P-153	85.36	2	0	2	170.72
frit-in-a-ferrule 2 um for 1/8" tubing	P-372	6.65	0	2	2	13.3
extender tool for headless nuts	P-297	10.55	1	1	2	21.1
					0	0
					0	0

## Lee Valve

Description	Part #	Cost	Qty Needed	Qty Spare	Qty	Total
semi-inert hdi 3-way valves, face-mount	LHDA1221515H	request quote	40	10	50	#VALUE!
mounting screw support for 2 valves	LHDX0307130A	request quote	20	5	25	#VALUE!

## Clippard

Description	Part #	Cost	Qty Needed	Qty Spare	Qty	Total
epdm gaskets - 25 pack	11761-7-PKG	1.96	12	6	18	35.28
12 port manifold 10-32 fittings x 1 1/8-27 NPT fit MAN-12		6.27	8	2	10	62.7
10-32 screw plug, nickel plated, pack of 10	11755-ENP-PKG	3.05	6	2	8	24.4
10-32 to 1/16" single barb, pack of 10	11752-5-PKG	4.64	12	4	16	74.24
10-32 to 1/8" single barb, pack of 10	11752-4-PKG	4.64	0	2	2	9.28
10-32 to 1/8" OD compression, pack of 10	11923-PKG	12.29	10	4	14	172.06
8 port manifold 1/8 NPT fittings	MAN-ASF1-08	16.48	1	0	1	16.48
manifold mounting hardware	MAN-MH	2.06	1	0	1	2.06
replacement nut and ferrule, pack of 10	15155-PKG	6.7	0	2	2	13.4
10-32 to 1/16" OD compression, pack of 10	15160-ENP-PKG	18.16	4	4	8	145.28
minimatic fittings kit		106.81	0	1	1	106.81

note: needed quantities are approximate & may be overestimates; I requested ENP (electroless nickel plating) when available in stock. All buna-n gaskets must be swapped out for epdm

## Swagelok

Description	Part #	Cost	Qty Needed	Qty Spare	Qty	Total
brass tee; 1/4 x 1/4 x 1/8 NPT	B-400-3TTM	9	4	1	5	45
1/8" tube fitting to 1/8" NPT F, stainless	SS-200-7-2	9.4	3	0	3	28.2
1/4" tube fitting to 1/8" NPT M, stainless	SS-400-1-2	6.9	6	0	6	41.4
1/8" tube fitting to 1/8" NPT M, stainless	SS-200-1-2	7.5	6	0	6	45
1/4" to 1/8" swagelok adapter, brass	B-400-6-2	3.6	3	3	6	21.6
brass tee; 1/4 x 1/4 x 1/4	B-400-3	9	2	2	4	36
brass 1/4" tube to 1/4" NPT	B-400-1-4BT	2.9	1	2	3	8.7
brass cap for 1/4" tubing	B-400-C	1.7	1	3	4	6.8
brass plug for 1/4" tube fitting	B-400-P	1.7	0	2	2	3.4
brass pipe plug 1/4" male NPT	B-4-P	2.8	1	2	3	8.4
brass pipe plug 1/8" male NPT	B-2-P	2.2	4	4	8	17.6

pfa tubing, 1/8" OD x 0.03 wall; 100 feet	<a href="#">PFA-T2-030-100</a>	96.4	1	0	1	96.4
1/4" od tube bender; 3/4" bend radius	<a href="#">MS-HTB-4</a>	129.9	1	0	1	129.9
tubing cutter	<a href="#">MS-TC-308</a>	46.4	1	0	1	46.4
tube deburring tool	<a href="#">MS-TDT-24</a>	34.9	1	0	1	34.9
brass 3-way switching ball valve	<a href="#">B-42XS4</a>	44.1	1	0	1	44.1
brass hose connector 1/4" male NPT to 3/8" host	<a href="#">B-6-HC-1-4</a>	3.4	1	1	2	6.8
brass swagelok 1/4" to F NPT 1/4"	<a href="#">B-400-7-4</a>	3.4	1	1	2	6.8
brass hose connector 1/4" male NPT to 1/2" host	<a href="#">B-8-HC-1-4</a>	5.2	0	1	1	5.2
brass replacement ferrules 1/4"	<a href="#">B-400-SET</a>	0.74	0	10	10	7.4
brass replacement ferrules 1/8"	<a href="#">B-200-SET</a>	0.76	0	10	10	7.6

**McMaster-Carr**

Description	Part #	Cost	Qty Needed	Qty Spare	Qty	Total
corrosion-resistant muffler 1/8" NPT M	<a href="#">4402K51</a>	8.32	3	1	4	33.28
cleaned and capped copper tubing 1/4" OD	<a href="#">5174K3</a>	43.38	1	0	1	43.38
fep lined tygon tubing 1/16" ID x 1/8" OD	<a href="#">5046K16</a>	1.21	50	0	50	60.5
black PVC tubing 3/8" ID x 1/2" OD	<a href="#">5231K6</a>	0.43	25	0	25	10.75
tube clamps	<a href="#">9579K66</a>	9.08	1	0	1	9.08
6" cable ties	<a href="#">7130K41</a>	4.01	1	0	1	4.01
cable tie assortment	<a href="#">7338K53</a>	12.32	0	1	1	12.32
EPDM O-Ring AS568A Dash Number 282, 2 pack	<a href="#">9557K282</a>	6.65	1	1	2	13.3
EPDM O-Ring AS568A Dash Number 213, packs o	<a href="#">9557K482</a>	5.6	1	0	1	5.6
EPDM O-Ring AS568A Dash Number 212, packs o	<a href="#">9557K481</a>	5.45	0	1	1	5.45
EPDM O-Ring AS568A Dash Number 210	<a href="#">9557K478</a>	5.89	1	0	1	5.89
EPDM O-Ring AS568A Dash Number 211	<a href="#">9557K479</a>	5.28	1	0	1	5.28
green nylon tubing 1/4" OD	<a href="#">5635K53</a>	0.39	50	0	50	19.5
nylon screws 2-56 x 3/8	<a href="#">94607A079</a>	4.99	1	0	1	4.99
nylon screws 2-56 x 7/16	<a href="#">94607A080</a>	5.01	1	0	1	5.01
adhesive back uhmw plastic bumper 1/16" heigh	<a href="#">8962T31</a>	5.65	1	0	1	5.65
nylon spacer, #4 3/16" OD, 100 pk	<a href="#">94639A704</a>	7.08	1	0	1	7.08
SHCS 4-40 x 3/8, 100 pk	<a href="#">92196A108</a>	2.87	1	0	1	2.87
SHCS 4-40 x 1/2, 100 pk	<a href="#">92196A110</a>	3.13	1	0	1	3.13
adhesive backed fep film 12" square	<a href="#">5805T11</a>	13.94	2	0	2	27.88
Push-in Tapered Colored Rubber Plug Red, Fits 1"	<a href="#">9277K38</a>	10.48	2	0	2	20.96
Push-in Tapered Round Plug with Flange Std, Fits	<a href="#">40025K26</a>	11.91	0	2	2	23.82

**80/20**

Description	Part #	Cost	Qty Needed	Qty Spare	Qty	Total
hinged clamp for pneumatic compression	see separate bill of materials	381.45	1	0	1	381.45
enclosure	see separate bill of materials	1710.44	1	0	1	1710.44

**National Instruments**

Description	Part #	Cost	Qty Needed	Qty Spare	Qty	Total
NI USB 6008; USB based analog input/output dev	779051-01	169	2	0	2	338

**Baseline-Mocon**

Description	Part #	Cost	Qty Needed	Qty Spare	Qty	Total
Pidtech Plus Black (0.05 to 2000 ppm)	<a href="#">ZPP6018001 042-208</a>	540	2	0	2	1080
Pidtech Plus Silver (<5ppb to 20 ppm)	<a href="#">ZPP6018002 042-209</a>	675	1	0	1	675

**Custom electronics**

valve controller board	separate pcb and parts list
led light bars	separate pcb and parts list

**Aalborg**

Description	Part #	Cost	Qty Needed	Qty Spare	Qty	Total
gas flow controller; aluminum housing; viton sea GFC17A-VADL2-C0A		852	3	0	3	2556
calibrated for air 5L/min	3AB-09-SS		1	0	1	0
calibrated for air 100ml/min	3AB-04-SS		2	0	2	0
flow meter - housing	P11A3-TA0A	277	1	0	1	277
flow meter - flow tube 0-10 L/min direct reading	102-16-CA-TN		1	0	1	0

12V computer power supply

basic electronic supplies (wires, connectors, solder, etc.)

tools (wrenches, allen wrenches, t-handle ball driver, etc.)

hardware (screws, nuts, etc. I've tried to put hardware into list, but I'm sure there's stuff missing)

Additional components will be required.

Need to provide clean filtered air (charcoal filtered &amp; filtered at 35 microns or better) at 20 psi to mass flow controllers and air to pneumatic clamp at adjustable pressure ~10 psi

Need camera, acquisition board, computer, etc. for acquisition



## AutoQuoter Bill of Materials

# of Kits: 1  
 Req. Del. Date: 03/16/2012

Dist. PO:  
 Contact #1:  
 Contact #2:  
 Dist. Email:

Cust. PO:  
 Cust. Ref:  
 Cust. Contact: Alison Howard  
 Cust. Email: howarda@janelia.hhmi.org

# 80/20 Inc.

*The Industrial Erector Set®*

1701 South 400 East  
 Columbia City, Indiana 46725-8753  
 P: 260.248.8030 F: 260.248.8029  
[www.8020.net](http://www.8020.net)

**Distributor:**

**Customer:**  
 Marta Zlatic  
 19700 Helix Drive  
 Janelia Farm, RM 3C, 223  
 Ashburn, VA 20147

**Notes:**

TAG Part #	Qty	Length Each (or area)	Units	Total Wgt (lbs)	Description	Note: all extrusion dimensions start at the left end.	
						Each \$	Price \$
A 1010	2	18.000	IN	1.58	7042 in A Left	4.140	8.28
B 1010	3	14.000	IN	1.85	1" X 1" T-SLOTTED EXTRUSION	3.220	9.66
C 1010	2	12.000	IN	1.06	1" X 1" T-SLOTTED EXTRUSION	2.760	5.52
D 1010	2	5.000	IN	0.44	1" X 1" T-SLOTTED EXTRUSION	1.150	2.30
E 1010	2	4.000	IN	0.35	7042 in C Left	0.920	1.84
F 1010	2	4.000	IN	0.35	1" X 1" T-SLOTTED EXTRUSION	0.920	1.84
G 1020	1	12.000	IN	0.94	1" X 2" T-SLOTTED EXTRUSION	4.680	4.68
H 1030	1	12.000	IN	1.37	7042 in H Left; 7042 in E Left; 7042 in H Right; 7042 in E Right	6.600	6.60
7000	1		EA		Cut to Length 1" x 2" T-Slot and Tube	1.950	1.95
7003	1		EA		Cut to Length 1" x 3" T-Slot and Tube	1.950	1.95
7005	13		EA		Cut to Length 1" x 1" T-Slot and Tube	1.950	25.35
7042	8		EA		Anchor Fastener Counterbore for 10 Series	2.250	18.00
I 2053	2		EA	0.46	DEADBOLT W/ TOP LATCH	18.900	37.80
J 4081	6		EA	0.75	10 S 5 HOLE "L" JOINING PLATE	6.550	39.30
K 4118	10		EA	0.45	10 S 3 HOLE JOINING STRIP	4.300	43.00
L 4119	2		EA	0.05	10 S 2 HOLE INSIDE CORNER BRACKET	2.900	5.80
M 4132	2		EA	0.08	10 S 2 HOLE INSIDE CORNER GUSSET	3.950	7.90
N 4171	1		EA	0.39	10 S 2" UNIVERSAL LIVING HINGE W/ CORNER BRACKET	19.200	19.20
O 4260	2		EA	0.11	10 S 4 HOLE SLOTTED CORNER BRACKET	5.600	11.20
3275	12		EA	0.10	10 S ECON T-NUT 8-32 THREAD	0.160	1.92
3280	12		EA	0.24	10 S DBL ECON T-NUT 1/4-20 THREAD	0.690	8.28
3287	12		EA	0.30	10 S TRIPLE ECON T-NUT 1/4-20 THREAD	0.790	9.48
3313	12		EA	0.09	10 S 1/4-20 DROP-IN W/SET SCREW	2.400	28.80
3321	68		EA	1.36	1/4-20 X 1/2" FBHSCS & ECON T-NUT	0.500	34.00



## AutoQuoter Bill of Materials

Pg 59

# of Kits: 1  
**Req. Del. Date:** 03/16/2012  
**Dist. PO:**  
**Contact #1:**  
**Contact #2:**  
**Dist. Email:**

**Cust. PO:**  
**Cust. Ref:**  
**Cust. Contact:** Alison Howard  
**Cust. Email:** howarda@janelia.hhmi.org

### Distributor:

**80/20 Inc.**  
*The Industrial Erector Set®*  
 1701 South 400 East  
 Columbia City, Indiana 46725-8753  
 P: 260.248.8030 F: 260.248.8029  
[www.8020.net](http://www.8020.net)

### Customer:

Marta Zlatic  
 19700 Helix Drive  
 Janelia Farm, RM 3C, 223  
 Ashburn, VA 20147

### Notes:

TAG Part #	Qty	Length Each (or area)	Units	Total Wgt (lbs)	Description	Note: all extrusion dimensions start at the left end.	Each	Price
3375	12		EA	0.11	10 S DROP IN T-NUT 10-32		1.700	20.40
3393	8		EA	0.14	1/4-20 X 1/2" BHSCS, ECON T-NUT		0.400	3.20
3395	8		EA	0.24	10 S ANCHOR FASTENER ASSEMBLY		2.900	23.20

Weight per Kit: 12.80

Total Amount per Kit: \$381.45

**AutoQuoter Version:** 1.10.13.14**Price Release Date:** January 15, 2007**Drawing FileName:** C:\Documents and Settings\XPMUser\My Documents\autocad plans\hinge for lady gaga 2\pneumatic clamp.dwg

**AutoQuoter Bill of Materials**

<b>TAG Part #</b>	<b>Qty</b>	<b>Length Each (or area)</b>	<b>Units</b>	<b>Total Description</b> <b>Wgt Note: all extrusion dimensions start at the left end.</b>	<b>Each \$</b>	<b>Price \$</b>
				(lbs)		
A	1010	4	38.000	IN 6.69 7042 in A Left; 7042 in A Right	8.740	34.96
D	1010	2	36.000	IN 3.17 7042 in D Left; 7042 in D Right	8.280	16.56
C	1010	2	36.000	IN 3.17 1" X 1" T-SLOTTED EXTRUSION	8.280	16.56
B	1010	6	36.000	IN 9.50 7042 in A Left; 7042 in A Right	8.280	49.68
E	1010	4	24.000	IN 4.22 1" X 1" T-SLOTTED EXTRUSION	5.520	22.08
F	1010	6	24.000	IN 6.34 7042 in A Left; 7042 in A Right	5.520	33.12
G	1020	1	36.000	IN 2.81 7042 in E Left; 7042 in H Left; 7042 in E Right; 7042 in H Right	14.040	14.04
H	1030	2	24.000	IN 5.47 7042 in JJ Left; 7042 in I Left; 7042 in JJ Right; 7042 in I Right	13.200	26.40
I	2020	4	60.000	IN 29.52 7064 Right	34.200	136.80
J	2454	2	2.500	SQ FT 13.40 0.187" MILL FINISH ALUM PANEL 6061-T6 <b>**PER DRAWING**</b> <b>** with additional machining; see drawing **</b> (AD) 26IN x (AB) 12IN	48.130	96.26
K	2614-S	1	17.500	SQ FT 17.41 3/16" Black Haircell ABS (Smooth Side Up) (AD) 58.5IN x (AB) 36.5IN	77.000	77.00
L	2614-S	1	10.500	SQ FT 10.45 3/16" Black Haircell ABS (Smooth Side Up) (AD) 38.5IN x (AB) 34.5IN	46.200	46.20
M	2614-S	2	10.000	SQ FT 19.90 3/16" Black Haircell ABS (Smooth Side Up) (AD) 47.5IN x (AB) 24.5IN	44.000	88.00
O	2614-S	1	8.750	SQ FT 8.71 3/16" Black Haircell ABS (Smooth Side Up) (AD) 38.5IN x (AB) 24.5IN	38.500	38.50
N	2614-S	1	8.750	SQ FT 8.71 3/16" Black Haircell ABS (Smooth Side Up) <b>**PER DRAWING**</b> (AD) 40IN x (AB) 28IN 7507 on side AB @ 0.500; 7507 on side AB @ 27.500; 7507 on side CD @ 0.500; 7507 on side CD @ 27.500	38.500	38.50
	7000	1		EA Cut to Length 1" x 2" T-Slot and Tube	1.950	1.95
	7003	2		EA Cut to Length 1" x 3" T-Slot and Tube	1.950	3.90
	7005	24		EA Cut to Length 1" x 1" T-Slot and Tube	1.950	46.80
	7012	4		EA Cut to Length 2" x 2" T-Slot and Tube	2.050	8.20
	7042	48		EA Anchor Fastener Counterbore for 10 Series	2.250	108.00
	7064	4		EA 1/4-20 (1.125") Tap For 2020 Extrusions	7.650	30.60
	7150	5		EA Cut to Length Panel All Sides <= 48in	10.500	52.50
	7155	1		EA Cut to Length Panel Any Side > 48in	17.350	17.35

7167	2	EA	Cut to Length Panel All Sides <= 48in	15.500	31.00	
7507	4	EA	DRILL THRU 0.281" IN PANEL 1/2" FROM EDGE	2.100	8.40	
7180	22	EA	DRILL THRU ALUMINUM PANEL	2.500	55.00	
7175	8	EA	CIRCULAR CUTOUT ALUMINUM PANEL > 1"	6.300	50.40	
P	2053	2	EA	0.46 DEADBOLT W/ TOP LATCH	18.900	37.80
Q	2062	2	EA	0.12 SMALL PLASTIC DOOR HANDLE-BLACK	4.200	8.40
R	2066	6	EA	0.96 10 S HEAVY DUTY HINGE	20.800	124.80
S	2116	1	80.000 FT	1.60 10 S RUBBER PANEL GASKET	29.600	29.60
T	2427	8	EA	0.40 10 S PANEL MOUNT BLOCK	5.800	46.40
U	2500	18	EA	0.09 1/8" SINGLE TUBE CLAMP	0.210	3.78
V	2501	18	EA	0.09 1/4" SINGLE TUBE CLAMP	0.270	4.86
W	4108	4	EA	0.08 10 S 2 HOLE INSIDE CORNER BRACKET	2.750	11.00
X	4167	2	EA	0.15 10 S 4 HOLE JOINING PLATE	4.800	9.60
Y	4265	6	EA	0.15 10 S 2 HOLE SLOTTED CORNER BRACKET	3.550	21.30
Z	6000	1	EA	3/16" T HANDLE HEX WRENCH	5.250	5.25
AA	6110	1	EA	5/32" "T" HANDLE HEX WRENCH	5.000	5.00
AB	6111	1	EA	BONDHUS STANDARD BALL END L-WRENCH SET	20.500	20.50
AC	8030	1	EA	0.05 80/20 ATTITUDE PIN	0.270	0.27
	3063	8	EA	0.08 1/4-20 X .625" BHSCS	0.230	1.84
	3064	12	EA	0.17 1/4-20 X .75" SHCS	0.210	2.52
	3071	12	EA	0.19 1/4-20 X 1" SHCS	0.260	3.12
	3072	12	EA	0.22 1/4-20 X 1.25" SHCS	0.320	3.84
	3275	18	EA	0.14 10 S ECON T-NUT 8-32 THREAD	0.160	2.88
	3276	12	EA	0.10 10 S ECON T-NUT 10-32 THREAD	0.160	1.92
	3280	6	EA	0.12 10 S DBL ECON T-NUT 1/4-20 THREAD	0.690	4.14
	3321	20	EA	0.40 1/4-20 X 1/2" FBHSCS & ECON T- NUT	0.500	10.00
	3342	4	EA	0.04 1/4-20 X 1/2" FLANGED BHSCS	0.300	1.20
	3375	6	EA	0.05 10 S DROP IN T-NUT 10-32	1.700	10.20
	3376	24	EA	0.19 10 S DROP IN T-NUT 1/4-20	1.700	40.80
	3382	30	EA	0.30 10 S ECON T-NUT 1/4-20 THREAD	0.210	6.30
	3386	8	EA	0.14 1/4-20 X 3/8" FBHSCS & ECON T-NUT	0.460	3.68
	3395	48	EA	1.44 10 S ANCHOR FASTENER ASSEMBLY	2.900	139.20
	3491	4	EA	0.08 1/4-20 X 1/2" SHCS, ECON T-NUT	0.370	1.48

Weight per Kit:

Total Amount per Kit:

**1710.44**

157.26

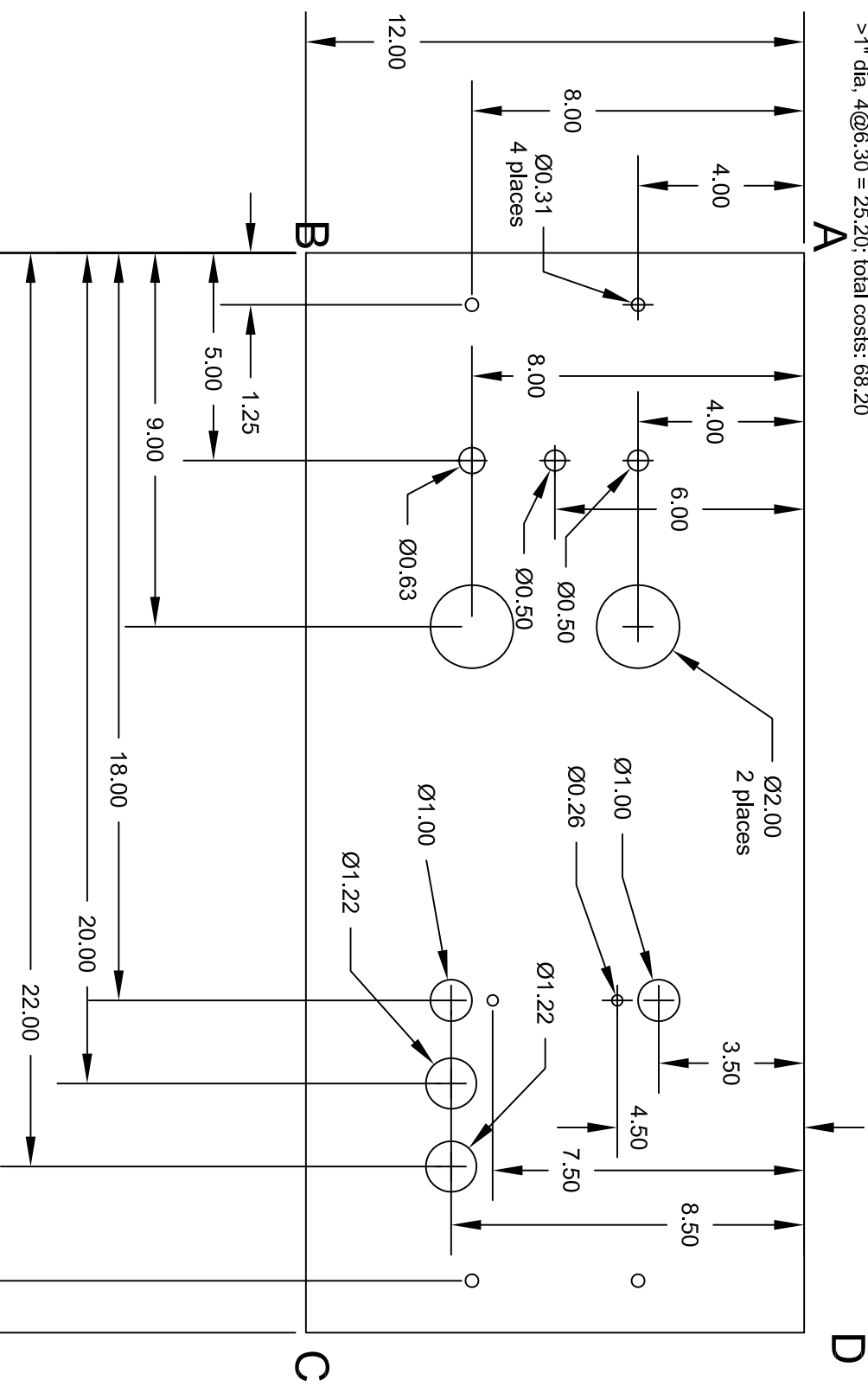
**AutoQuoter Version:** 1.10.13.14

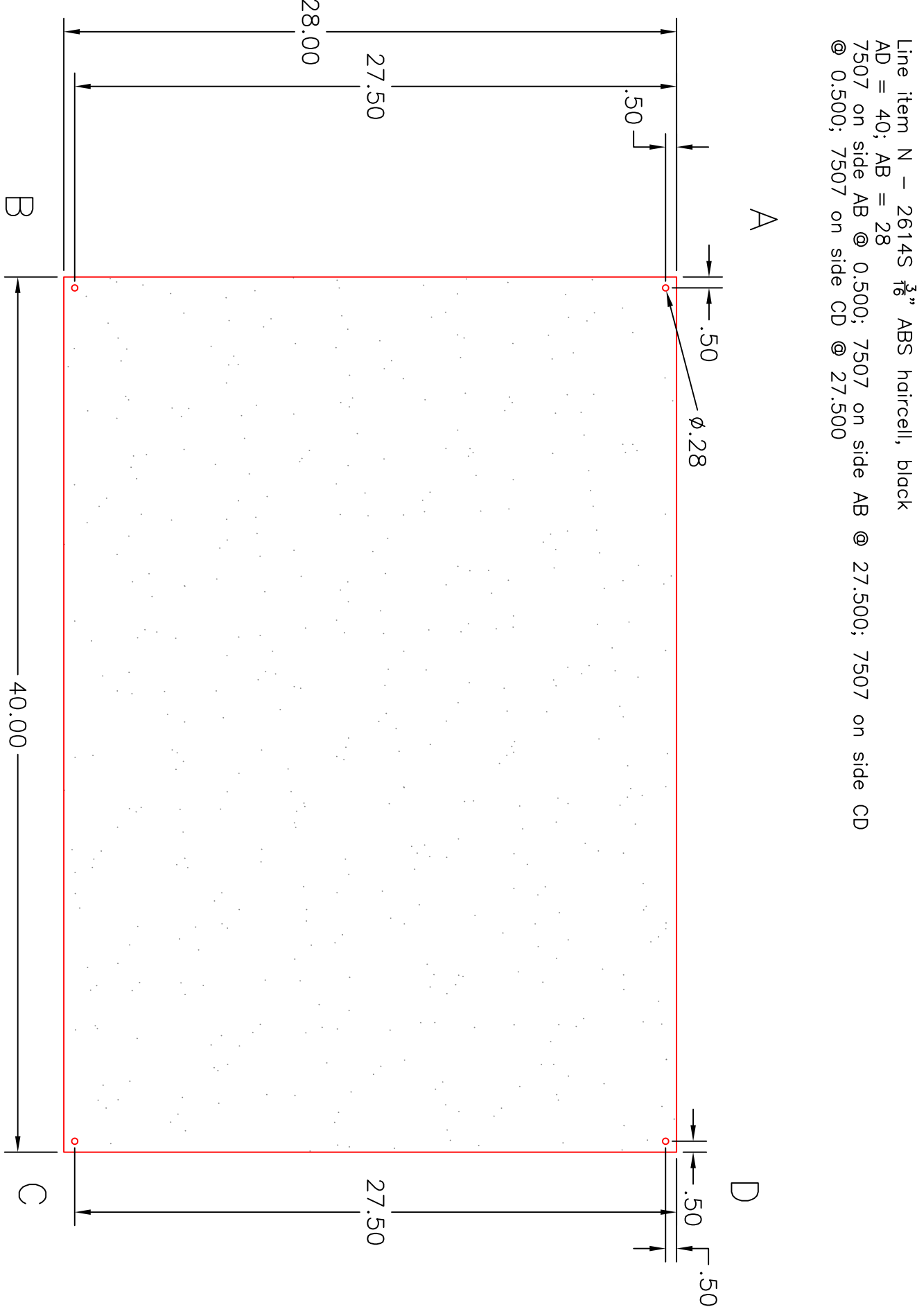
**Drawing FileName:** C:\Documents and Settings\XPMUser\My Documents\autocad plans\lady gaga large enclosure\frame and panels.dwg

Line Item J: 2454,  $\frac{3}{16}$ " aluminum panel, AD = 26", AB = 12" -- 2 panels  
 7180 -  $\frac{5}{16}$ " DIA along AB, 1.25" from edge, @4" and @8"  
 7180 -  $\frac{5}{16}$ " DIA along CD, 1.25" from edge, @4" and @8"  
 7180 -  $\frac{1}{2}$ " DIA 5" from side AB, @4" and 6" from AD

7180 -  $\frac{5}{8}$ " DIA 5" from side AB @ 8" from AD  
 7175 - 2.00" DIA 9" from side AB @4" from AD and @8" from AD  
 7180 - 1.00" DIA 18" from side AB @3.5" from AD and 8.5" from AD  
 7180 - 0.261" DIA 18" from side AB @4.5" from AD and 7.5" from AD

7175 - 1  $\frac{7}{32}$ " DIA 20" from side AB @ 8.5" from AD  
 7175 - 1  $\frac{7}{32}$ " DIA 22" from side AB @ 8.5" from AD  
 Total # of holes: 15 (4 @  $\frac{5}{16}$ " DIA, 2 @ 2" DIA, 2 @  $\frac{1}{2}$ " DIA, 1 @  $\frac{5}{8}$ " DIA, 2 @ .261" DIA, and 2 @ 1  $\frac{7}{32}$ " DIA)  
 Machining costs (per panel): 7167, cut to size, 15.50; 7180, drill thru aluminum panel, 11 @ 2.50 = 27.50; 7175 circular cutout >1" dia, 4@6.30 = 25.20; total costs: 68.20





Line item N - 2614S  $\frac{3}{16}$ " ABS haircell, black  
AD = 40; AB = 28  
7507 on side AB @ 0.500; 7507 on side CD  
@ 0.500; 7507 on side CD @ 27.500